The Dissertation Committee for Jordan Reynolds Keith
certifies that this is the approved version of the following dissertation:

# Investigations into ion transport properties of polymerized ionic liquids and related materials

Committee:

Venkat Ganesan, Supervisor

Joan Brennecke

Nathaniel Lynd

Pengyu Ren

Thomas Truskett

# Investigations into ion transport properties of polymerized ionic liquids and related materials

**by**

**Jordan Reynolds Keith**

**DISSERTATION**

Presented to the Faculty of the Graduate School of

The University of Texas at Austin

in Partial Fulfillment

of the Requirements

for the Degree of

**DOCTOR OF PHILOSOPHY**

THE UNIVERSITY OF TEXAS AT AUSTIN

August 2019

Dedicated to my tenth-grade chemistry teacher, Colonel Mark Mondl, whose teaching first inspired me to embrace science.

# Acknowledgments

I wish to thank my advisor, Dr. Venkat Ganesan, for four years of financial and intellectual support during graduate school. Thanks is also owed to my committee members, and all other faculty at the University of Texas who enabled my attendance and progression toward completion of the degree requirements. Specifically, I want to recognize the following faculty members: Hal Alper and the McKetta Chemical Engineering Department's graduate student selection committee in 2014, who granted me the opportunity to study at the University of Texas; Venkat Ganesan, Isaac Sanchez, Juan Ruiz, Gyeong Hwang, Nicholas Peppas, Roger Bonnecaze, Jean Anne Incorvia, and Benny Freeman, from whom I took classes; Brian Dinsmoor and Michael Poehl, who were supportive mentors during my stints as a teaching assistant; and Michael Baldea, with whom I shared stories and took advice on a plane ride to the AIChE conference in Pittsburgh, PA.

I also wish to recognize the professionals who groomed and guided me in my early career. To professors and advisors who issued recommendation letters and employed me as an undergraduate research assistant: Dr. Lisa Bullard, Dr. Phil Westmoreland, and Dr. Steve Peretti of the Department of Chemical and Biomolecular Engineering at North Carolina State University; and Dr. Mark Bathe of the Department of Biological Engineering at the Massachusetts

Institute of Technology. To notable colleagues and mentors (there are too many to name them all) at Eastman Chemical Company: Richard Lorenzo, Dave Schubert, Bob Kline, Ed Hicks, Brad Killen, Steve Miller, and Jerry Bewley; thank you for your patience and dedication in mentoring me as a developing engineer.

I cannot go without acknowledging the tremendous support that I received from my research group. Dr. Santosh Mogurampelly was instrumental in beginning our polymerized-ionic-liquids research program, and I owe him a tremendous debt for smoothing my transition to graduate research and inspiring the first two projects in this dissertation. I am also particularly grateful for mentorship from Dr. Zidan Zhang, who helped me expand my molecular dynamics tool set, which facilitated a quick and successful conclusion to my doctoral studies and armed me with a host of new capabilities. Dr. Dylan Kipp, who is a friend and colleague, deserves thanks for his role in connecting me with my future employer. I am also deeply appreciative for all other members of our research team: Dr. Vaidya Sethuraman, Dr. Dipak Aryal, Dr. Amir Taghavi Nasrabadi, Bill Wheatle, Rituparna Samanta, and Sanket Kadulkar; your intellectual support and friendship has been essential, and is greatly appreciated.

Of course, this list would be incomplete without acknowledgments for my family and friends. First and foremost, to my wife, Amanda Howes-Keith: for sacrificing your career gains and moving to a new city, giving me the chance to grow as a professional and pursue my dreams. To my parents and father-

in-law, Nancy Keith, Scott Keith, and David Howes: for numerous visits, emotional and financial support, and availability whenever I needed advice or a simple sounding board. To my aunt and uncle, Kae and Ben Keith: for allowing me to visit often, and giving me the right advice at the right time. To my local friends: Bill Wheatle, Kevin and Lauren Reimnitz, Alejandro Leal, Abby Leistra, Tommy and Caitlin Bentley, Gosia Chwatko, Kevin Baldridge, Jeff Thompson, and Aaron Burkey; for joining me for board games and other fun activities throughout the years. To my movement community: Josh Grant, Matt Johnson, and everyone involved with the Jungle Movement Academy; I'm so proud of you, and thank you for understanding when I had to reduce involvement to chase my dreams in graduate school. To my long-time friends: Ben Cowen, Michael DeMaria, Joe Puhr, Brandon Stevens, Richard Lorenzo, Zach Powell, John Hoyle, and Sam Thomson; you all have been there for me, for phone calls of support and celebration, and I appreciate the fact that all of you are still in my life in a meaningful way.

Finally, I want to acknowledge Jason Stapleton, host of the podcast "Wealth, Power, and Influence with Jason Stapleton," and all of the members of his Infuencer Community. Although Jason and I are not personal friends, his passion and message resonate, pushing me to strive for increase in every aspect of my life.

# Investigations into ion transport properties of polymerized ionic liquids and related materials

Publication No. _____

Jordan Reynolds Keith, Ph.D.
The University of Texas at Austin, 2019

Supervisor: Venkat Ganesan

The body of work on polymerized ionic liquids has been growing rapidly in recent years as researchers expand the synthesis space to achieve novel membrane materials with high conductivity, excellent mechanical stability, and high transference number. Despite progress in identifying specific new polymers and useful properties, there has been limited agreement over the mechanism for ion transport in these materials. It is essential that we resolve said mechanism for polymerized-ionic-liquid conduction, with the goal of streamlining future material design. Molecular dynamics is an excellent tool for analyzing local coordination behavior, ion-hopping pathways, and other phenomena of length- and time-scales that are currently inaccessible to direct experimental observation.

Ion transport is seen to proceed via a "climbing the ladder" mechanism involving the formation and breaking of ion-association pairs with, on average,

four polymerized ions from two polymer chains. This results in a link between ion-association lifetime and diffusivity for chemically similar polymerized ionic liquids, a feature that distinguishes polymerized ionic liquids from a broad class of polymer electrolytes and low fragility ionomers. This is also shown to be the case for a set of backbone-polymerized ionic liquids, when compared to a chemically similar pendent-polymerized ionic liquid. This is particularly interesting because the pendent architectural motif proves to have significantly higher reversibility of ion-hopping events. The application of design rules inspired by this research has already led to the experimental discovery of highly decoupled polymerized ionic liquids with excellent conductivity at ambient temperature.

Parametric simulation studies of poly(vinylimidazolium) polymerized ionic liquids and counterion variants have revealed a decoupling of ion mobility from polymer segmental dynamics. Small counterions are generally more decoupled, but results show that size is not the sole arbiter. For this set of different chemical components, encompassed by the anionic study, ion-association relaxation time, rather than lifetime, was proven to better correlate with diffusivity. Similar physics is observed between polymerized ionic liquids and salt-doped polymerized zwitterions for the population of mobile ions whose polymerized counter-charge is located on the end of a monomeric pendant. However, the cage-relaxation timescale appears to correlate better with diffusivity for the opposite ion in such materials.

# Table of Contents

# List of Tables

# List of Figures

# Chapter 1

# Introducing polymerized ionic liquids for battery electrolytes

In 2017 and 2018, the United States government released coupled installments of the fourth national climate assessment [249, 336]. Therein, the authors asserted that global temperature change over the past century is consistently attributed to human activities, especially through the emission of greenhouse gases such as carbon dioxide. Industrial emissions and fossil-fuel-sourced electricity can be curbed using capture, storage, and utilization technologies [8, 150, 171]. We already collectively use a diverse mixture of energy sources for producing electricity, ranging from traditional fossil fuels and nuclear power to renewable technologies such as wind and solar. Transitioning the transportation sector to electric power can boost results further. Simultaneously, improvements in energy storage technologies are required for terrestrial-grid applications, to ensure that the lights stay on during peak consumption periods, as well as during non-generating hours for renewable sources. The central need of both of these challenges is improved battery technology.

## 1.1 Background and Motivation

What are the canonical challenges in battery design and performance optimization? Tarascon reviews them in a 2001 article, highlighting electrode capacity/resistance and resistive-layer deposition during operation, along with various features of electrolyte design [303]. Specifically, the electrolyte must be a good ionic conductor and electronic insulator, inert to other cell components, thermally stable, non-volatile at operating temperatures, sustainable, and cheap [175]. It must also be mechanically stable. In lithium-ion batteries, a compressible electrolyte requires a shear modulus of greater than that of the electrode to maintain interfacial stability [221]. Instability can lead to surface roughness or dendrite formation. Dendrites are formed by targeted ion deposition that branches through the electrolyte. When branches reach the opposite electrode, it causes a short circuit, which can lead to rapid and potentially explosive discharge of stored energy [173, 264]. This has been documented to cause safety issues, including overheating and flammability in lithium-ion batteries [128, 155].

Safety is a critical aspect of battery electrolyte design. Flammability has already been addressed, in part, with respect to dendrite formation [128]. Enhanced chemical stability of electrolyte components prevents decomposition products from leaking, volatilizing, or causing uncontrolled decomposition, leading to runaway reactions. Non-volatility is an important property for any native and decomposition products, since flammability is often predicated on a non-negligible vapor pressure [66]. Furthermore, non-volatility prevents vapor

pockets from forming internally, which could pose explosion risks, as well as reduce battery performance. Non-toxicity is also a key property, in case leaks occur where batteries are deployed to countless applications where people and animals could come into contact with the encased electrolyte or additives [175].

Finally, we wish to maximize battery performance, including conductivity and ion selectivity, which is quantified by the lithium-transference number in lithium-ion batteries. An improved lithium-transference number reduces the buildup of counterions near an electrode, termed concentration polarization [140, 197, 198].

What material design strategies are being used to progress the field? Polymer electrolyte membranes have been a keen target for researchers, with improved mechanical strength and discharge rate, which enhance the safety characteristics of the electrolyte. However, they do show reduced conductivity compared with their liquid-media counterparts. A enormous body of work has been devoted to understanding the transport mechanism of ions in polymer electrolytes due to their importance in battery-electrolyte membranes.

Intra-chain, inter-chain, and cooperative motion have all been explored as possible contributors to lithium conduction in salt-doped electrolytes. Diddens et al. explored a lithium salt in poly(ethylene-oxide) membranes, identifying a common motif of two chains solvating a lithium, with motion of lithium along each chain, independent of the others [76]. They concluded that intra-chain motion better predicts ion-transport behavior, a conclusion which was supported by Borodin [29]. Borodin wrote, in numerous studies, that

there is strong coupling between lithium diffusion and monomeric displacement via polymer segmental relaxation, which was investigated further using many-body polarizable force fields in simulation [27, 30, 31, 33–35]. Borodin later posed two key mechanisms for lithium diffusion in solvent-containing polymer-electrolyte membranes: vehicular diffusion and solvent exchange [32].

More recently, it has been discovered that there is a competition between increasing concentration of charge carriers and slowing polymer segmental relaxation dynamics in salt-doped polymer electrolytes [220, 330, 331]. And some extent of decoupling has been observed between conductivity and polymer segmental dynamics for systems with continuous paths of solvation sites, allowing lithium to shuttle along the polymer [239, 328].

Non-ionic-liquid single-ion conductors have also been explored in an effort to increase transport selectivity [103, 350]. Over a decade of study led to the unearthing of a novel ion-transport mechanism. Some studies continued to show strong coupling between polymer segmental dynamics and conductivity, arguing that single-ion conductors should be designed with weakened ionic interactions and faster backbone relaxation rates [80, 95, 177, 322]. Others showed strategies for improving conductivity without sacrificing segmental dynamics. Liang et al. were able to improve conductivity relative to glass-transition-normalized temperature by manipulating the backbone (polysiloxane for flexibility and low viscosity) and anion electronegativity (borate rather than nitrogen- or fluorine-containing compounds) [176].

Ionic aggregation has also been widely explored as a key to ion conduc-

tion in these materials. Several studies reported on chain-like aggregates that demonstrate fast ion conduction, despite aggregation [178, 284, 285]. Meanwhile, more aggregation and superior conductivities were reported in monomers with long side chains, further supporting the notion that aggregation increases conductivity [59]. Many studies explored ion transport in precise ionomers, which consist of ionic repeat units with a precise number of backbone atoms separating each ionic unit [41–43, 307, 308]. Hall and coworkers, in a series of studies, contributed deep understanding of structure in precise ionomers and reported faster dynamics once the ionic aggregates became percolated [41–43, 119, 121, 122].

Other researchers produced some of the earliest reports of ion-hopping mechanisms in single-ion-conducting materials. Milner and coworkers used coarse-grained molecular dynamics to show that ion transport is mediated through consecutive coordination with ion pairs [192,193]. Reports of transient triple ions with two ions and one covalently bound counterion informed a proposed hopping mechanism in related studies [95, 160].

Introducing a more delocalized charge distribution in the tethered ions has demonstrated improvement in ion conductivity and transference number in single-ion conductors [196, 245]. Ionic liquids consist of salt-components which have highly delocalized charge distributions, reducing intermolecular interactions and lowering boiling point. Ionic liquids have been explored as candidates for battery electrolytes, owing to their excellent chemical stability, low volatility, and compatibility with battery components [9, 115, 231]. How-

ever, because of their liquid nature, ionic liquids suffer from the effects of charge polarization, the phenomenon of coordinated diffusion that can lead to high impedance, voltage loss, and unwanted side reactions. Their liquid nature also bestows poor mechanical properties, which are unsuitable for stopping dendrite penetration. They also suffer other negative effects, including leaching, swelling, and potential containment loss [177, 204, 300, 326].

Incorporating ionic-liquid components into single-ion conductors increases charge delocalization and conductivity while maintaining mechanical strength. Considering the preceding discussion, we conclude that polymerized ionic liquids are a target for improved battery electrolyte membranes. The remainder of this chapter will be devoted to exploring the current state of polymerized-ionic-liquid research, especially the knowledge base on ion-transport mechanisms in such materials. Many reviews have been written on the subject of polymerized ionic liquids. In 2019, Ganesan published a comprehensive review of ion-transport properties in polymerized ionic liquids, largely inspired by the results in and peripherally related to this project [103]. Several other groups reviewed synthesis and application of polymerized ionic liquids [112, 209, 347].

Polymerized ionic liquids are rapidly ascending as integral materials in battery electrolyte research. Several recent reviews are available, covering the breadth of device applications sought through polymerized ionic liquids [2, 112, 209, 229, 347]. While there has been a large contribution of simulation research in modeling ion transport in non-ionic polymers, polymers mixed

with additives, and co-polymers of highly conductive and mechanically strong elements [214], no studies, prior to the contained set of reported works, have examined ion-transport mechanisms in polymerized ionic liquids.

The goal of this project is to identify and explain ion-transport mechanisms in polymerized ionic liquids using atomistic molecular dynamics simulations. Optimization of ion transport of polymerized ionic liquids has been hampered by a lack of fundamental mechanistic understanding. Indeed, while ion transport is understood to be governed by the ion-association structural relaxation times in pure ionic liquids [352], and by the polymer backbone segmental dynamics in polymer electrolytes such as poly(ethylene oxide) [16, 28, 29, 33, 77, 199, 200, 213, 227], little clarity exists on the mechanisms prevailing in ionic-liquid-based single-ion conductors.

Original reports suggested that ionic conductivity in polymerized ionic liquids are slaved to polymer segmental motion [168, 230]. Indeed, such a conclusion may be correct for backbone ionomers (ions incorporated directly into polymer backbone) as reported in a number of studies from Colby and coworkers [94, 95, 315, 322]. Nakamura and coworkers were the first to demonstrate a decoupling between the timescales of ion and segmental motion for polymerized ionic liquids [224–226]. They utilized both dielectric and viscoelastic relaxation spectra to argue that a broadband dielectric spectroscopy peak, once attributed to segmental relaxation, was actually due to ion-pair relaxation. This represented the first appearance of the ion-hopping mechanism in polymerized-ionic-liquid literature. Still, the segmental-motion mech-

anism was persistent, being utilized to explain conductivity behavior by high profile contributors, including Winey, Runt, and Colby all the way through 2015 [59–61, 253].

With better understanding of existing analysis techniques and the advent of new techniques for identifying specific relaxation modes, the decoupling between ionic conductivity and structural dynamics in polymerized ionic liquids reemerged as a central issue [73, 86, 98, 134, 162, 256, 333]. Such considerations motivate the questions considered in this project, *viz.*, "What are the mechanisms and time scales underlying ion transport in polymerized ionic liquids?", "What is the origin of differences, if any, in ion-transport phenomena between polymerized and pure ionic liquids, and their relationship to the structural relaxation dynamics?", "Are the ion transport properties of polymerized ionic liquids indeed decoupled from the segmental relaxations and glass-transition temperatures?" Progress in answering the above questions should provide valuable insight into the design of new materials for battery and fuel cell electrolytes, electrode binders, gas separation membranes, and other applications.

## 1.2 Outline of Dissertation

### 1.2.1 Methods

In this chapter, we address common approaches for all of the work included in this dissertation. To begin, we discuss the Optimized Potential for Liquid Simulations, which was deployed to model inter-atomic and intra-

molecular interactions. We also address the assignment of partial charges, and support the decision to use constant scaled partial charges to reflect an average polarization effect. We then discuss the approach to setting up simulations and bringing the resulting initial configuration to equilibrium.

For the remainder of the chapter, we build the suite of analysis methods used in this project. The fundamental transport property probed among these works in the self-diffusivity, which is traced from the mean-squared displacement. Structure functions, including the radial distribution function and the structure factor are revealed next. We then explore ion-association analysis, followed by the ion-association autocorrelation functions (intermittent and continuous) whose fundamental timescales are the ion-association structural relaxation time and lifetime. Finally, we reveal our approach to evaluating ion hopping using ion-coordination states at consecutive timesteps.

### 1.2.2 Probing mechanistic differences in ionic liquids and polymerized ionic liquids by varying the number of repeat units

We report the results of atomistic molecular dynamics simulations on polymerized 1-butyl-3-vinylimidazolium hexafluorophosphate ionic liquids, studying the influence of the polymer molecular weight on the ion mobilities and the mechanisms underlying ion transport, including ion-association dynamics, ion hopping, and ion-polymer coordinations.[1] With an increase in polymer molec-

[1]Jordan R. Keith, et al. Influence of molecular weight on ion-transport properties of polymerized ionic liquids. *Phys. Chem. Chem. Phys.*, 19:29134, 2017. – Reproduced by permission of the PCCP Owner Societies.

ular weight, the diffusivity of the hexafluorophosphate counterion decreases and plateaus above seven repeat units. The diffusivity is seen to correlate well with the ion-association structural relaxation time for pure ionic liquids, but becomes more correlated with ion-association lifetimes for larger-molecular-weight polymers. By analyzing the diffusivity of ions based on coordination structure, we unearth a transport mechanism in which the hexafluorophosphate moves by "climbing the ladder" while associated with four polymeric cations from two different polymers.

### 1.2.3 Identifying variation of ion-transport mechanisms in polymerized ionic liquids with different polymerized cation chemistry

We used atomistic molecular dynamics simulations to study the properties of polymerized 1-*alkene*-3-butylimidazolium hexafluorophosphate, a polymerized ionic liquid electrolyte, and characterized the influence of the linear alkene length on the mobility of the hexafluorophosphate ions.[2] Consistent with experimental observations, our simulations indicate that as the alkene length increases, the diffusivity of hexafluorophosphate anion monotonically increases. We demonstrate that such a trend arises from the influence of linker segments on the intermolecular ion hopping rates, which is in turn modulated by intermolecular cationic separation distances.

[2]Reproduced with permission from Jordan R. Keith, et al. Influence of side chain linker length on ion-transport properties of polymeric ionic liquids. *J. Poly. Sci. Part B: Polymer Physics*, 55(23):1718-1723, 2017. Copyright 2017 John Wiley and Sons.

### 1.2.4 Analyzing the influence of varying mobile-anion chemistry on ion transport in polymerized ionic liquids

We use all-atom molecular dynamics simulations of cationic polymerized ionic liquids to probe the influence of size and shape of counterions on ion mobilities in relation to polymer segmental dynamics.[3] Our results demonstrate that the size, or ionic volume, of the counterion, cannot fully explain the mobility trends. Within certain geometric and chemical-specific classes, small ions generally show a higher degree of decoupling from polymer segmental dynamics. However, even such a size effect is observed to be not universal, and appears to be overcome when substantial delocalization of cation-anion coordination manifests. We demonstrate a universal inverse correlation between ion-association structural relaxation time and the conductivity for these polymerized ionic liquids, supporting the ion-hopping interpretation of ion mobility in polymerized ionic liquids.

### 1.2.5 Characterizing the impact of backbone- versus pendant architecture on ion transport in polymerized ionic liquids

We use atomistic computer simulations to examine ion-transport phenomena for backbone polymerized cationic liquids with bistrifluorosulfonylimide ($TFSI^-$) counterions. We consider a system in which the polymerized cation moiety is the imidazolium ring, and study the structural characteristics

[3]Reproduced with permission from Jordan R. Keith, et al. Influence of Counterion Structure on Conductivity of Polymerized Ionic Liquids. *ACS Macro Letters*, 8:387-392, 2019. Copyright 2019 American Chemical Society.

and ion mobilities for cases in which the cations are separated by four, six, and eight methylene units on the backbone. A pendant polymerized ionic liquid, 1-butyl-3-vinylimidazolium, is compared to the backbone series across ion coordination and hopping features. The anion diffusivity in backbone polymerized cationic liquids is found to decrease with increasing spacer length, which is shown to result from a decrease in intra and intermolecular hopping frequencies due to an increasing distance separating imidazolium moieties. In comparison to pendant polymerized ionic liquids, we observe that the participation rates of intermolecular hopping events in the backbone polymers far exceed that of the pendant, and the intrapolymeric ionic coordination profile shows the $TFSI^-$ of the pendant polymer with a high propensity for coordination by multiple imidazolium, compared with one monomer from a given polymer for the backbone series. Despite these differences, backbone polymerized ionic liquids are seen to possess correlated diffusivity and ion-association relaxation times, in a manner similar to the results observed in past studies for pendant variants.

### 1.2.6 Extending principles of ion motion in polymerized ionic liquids to polymerized zwitterions for battery electrolytes

Polyzwitterions (polyZIs), macromolecules with repeating ampholytic monomers, are a novel class of materials with attractive properties for battery electrolytes. In this study, we test two salt-doped ($Li^+$-$TFSI^-$) polyZIs of similar composition with contrasting zwitterion (ZI) ionic organization: pendant monomers organized via backbone-anion-cation (B-$ZI^-$-$ZI^+$, motif B) and

backbone-cation-anion (B-$ZI^+$-$ZI^-$, motif C). Within motifs B and C, the counterion of the pendant-end ZI moiety shows higher mobility. Similarly, when comparing $Li^+$ or $TFSI^-$ across motifs, it is seen that the respective pendant-end counterion possesses higher mobility than its backbone-adjacent counterpart. Furthermore, when comparing counterions to same-position ZI moieties, $TFSI^-$ is seen to possess higher mobility than $Li^+$ in each case. This latter phenomenon results from lower interaction strength between the $TFSI^-$ and $ZI^+$, but these results suggest that there are different physics governing the mobilities of ions based on the pendant position of their ZI countercharge. Indeed, the mobility of countercharges to the pendant-end ZI moiety are shown to correlate with the ion-association relaxation timescale, similar to polymerized ionic liquids in past studies. However, the mobility of countercharges to the backbone-adjacent ZI moiety are correlated with a cage relaxation time, incorporating the combined effects of i) frustrated motion due to the presence of the polymer backbone and pendant-end ZI moiety and ii) heightened mobility in a population of lightly zwitterion-coordinated ions.

### 1.2.7 Prospects for the future of the field

This chapter discusses a collection of questions that could motivate future projects, extending the encompassed work of this dissertation. Specifically, there are two thrusts presented herein. First, polymerized-ionic-liquid block copolymers are an area of scrutiny in the experimental community. But they have been underserved by simulations due to the challenge of marrying

mesoscale morphological characterization with atomistic-scale transport modeling. The first section discusses the dissipative-particle-dynamics framework and its role in modeling mesoscale phase behavior, and poses a series of unknown transport phenomena as they relate to morphology. The second section delves into confined ionic materials, with the goal of establishing prior work on confined ionic liquids as a springboard to analyzing ion transport in confined polymerized ionic liquids. We discuss modeling and analysis techniques to establish the current state-of-the-art, and propose an assortment of motivating questions related to confined ionic structure and transport phenomena in polymerized ionic liquids.

# Chapter 2

# Methods

## 2.1 Simulation methods

### 2.1.1 Potential energy and parameters

We utilized the optimized potential for liquid simulations (OPLS), an all-atom molecular dynamics force field designed to model complex organic molecular liquids [144]. The OPLS all-atom force field has been utilized in past studies to model the physical properties of ionic liquids and polymers [19, 47, 79, 219, 254]. Such efforts have been mostly successful in matching experimental structural and thermodynamic properties, including density and heats of vaporization [254]. However, apart from Bhargava and Balasubramanian, who demonstrated good agreement with experimental diffusion coefficients, these studies did not reproduce transport properties [19].

Polarizable force fields have been utilized in some studies to improve the accuracy of dynamical properties in ionic liquids [25, 26, 35, 208, 288]. But, they are computationally expensive, even for non-polymerized ionic materials. Others have circumvented the computational expense of such methods by scaling partial atomic charges to study ionic-liquid systems [19, 53, 54, 218, 222, 301, 344, 351, 353, 353]. Several studies demonstrated that uniformly scaling partial atomic charges by 0.7-0.9 (depending on ionic liquid) was successful

in matching structural and transport properties [19, 53, 54, 218, 301]. Based upon the efficiency and accuracy of such methods, we have utilized the charge scaling approach with a 0.8 scaling factor, whose success for a $PF_6^-$-based ionic liquid was demonstrated by Bhargava and Balasubramanian [19]. Section 2.1.2 provides more detailed discussion and defense of this choice, and its relevance beyond $PF_6^-$-based polymerized ionic liquids. We also address with methodology for determining atomic partial charges in this next section.

The OPLS potential energy takes the form

$$U = \sum_r U_{bond}(r) + \sum_\theta U_{ang}(\theta) + \sum_\phi U_{dih}(\phi) + \sum_\phi U_{imp}(\psi) + \sum_{ij} U_{nb}(r_{ij}). \quad (2.1)$$

Equation 2.1 includes terms for bond interactions, $U_{bond}(r) = k_r(r - r_0)^2$, and angle interactions, $U_{ang}(\theta) = k_\theta(\theta - \theta_0)^2$, with spring constants, $k_r$ and $k_\theta$, and equilibrium bond length, $r_0$ and angle $\theta_0$. The energy contributions from dihedral angles,

$$U_{dih}(\phi) = \frac{1}{2}\sum_{n=1}^{4} K_n[1 + (-1)^{n+1}\cos(n\phi)], \quad (2.2)$$

and improper angles, $U_{imp}(\psi) = 1.1[1 - \cos(2\psi)]$, complete the bonded energy description. Early efforts in this project conceptualized and specified the improper angles incorrectly, so reference to the specific parameters should be avoided. The above description is accurate and can be used to determine parameters for previously modeled and new imidazolium-based materials.

We complete the energetic description with the contributions of non-bonded interactions. Such interactions include long-range Coulombic (electrostatic) attraction/repulsion ($r^{-1}$), attraction via short-range electron-dispersion

($r^{-6}$), and an empirical fast-decaying repulsive potential used to avoid atom overlap ($r^{-12}$). This description manifests as the traditionally used Lennard-Jones (LJ) 6-12 potential and the well-known Coulombic potential:

$$U_{nb}(r_{ij}) = 4\epsilon_{ij}\left[\left(\frac{\sigma_{ij}}{r}\right)^{12} - \left(\frac{\sigma_{ij}}{r}\right)^{6}\right] + \frac{Cq_iq_j}{r}. \tag{2.3}$$

OPLS non-bonded parameters include potential-well depth $\epsilon_{ij}$ and the LJ-radius $\sigma_{ij}$ for pair $ij$. Cross terms were calculated using a geometric mixing rule such that $\epsilon_{ij} = \sqrt{\epsilon_i\epsilon_j}$ and $\sigma_{ij} = \sqrt{\sigma_i\sigma_j}$. Finally, equation 2.3 includes the partial atomic charges, $q_i$ and $q_j$, in elementary units of charge and a constant, $C = 5.514 \times 10^{-22}$ kcal-Å/e$^2$.

Non-bonded forces were scaled to 0.0 for first- and second-order bonded atoms. In other words, atoms that are directly bonded, or connected within two bonds, were not considered to interact via electrostatic or dispersion forces. Third-order bonded atoms, or atoms connected within three bonds, included non-bonded forces scaled by 0.5. All other atom-atom pairs interact using the full non-bonded energy description in equation 2.3.

The most important monomer platform for this research has been the 1-butyl-3-vinyl imidazolium (pBvIm$^+$) cation, initially introduced by Mogurampelly, myself, and Ganesan [216]. We adapted most of the intra- and inter-molecular force field parameters for this polymer from earlier studies on organic liquid force fields and molecular dynamics modeling of ionic liquids [19,144,254]. The OPLS all-atom force field and parameter set originated in Jorgensen's all-atom optimized potential for liquid simulations force field

(OPLS-AA) [144]. Bhargava and Balasubramanian reported improved parameters for 1-butyl-3-methylimidazolium($BmIm^+$)-$PF_6^-$ to accurately reproduce experimental density and diffusion coefficients [19]. This improvement was essential for a series of studies, like ours, that focuses on dynamic properties and transport mechanisms.

Sambasivarao et al. contributed further refinements to the intramolecular parameters for the ionic liquid $BMIm^+$-$PF_6^-$, particularly for the energy contribution of dihedral angles, which were incoporated into our early models of pBvIm-$PF_6^-$ [254]. The original contribution from Mogurampelly, which used the precise improvements noted above, modeled pBvIm$^+$-$PF_6^-$ with $n = 32$ repeat units [216]. Additionally, Mogurampelly spearheaded efforts to develop new dihedral-angle potentials for backbone-containing angles, which had never been modeled. The dihedral parameters developed as part of this study were extended to other studies in this project, including ones on molecular-weight and counterion effects [147,149]. These studies used the same polymerized-cation platform, making them easy candidates for extension of the prior work.

Another early study contained in this project, which probes linker effects in chemically similar polymerized ionic liquids, extended this dihedral-fitting approach to capture new angles for novel simulation materials [148]. However, for later studies in this project, we increasingly viewed the OPLS platform as a conduit for fast material screening and actionable modeling. In order to increase the speed of development and the richness of chemical diversity in our efforts, we discarded the dihedral-fitting procedures, relying on

built-in parameters from the latest iteration of the OPLS database, the LigParGen server [78, 145]. This online tool allows a researcher to upload a PDB file of the molecule of interest, which the server returns as a variety of starting points for various simulation packages that support the OPLS equations. This includes properly specified topology, along with force field parameters in the OPLS style. While there may be enormous differences in the parameters of the OPLS database and those generated by the procedure used in our early works, our contention is that such differences are inconsequential to the overall system energy and the properties probed in our simulations.

### 2.1.2 Effective polarization

Dommert et al. authored a seminal review on polarization phenomena in molecular dynamics simulations of ionic liquids [79]. There are two accepted approaches to modeling such phenomena: 1) explicit polarization through the use of polarizable force fields and 2) effective polarization using reduced constant partial atomic charges. Models with explicit polarizability align more closely with the physics of real materials. And, although polarizable force fields have been used with success to compute transport properties, they are computationally expensive. This issue is magnified for atomistic modeling of polymerized ionic liquids because of their slow relaxation timescales.

Fortunately, charge transfer phenomena can be qualitatively captured as an average effect, yielding an effective reduction in partial charges, such as the ones explored by these earlier studies. A reduced constant partial charge

yields an "average effective description of polarization" [79] that apparently reproduces structural and dynamic properties in ionic liquids [19, 54, 183, 294, 351, 352]. Morrow and Maginn were the first to use reduced partial charges in ionic liquids. Each ion from the ion pair $BmIm^+$-$PF_6^-$ was assigned a total charge of $\pm 0.904$ from vapor-phase electrostatic mapping [222]. Now, studies on materials including ionic liquids, zwitterions, polyampholytes, and polymerized ionic liquids have employed a similar approach.

Julian and Jarrold proved the existence of internal charge-separation in zwitterions, for example, using gas-phase quantum chemical optimization and electrostatic mapping [146]. Early models of zwitterions by Shao et al. used a non-polarizable potential with partial charges developed from the electrostatic potential map of molecules optimized in a polarizable-continuum implicit solvent [272]. But, they did not include the implicit solvent model in later studies, and instead, optimized molecules in the gas phase, which justified our choice of the same approach [273]. The spirit of the former approach is certainly sound, considering the potential influence of the immediate chemical environment on charge dispersion. Ultimately, we are convinced to employ the simpler, latter approach, whose effectiveness has been demonstrated in numerous adjacent material classes.

Specifically, several recent simulation studies revealed improvements to dynamic properties such as diffusivity over non-charge-scaled models [19, 54, 183, 294, 351, 352]. The work of Bhargava and Balasubramanian on $BmIm^+$-$PF_6^-$ established the basis for our investigations into polymerized ionic liquids.

They reported accurate densities and low deviations from experimental diffusivities, using a uniform scaling factor of 0.8 on vapor-phase partial charges for $BmIm^+$-$PF_6^-$ ionic liquid [19]. Zhang and Maginn also reported accurate diffusivities for $BmIm^+$-$PF_6^-$ ionic liquid with the same scaling factor [351].

Success in improving atomistic-modeling accuracy extends beyond $BmIm^+$-$PF_6^-$. Chaban et al. determined that uniform scaling of charges for $BmIm^+$-$BF_4^-$ ionic liquids accurately reproduced experimental diffusivities and densities with a scaling constant of 0.807 [54]. Sprenger et al. reported diffusivity errors of 11.0% ($BmIm^+$) and 18.7% ($TFSI^-$) using the uniform scaling factor of 0.8 [294]. In an earlier work on an imidazolium-series of cations with $TFSI^-$, Liu and Maginn showed similar agreement with experimental results for the same scaling factor [183]. Later, Zhang and Maginn demonstrated the applicability of the uniform charge-scaling constant 0.8 to 29 ionic liquids containing four distinct anions (including $TFSI^-$ and $PF_6^-$) with a series of imidazolium-based cations [352].

After considering the evidence presented above, we elected to incorporate effective polarization through the use of reduced vapor-phase partial charges for the studies pursued under the umbrella of this work. The specific approach to obtaining the unscaled partial charges differs among the projects included in this thesis. However, the following approach, or one employing a more detailed method and/or a higher-level basis set for optimization, is recommended for future efforts. In short, the use of low-level basis sets or less rigorous methods changes the electrostatic potential map, and alters the result-

ing distribution of partial atomic charges. Although we cannot guarantee that our chosen method is accurate, the current method and basis set are proven based on their use in past work from the simulation community [146, 273].

We optimized molecules using the B3LYP hybrid functional with the 6-311++G** basis set using Gaussian16 [99]. This basis set is chosen to incorporate both polarization (++) and diffuse functions (**). Polarization captures electronic shifts when atoms approach each other. Diffuse functions capture the behavior of loosely held electrons, such as those in the valence shell of a large atom or an anion. Diffuse functions are critically important to capturing the correct geometry and partial charge distribution of anions.

Calculation time in quantum chemistry scales quickly with an increasing number of atoms, so it is important to keep the atom-count low. But for polymer molecules, this means that one must choose a representative piece of the molecule, such as a monomer, to capture partial charge distribution. Several approaches have been taken in the works included in this thesis, including the use of monomers, dimers, and trimers for optimization and electrostatic mapping. The choice of polymer fragment was mostly based on monomer complexity, and it is our belief that a simple monomer representation often satisfies needs for speed and accuracy. The electrostatic potential should be mapped at Merz-Singh-Kollman points, with partial charges computed using Amber Antechamber (or similar) and scaled by 0.8, a scaling constant used in previous work to mimic charge transfer and capture average polarization effects [17, 283, 319, 320].

### 2.1.3 Simulation setup

Simulations can be prepared in a variety of ways, but we will briefly highlight our chosen methodology, which remained largely consistent throughout this project. Details that are unique to individual studies can be found in their respective chapter, while general aspects encompassing all studies can be found here. Using molecular topologies of each component species, we packed the requisite composition of molecules into a simulation box at a density of 0.01 g/cm$^3$ using PACKMOL, a free tool available to pack simulation boxes with molecule PDB files [206].

We utilized the LAMMPS software package for all molecular simulations [243]. The topology generated in PACKMOL was energy minimized via a steepest-decent and subsequent conjugate-gradient minimization, each with an energy tolerance of $1 \times 10^{-5}$. The resulting topology was fed to a series of initialization, minimization, and equilibration steps, which are study-specific, but are simply combinations of unique arrangements and simulation times for the same set of procedures. After testing different approaches, we have settled on the following as a reproducible method that requires minimal user-interference, and generally avoids thorny simulation crashes.

Since the box begins at low density, we must compress the contents of the box to a realistic density. The contents of the box are also initially frozen, so we must use some method to initialize particle velocities. This can be done using a method, such as "velocity create" in LAMMPS, which can initialize velocity in a uniform or Gaussian distribution, and even conserve linear and

angular momenta. However, this approach is particularly dangerous for our starting topology because initialization at the target temperature, followed by compression to the desired density will lead to a large positive departure from the intended temperature, and will likely lead to simulation failure due to high particle velocities. The above-mentioned method can be modified by using a gradual velocity (temperature) increase, but this option was not explored in the context of this project. Additionally, options exist within LAMMPS to force box-dimension changes, but none of these tools were explored for our purposes.

Instead, we elected to use the Langevin thermostat and Berendsen barostat to direct our system into a stable temperature/pressure configuration. The Langevin thermostat couples the emsemble temperature of explicit particles to that of an implicit solvent sink [261]. The methodology used in this case is similar to that employed in the context of dissipative particle dynamics, which is discussed in some detail in chapter 8. The force on a particle is determined by the sum of a conservative force, a frictional drag term proportional to the particle's velocity, and a random force related to the drag through the fluctuation-dissipation theorem. In LAMMPS, the "fix langevin" command uses uniform, not Gaussian, random numbers to determine the magnitude and direction of the random force, which improves algorithm speed [81]. The Berendsen barostat, "fix press/berendsen" in LAMMPS, is used to reset the pressure of the system by adjusting volume and atom positions, accordingly [15].

These two fixes do not perform time integration in LAMMPS, so they must be combined with a microcanonical integrator such as "fix nve" to integrate the equations of motion [63,65]. Specifically, the integrator that we chose was "nve/limit," which uses the same equations as "fix nve," but does not allow atoms to move further than a maximum distance in one timestep [64]. This approach prevented atoms in the simulation from traveling too fast, which often led to simulation failure. We perform this simulation from a starting temperature/pressure to an ending temperature/pressure with a 0.01 fs timestep at a rate of 0.1 K/fs. Both damping parameters are set to 100 fs, and atoms could move a maximum of 0.1 Å/timestep.

Simulations of this type were carried out without including long-range Coulombic forces. The particle-particle particle-mesh (PPPM) method, which we used for evaluating long-range electrostatic interactions, relies on a grid construction overlaying the simulation box. During periods of rapid volume change, the grid may not respond to changes in the box volume, causing simulation failure. Even in constant pressure ensembles at high temperature, box volume may change rapidly, leading to unpredictable PPPM failure.

Long-range electrostatic interactions were incorporated for equilibration and production simulations. Forces and positions were evaluated every 1.0 fs at a given temperature and 1.0 atm using a Nosé-Hoover thermostat and a Parinello-Rahman barostat [207, 238, 279, 296, 314]. LJ and Coulombic pair energies were evaluated using equation 2.3 up to a 10 Å cutoff. Long-range LJ interactions were included with a Van der Waals tail correction. Coulombic

interactions beyond the direct-evaluation cutoff were incorporated using the PPPM solver with a tolerance of $1 \times 10^{-5}$ [131, 244]. A more rigorous tolerance, while desired for electrostatic accuracy, must be balanced with the speed of the simulation. We recommend the use of a tolerance of $1 \times 10^{-6}$ if one's computational resources allow for its practical application.

## 2.2 Analysis methods

### 2.2.1 Diffusivity and conductivity

Diffusivity is computed from the mean-squared displacement via the Einstein relation,

$$D = \lim_{t \to \infty} \frac{1}{6t} \left\langle \big(\mathbf{r}(t) - \mathbf{r}(0)\big)^2 \right\rangle. \tag{2.4}$$

When computing diffusivity from a simulation of finite time, a good approximation of the true diffusivity can be found by fitting a representative time range to a power-law fit,

$$\left\langle \big(\mathbf{r}(t) - \mathbf{r}(0)\big)^2 \right\rangle = Ct^{\beta}, \tag{2.5}$$

and if the parameter $\beta$ is close to unity, then the apparent diffusivity is calculated from

$$D_{apparent} = \frac{1}{6}C. \tag{2.6}$$

Obviously, this analysis relies on $\beta = 1.0$, so $\beta$ is a good indicator of the fitness of the data. If the species of interest has not reached $\beta = 1.0$, then it has not reached the diffusive regime, and diffusivity cannot be extracted.

While diffusivity is effective for quantifying ion mobility, conductivity is a more important feature for designing materials for electrochemical devices. The Nerst-Einstein conductivity ($\sigma_{NE}$), given by

$$\sigma_{NE} = \frac{N_{pair}}{V k_B T}\left(q_+^2 D_+ + q_-^2 D_-\right) \tag{2.7}$$

for a bicomponent ionic system, is sometimes used in computational studies due to the ease of computing diffusivity, as discussed above. The ideal conductivity is particularly useful in polymerized ionic liquids since the polymerized ion has limited mobility. This means that, effectively, $D_+ \approx 0$ for a polymerized cation. There is still some debate over this, given that ions of the same charge can move in a correlated or anti-correlated manner, impacting the value of conductivity.

For systems where self-diffusivity alone does not control conductivity, the dc conductivity captures the effect of correlated motion, which can reduce or improve conductivity.

$$\sigma_{dc} = \lim_{t\to\infty} \frac{e^2}{6tVk_BT} \sum_{ij}^{N} z_i z_j \Big\langle \big[r_i(t) - r_i(0)\big]\big[r_j(t) - r_j(0)\big] \Big\rangle. \tag{2.8}$$

We extracted the slope of the long-time average to obtain the dc conductivity. Due to significant fluctuations at large $t$, we are typically forced to discard time scales of greater than 50% of simulation times. In addition, to quantify the uncertainty inherent in our approach, we chose to represent the ultimate conductivity as the average of a series of linear fits on distinct data ranges from 0-50% of the simulation time. This average value, and its associated standard deviation, provided the reported results for $\sigma_{dc}$ and the associated error bars.

### 2.2.2 Structure functions

Local coordination behavior is succinctly captured in the radial distribution function,

$$g(r) = \frac{\rho(r)}{\rho_0}, \tag{2.9}$$

where $\rho(r)$ denotes the local density of components in a thin spherical shell a distance $r$ from a reference particle. The value $\rho_0$ is the theoretical density of the shell given a uniform density of subject particles. Sets of particles with short-distance coordination patterns yield a naturally defined cutoff distance, which can be used to establish the coordination of ionic groups.

While radial distributions are not obtained naturally from experimental methods, structure factors are available from a number of scattering analyses. X-ray scattering is a useful way to probe coordination distances at atomic resolutions. For comparison with these results, we developed a structure factor from density-normalized radial distribution functions using a Fourier transform method reported by Frischknecht and Winey [100],

$$S(q) = \sum_i c_i f_i^2 + 4\pi\rho \int_0^\infty dr w(r) \frac{\sin(qr)}{qr} r^2 \sum_{i,j} c_i c_j f_i f_j \Big( g(r) - 1 \Big). \tag{2.10}$$

The revised Lorch window function,

$$w(r) = \frac{3}{(2\pi r/L)^3} \left[ \sin(2\pi r/L) - \frac{2\pi r}{L} \cos(2\pi r/L) \right], \tag{2.11}$$

"was used to remedy the cutoff ripple artifact due to the Fourier transform" [100]. Equation 2.10 contains summations over the atom indices of species sets or subsets $i$ and $j$, which can be different or the same. Here, $c_i$ refers to

the mole fraction of species set $i$, and $f_i$ is the atomic scattering function for species $i$,

$$f_i(q) = \alpha_i + \sum_{k=1}^{4} a_{ik} \exp\big( - b_{ik}(q/4\pi)^2\big). \tag{2.12}$$

We used atomic-scattering function coefficients $a_{ik}$, $b_{ik}$, and $\alpha_i$ by Brown et al. to ensure accurate modeling of low-frequency scattering intensities [40]. One has to ensure that the frequency $q$ is properly normalized as $2\pi/L$, where $L$ is the length of a side of the simulation box. This approach assumes that the simulation box is cubic and the material is isotropic, meaning that the interactions are not expected to vary depending on the orientation of the wavevector.

### 2.2.3 Ion-association analysis

In dense ionic systems, such the ionic liquids, polymerized ionic liquids, and polymerized zwitterions explored in this project, we often seek to characterize the association behavior of ionic species or intra-molecule atom groups. The purpose of this section is to introduce the reader to the mathematical language used to identify sets of atoms, molecules, or groups that participate in coordination relationships.

While condensing a group of atoms into a center-of-mass for association analysis is a viable approach, there are several disadvantages that made me seek alternative means. First, calculating a center-of-mass can be challenging from a simple programming standpoint. Much of the work in this project was done using basic Fortran programs, and evaluating centers of mass on the fly

was difficult. Second, for some asymmetric and non-spherical molecules, the center-of-mass can be found outside of the molecule boundaries, potentially leading to overlap with other molecules' centers-of-mass. Third, this approach can lead to interaction-smearing phenomena, whereby coordination distances increase and first-coordination shells blur since the real association sites are irrelevant. In some cases, this may even cause misleading conclusions regarding the true association state of two species. Finally, and closely related to the last point, this approach makes it difficult to reliably compare chemically distinct systems due to fundamental differences in close-range association behavior. For an excellent example, we refer the reader the chapter 5, where we evaluate the counterion effect.

MDAnalysis is a python-based molecular-dynamics toolset, which contains trajectory readers and writers, coordinate manipulators, and many other useful tools for analyzing molecular dynamics trajectories [110, 212]. While it does contain a center-of-mass module, we still feel that this is not the best approach. It is much easier to evaluate distances between atoms using the fast distance array tools of MDAnalysis. Usually, an ionic center can be approximated as a single atom for this purpose. While this approach is easier than computing centers-of-mass for every component, it still suffers from the latter two drawbacks mentioned earlier. Namely, reliance on a single association "site" can produce smeared and sometimes misleading results.

We can instead utilize direct atomic correlations as the basis for all association analysis. This solution brings us closest to realizing the physi-

cally relevant basis of association behavior. Consider a subset of unique atom identifiers in $\mathrm{A} = \{a \in \mathbb{Z} \mid 1 \leq a \leq N_a\}$, where $N_a$ is the total number of atoms, consisting of only desired atom types, such as the oxygen from bistrifluoromethane-sulfonylimide ($\mathrm{TFSI}^-$) , $a_T = \mathrm{O_F}$,

$$\mathrm{A_T} \subseteq \mathrm{A} \mid a_T(a) \equiv \mathrm{O_F} \ \forall a \in \mathrm{A_T}. \tag{2.13}$$

We can designate a set $h(t)$ of association pairs $p = (a_1, a_2)$ at time $t$ such that the distance between each pair $r_{a_1,a_2}$ is less than or equal to a cutoff distance $r_{cut}$,

$$h_a(t) = \{p \mid a_1 \in \mathrm{A_{T,1}} \text{ and } a_2 \in \mathrm{A_{T,2}} \text{ and } r_{a_1,a_2} \leq r_{cut}\}. \tag{2.14}$$

The curly braces denote set notation. The components $p$ of the set from equation 2.14 are all inherently unique, but set notation ensures that a grouping that contains duplicate entries are winnowed down to only unique elements.

For ionic units that consist of a whole molecule, such as $\mathrm{Li}^+$ and $\mathrm{TFSI}^-$, we can then determine a unique set of whole-ion interactions. This is done using the system topology, which includes explicit molecule identifiers $m(a_i)$, revealing a set of molecule-association pairs $p_m = (m(\pi_1(p)), m(\pi_2(p)))$,

$$h_m(t) = \{p_m \ \forall p \in h_a(t)\}, \tag{2.15}$$

where $\pi_1(p)$ and $\pi_2(p)$ are the left- and right-projection of atom pair $p$. Remember that set notation implicitly reduces any number of non-unique interactions to a single unique instance.

Molecule assignments are too granular to maximize utility for polymerized ionic liquids or zwitterions. Often, we must identify ionic groups from different monomers, or even parts of monomers, as is the case for polymerized zwitterions. Unfortunately, there is no robust method for identifying these fragments. The user must be familiar with the simulation topology, using their underlying knowledge to manually or algorithmically identify the appropriate subsets of atoms belonging to each unit, $u(a_i)$. Then, similar to the molecule-association approach from equation 2.15, we can develop a set of unit-association pairs $p_u = (u(\pi_1(p)), u(\pi_2(p)))$,

$$h_u(t) = \{p_u \ \forall p \in h_a(t)\}. \tag{2.16}$$

The user can modify this construction, using combinations of $a_i$, $m(a_i)$, and $u(a_i)$ to maximize utility for a given application. We will now explore various analyses that utilize the coordination structure $h_a(t)$ and its variants from equations 2.15 and 2.16.

A set of ionic coordination states for $TFSI^-$ can be extracted from $h(t_0)$ (equation 2.14), where $\pi_1(p)$ and $\pi_2(p)$ represent the left ($TFSI^-$) and right ($Im^+$) indexes of pair $p$:

$$\begin{aligned} I(t_0) =&\{(i, |\{\pi_2(p) \ \mid \ \pi_1(p) \equiv i \ \forall \ p \in h(t_0)\}|) \\ &\mid \ \forall i \in \mathrm{I}\}. \end{aligned} \tag{2.17}$$

By manually assigning polymer identifiers $m(j)$ to the $Im^+$ index, we can recast the association set as

$$h_{\mathrm{poly}}(t_0) = \{(\pi_1(p), m(\pi_2(p)) \ \forall p \in h(t_0)\}. \tag{2.18}$$

This is an implicitly unique set of ion-polymer association pairs, which replaces $h(t_0)$ in equation 2.30 to yield a set of polymer association states $P(t_0)$ (in place of $I(t_0)$). The fraction of $TFSI^-$ coordinated with $N_I$ $Im^+$ at temperature $T$, averaged over $TFSI^-$ and time ($N_{\text{frames}}$) is

$$f_I(N_I, T) = \frac{\sum_{t_0} \mid \{\pi_1(p) \mid \pi_2(p) \equiv N_I \ \forall \ p \in I(t_0)\} \mid}{N_{\text{TFSI}} N_{\text{frames}}}. \tag{2.19}$$

A similar result is resolved for the simulation-averaged fraction of $TFSI^-$ associated with $N_P$ polymers, $f_P(N_P, T)$. The intrapolymeric ionic coordination number $N_{IP}$ is a related quantity that counts the number of $Im^+$ from a given polymer that are associated with a $TFSI^-$. Its distribution $f_{IP}$ is derived from $I_P(t_0)$, a set of triplets $q$ that includes the $TFSI^-$index $i$, the molecule identifier $M$, and $N_{IP}$ as shown here

$$\begin{aligned} I_P(t_0) = &\{(i, M, |\{\pi_2(p) \ \mid \ \pi_1(p) \equiv i \text{ and} \\ &m(\pi_2(p)) \equiv M \ \forall \ p \in h(t_0)\}|) \ \mid \ \forall i \in \mathrm{I}\}. \end{aligned} \tag{2.20}$$

The normalization factor is the sum of $|h_{poly}(t_0)|$ over time,

$$\begin{aligned} &f_{IP}(N_{IP}, T) = \\ &\frac{\sum_{t_0} \mid \{(\pi_1(q), \pi_2(q)) \mid \pi_3(q) \equiv N_{IP} \ \forall \ q \in I_P(t_0)\} \mid}{\sum_{t_0} |h_{poly}(t_0)|}. \end{aligned} \tag{2.21}$$

### 2.2.4 Association-relaxation functions

The intermittent ion-association autocorrelation function $C(t)$ represents the probability that two ions, which were associated at time $t = t_0$, are still associated at time $t$. To craft this function, we begin by defining the intersection of two association states for configurations $t_0$ and $t_0 + t$,

$$c_i(t_0, t) = h_i(t_0) \cap h_i(t_0 + t), \tag{2.22}$$

which captures their shared association pairs for $i = a$ or $m$ or $u$. The autocorrelation function is then defined as the fraction of remaining ion pairs, averaged over starting time $t_0$,

$$C_i(t) = \left\langle \frac{|c_i(t_0, t)|}{|h_i(t_0)|} \right\rangle_{t_0}. \tag{2.23}$$

The bracketing vertical bars represent the notation for "cardinality," similar to the magnitude of a vector. In this case, a mathematical set has a given number of elements, which equals its cardinality.

In a slightly different construction, the continuous ion-association autocorrelation function represents the probability that two ions, which are associated at time $t_0$, *remain* associated until time $t_0+t$. The association-intersection over all timesteps $\mathrm{T}(0, t) = \{0...t\}$,

$$s_i(t_0, t) = \bigcap_{\tau \in \mathrm{T}} h_i(t_0 + \tau). \tag{2.24}$$

Similarly, the autocorrelation function is defined as the fraction of remaining ions,

$$S_i(t) = \left\langle \frac{|s_i(t_0, t)|}{|h_i(t_0)|} \right\rangle_{t_0}. \tag{2.25}$$

Both functions, $C(t)$ and $S(t)$ can be fit to a stretched exponential function, for example:

$$C_i(t) = \exp\left( -\left(\frac{t}{\alpha_1}\right)^{\alpha_2} \right), \tag{2.26}$$

whose characteristic timescale of decay is computed as

$$\tau_{C,i} = \alpha_1 \Gamma\left(1 + \frac{1}{\alpha_2}\right). \tag{2.27}$$

The value $\tau_{C,i}$ is henceforth referred to as the average association structural relaxation time. The value $\tau_{S,i}$ is known as the average lifetime of an association pair.

These previous constructions have found application in different studies contained within this project, and have thus been valuable tools for analyzing ion transport phenomena. However, these two measures do have shortcomings. Because these measures compute average *pair* association lifetimes, one can miss critical information on the behavior of individual ions, especially in highly diverse coordination environments and when there are multiple associating species present. Furthermore, behaviors reliant on a collection of long-time association pairs can be lost due to the downward pressure on relaxation time of short-lived association pairs. The so-called "cage" relaxation analysis technique can address the myriad of challenges related to these pitfalls.

Association sets provide the building blocks for analyzing ion-on-ion caging effects. For example, consider three ionic species with unique integer identifiers: central ion $i$ and caging ions $j$ and $k$. These integers uniquely identify various molecules or units, as discussed previously. There exist association pairs of these species $p_1 = [i, j]$ and $p_2 = [i, k]$ with respective sets $h_1(t) = \{p_1 \mid r_{i,j} \leq r_{cut}\}$ and $h_2(t) = \{p_2 \mid r_{i,k} \leq r_{cut}\}$. The latter association sets can be developed using the methodology of equations 2.13-2.16, but the notation shown here is designed to clarify the correct order for identifiers in each pair structure. The central atom appears in the first projection, $\pi_1$ of each pair, while the caging ion appears in the second projection, $\pi_2$.

For some systems or analyses, an instantaneous snapshot of the association states, $h_1(t_0)$ and $h_2(t_0)$ is sufficient to capture the initial cage structure. In other words, the union of these two association sets initializes the cage environment,

$$h_{cage}(t_0) = h_1(t_0) \cup h_2(t_0) \tag{2.28}$$

In other cases, which perhaps exhibit weak interactions and fast dissociation relaxation rates, it will be necessary to capture the union of a series of consecutive association states to fully initialize the cage structure. Picking $n$ consecutive timesteps, $\mathrm{T} = \{0, 1...n-1\} \times \Delta t$, ensures that low-residence-time pairs, which play a relevant role as physical barriers of motion, are included in cage-classification. The union of association sets, $h_{cage}(t)$, over T,

$$c_{cage}(t_0) = \bigcup_{\tau \in \mathrm{T}} h_{cage}(t_0 + \tau) \tag{2.29}$$

captures a set of relevant pairs for the starting cage profile. Now, rather than quantifying simply the size of this set, it is important to capture the number of unique elements $j$ and $k$ in the second projection of each pair containing $i$ in the first projection,

$$\forall p \in c_{cage}(t_0),\ I(i, t_0) = \{\pi_2(p) \ \mid \ \pi_1(p) \equiv i\}. \tag{2.30}$$

We can then probe structural decay, or relaxation of the cage over time,

$$\mathfrak{I}(i, t_0, t) = I(i, t_0) \cap h_{cage}(t_0 + t), \tag{2.31}$$

to determine how many ions remain associated after $t$.

Once again, the fraction of ions is important, but we avoid quantifying an average of explicit fractional associations. Instead, we define a cutoff fractional association state $f_{cut}$, indicating when a cage is structurally relaxed, and set the cage state,

$$\mathfrak{I}(i,t_0,t) = \begin{cases} 1, & |\mathcal{I}(i,t_0,t)|/|I(i,t_0)| \geq f_{cut} \\ 0, & \text{otherwise.} \end{cases} \tag{2.32}$$

Finally, using the set of first-projection identifiers $\forall p \in c_{cage}(t_0),\ P(t_0) = \{\pi_1(p)\}$, we construct the intermittent cage relaxation function,

$$C_{cage}(t) = \left\langle \frac{\sum_i \mathfrak{I}(i,t_0,t)}{|P(t_0)|} \right\rangle_{t_0}. \tag{2.33}$$

This function can be fit using the stretched exponential formula of equation 2.26, and the cage relaxation time $\tau_{cage}$ can be extracted using equation 2.27. If $f_{cut} = 0$, $\tau_{cage}$ reveals the relaxation time of the longest-lasting cage pair, which we have found useful in characterizing vehicular transport of small ions. The physical meaning of $\tau_{cage}$ varies as $f_{cut}$ increases, but a range of values can generally be understood to mean the relaxation of cages to certain, specified count. For example, if $f_{cut} = 1/3$, then a cage initially containing four ions would have to lose coordination with three ions to be considered relaxed. As we will explore in chapter 7 on polymerized zwitterions, such measures can be useful for evaluating the underlying timescale of diffusion in materials where ions experience varying coordination environments.

### 2.2.5 Hopping analysis

In a 2017 study from our group [217], dynamical changes in the coordination states of ions were used as a means to identify the ion transport mechanisms in pure ionic liquids and polymerized ionic liquids. We continue such a line of investigation in this project, adopting the same definition of such an event, viz., the association or dissociation of a pair of ions over a specified time interval, always of 1 ps for our needs. In works directly encompassed by this project, we updated the two categories of hopping events, intra- and intermolecular, to reflect a new paradigm of the static coordination state of the ion in the *dissociated* frame [148]. Namely, in an intramolecular hopping event (type 1), ions move from monomer to monomer along the same polymer. To define this precisely, during the association or dissociation of a given $PF_6^-$-$Im^+$ pair, if one or more $Im^+$ from the same polymer as the participating $Im^+$ are associated with the $PF_6^-$ when the pair is *dissociated*, then the event is type 1. In contrast, for intermolecular hopping events (type 2), ion hopping occurs between different polymers. Again, to define this precisely, given an association or dissociation event involving a $PF_6^-$-$Im^+$ pair, if no other $Im^+$ from the same chain are associated with the $PF_6^-$ when the pair is *dissociated*, then the event is type 2.

To describe the above mathematically, we collect ionic or polymer associations that exist at time $t_0 \pm \Delta t$ (trajectory timestep $\Delta t$) and not at time $t_0$ using forward (+) and reverse (-) difference sets for $TFSI^-$ associated with a) $Im^+$, $\delta_I^{\pm} = h(t_0 \pm \Delta t) - h(t_0)$, and b) polymers, $\delta_P^{\pm} = h_{\text{poly}}(t_0 \pm \Delta t) - h_{\text{poly}}(t_0)$,

where $h_{poly}$ is defined in section 2.2.3. This enables acquisition of total type 2 hopping events via the summation of polymer-difference-set cardinalities over time

$$h_2 = \sum_{t_0} |\delta_P^+(t_0)| + |\delta_P^-(t_0)|. \tag{2.34}$$

The balance of hopping events reveals the total type 1 hopping events

$$h_1 = \left( \sum_{t_0} |\delta_I^+(t_0)| + |\delta_I^-(t_0)| \right) - h_2. \tag{2.35}$$

The values $h_1$ and $h_2$ are full-simulation totals, which can be normalized by $TFSI^-$ and/or an arbitrary timescale, to represent a hopping frequency, as was done in past studies [147, 217].

Figure 2.1, borrowed from the supporting information of reference 148, illustrates both categories of hopping events. These diagrams do not exhaustively define type 1 or type 2 events, but serve to illustrate the definitions. In Figure 2.1(a), polymer 1 in the left frame has three $Im^+$ associated with the $PF_6^-$ ion, evolving to a state in the right frame with two associated $Im^+$. As indicated by the dotted arrow, this is a type 1 *dissociation* event. The reverse, indicated by the solid arrow, is a type 1 *association* event. For both cases, in the frame where the ion pair in question is *dissociated* (right), at least one other $Im^+$ from the same chain is associated, indicating that the event is type 1. Figure 2.1(b) shows polymer 3 in the left frame with one $Im^+$ associated with the $PF_6^-$ ion, evolving to a state in the right frame where it has no $Im^+$ associated with the given $PF_6^-$. The dotted line represents a type 2 *dissociation* event, while the solid line depicts a type 2 *association* event. As

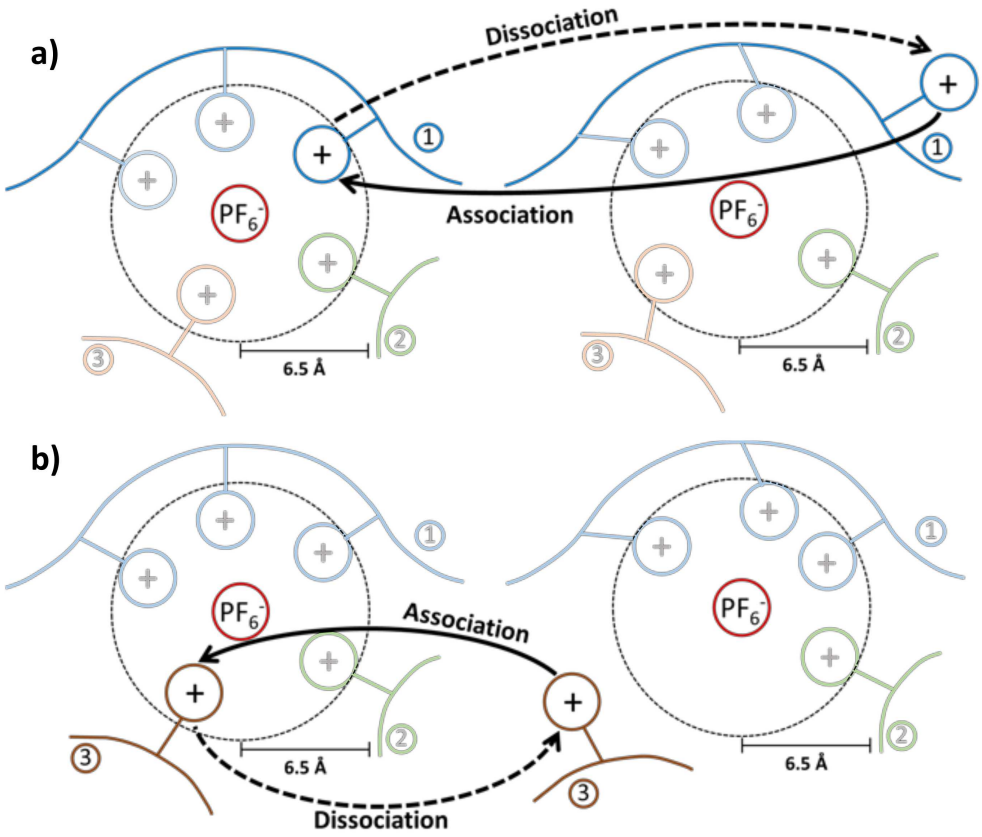


Figure 2.1: Diagrams depicting examples of (a) intramolecular (type 1) and (b) intermolecular (type 2) hopping events. Reprinted with permission from reference 148. Copyright 2017, reproduced by permission of the PCCP Owner Societies.

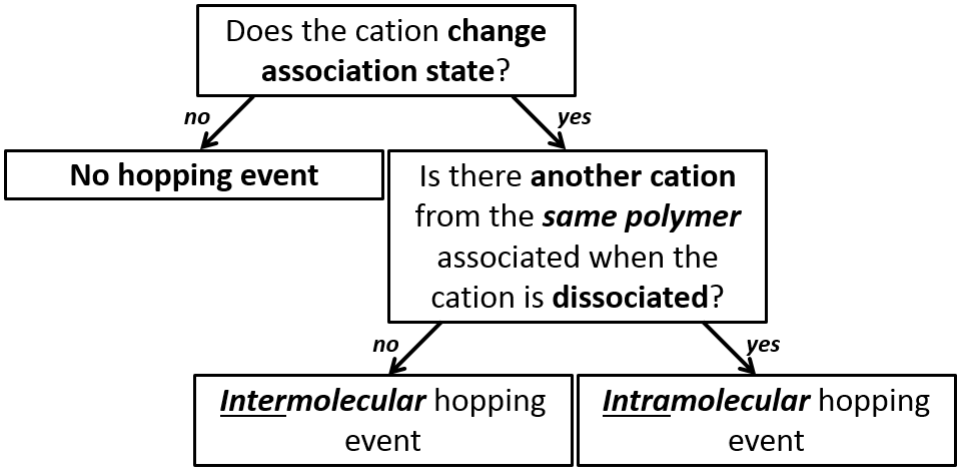


Figure 2.2: Flowchart depicting the logic sequence for defining and categorizing a hopping event. Reprinted with permission from reference 148. Copyright 2017, reproduced by permission of the PCCP Owner Societies.

in the previously example, and by definition, these are type 2 events because polymer 3 is not associated with the $PF_6^-$ ion when the $PF_6^-$ and $Im^+$ pair undergoing the event are not associated.

The following path of inquiry may help the reader understand the definition of a hopping event:

1. Was there a change in association state between a cation and an ion?

2. Were there any other associated cations with that ion from the same chain in the *dissociated* frame?

If the answer to the second question is "yes," then the hopping event is categorized as an *intramolecular* event. Otherwise, the hopping event is identified

as an *intermolecular* event. The dissociated frame can be found on the right for both examples in Figure 2.1. This logic flow is represented in Figure 2.2 to assist the reader in understanding the method.

Accounting for these events requires a cation-centered viewpoint. Every time a cation associates or dissociates from an ion, an intra- or intermolecular hopping event occurs. This means that multiple events can occur surrounding the same ion. By following this observation further, we know that intra- and intermolecular hopping events can occur on the same ion simultaneously. For clarity, we now reference two specific situations that will not likely be representative of the data collected, but must be addressed. First, if a monomer that is associated with an ion alone (or among cations from other polymers) dissociates at the exact moment that another monomer from the same polymer associates, then both of these events (the dissociation of the first and the association of the second) are considered *intramolecular* hopping events. Second, if two monomers from the same polymer associate or dissociate simultaneously from an ion that was not associated with said polymer, both events are considered *intermolecular*. In both cases, we feel that the resulting categorization is consistent with our intent.

# Chapter 3

# Probing mechanistic differences in ionic liquids and polymerized ionic liquids by varying the number of repeat units

## 3.1 Introduction

Polymerized ionic liquids have been explored as new materials for versatile solid polymer electrolytes since the pioneering experiments of Ohno and Ito [202, 230, 232, 289, 303].[1] Although experimental results have shown that polymerized ionic liquids exhibit lower conductivity compared to their non-polymerized counterparts [9, 56, 61, 87, 231], research has persisted due to the promise of improved mechanical stability [2, 62, 180, 326] and reduced charge polarization [7, 140, 153, 177, 193, 197, 198, 204, 300] for battery electrolyte applications [38, 59, 61, 168, 169, 253, 311, 317, 341].

Ion motion in conventional salt-doped polymer electrolytes, such as polyethylene oxide and other materials, is strongly slaved to the polymer segmental relaxation dynamics [28, 29, 33, 77, 199, 200, 227]. Such a coupling be-

[1] Jordan R. Keith, Santosh Mogurampelly, Faisal Aldukhi, Bill K. Wheatle, and Venkat Ganesan. Influence of molecular weight on ion-transport properties of polymerized ionic liquids. *Phys. Chem. Chem. Phys.*, 19:29134, 2017. My contributions include designing and performing the research, contributing new analytic tools, analyzing data, and writing the article – Adapted by permission of the PCCP Owner Societies.

tween the conductivity and the mechanical properties has proven to be a significant hurdle for the optimization and design of mechanically strong, but highly conductive, polymer electrolytes. In recent experiments of Sokolov, Sangoro and coworkers, the coupling between the structural relaxation time and ionic conductivity was found to be similarly applicable for pure ionic liquids [255,257,352]. However, for polymerized ionic liquids, a decoupling, manifesting as a "super-ionic" dependence of the conductivity on the structural relaxation times was observed [86,256,333]. Explicitly, Fan et al. demonstrated that long polymerized ionic liquids have a higher conductivity than short ones and pure ionic liquids when compared at the same glass-transition-normalized temperature ($T/T_g$) [86]. Such experimental results have raised interest in polymerized ionic liquids as potential candidate materials to overcome the trade-off between mechanical strength and conductivity that plagues many polymer electrolytes. In turn, such observations have also raised fundamental questions on the mechanisms and time scales underlying ion transport in polymerized ionic liquids, along with the origin of differences in ion-transport phenomena within polymerized ionic liquids and pure ionic liquids.

Motivated by the above issues, in a 2017 communication, we reported the results of atomistic molecular dynamics simulations on the mechanisms underlying ion motion and diffusivities in a specific model system of poly(1-butyl-3-vinylimidazolium) hexafluorophosphate ($pBvIm^+$-$PF_6^-$) polymerized-ionic-liquid polyelectrolytes containing 32 repeat units [217]. There, we demonstrated that anion transport in polymerized ionic liquids occurs through a

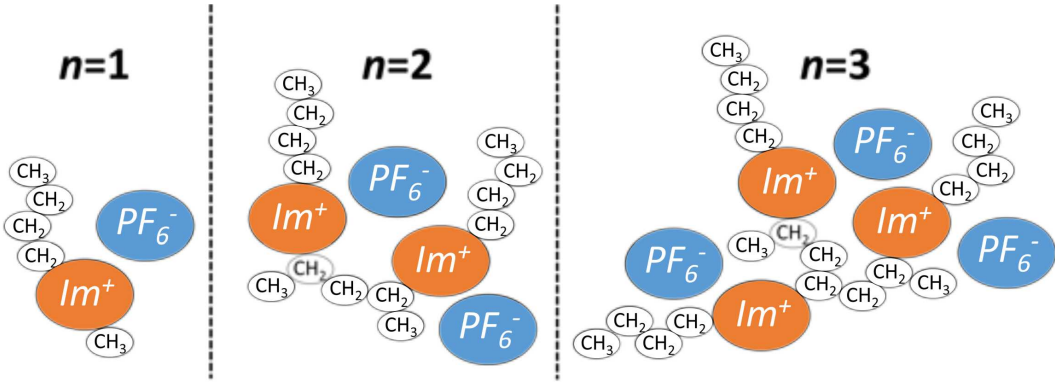


Figure 3.1: Chemical composition of molecules corresponding to $n = 1$, 2, and 3, where the imidazolium ring consists of resonance-stabilized carbon and nitrogen atoms. $n = 1$ corresponds to a pure ionic liquid, 1-butyl-3-methylimidazolium(BMIm)-$PF_6^-$, which was investigated in depth in our earlier study. [217] Polymers investigated in the present study contain $n$ butylimidazolium fragment bonded to repeating vinyl monomers, as shown for $n = 2$ and 3. Reference 147 – Reproduced by permission of the PCCP Owner Societies.

mechanism involving intra- and intermolecular ion hopping through the formation and breaking of ion associations involving four polymerized cationic monomers bonded to two different polymer chains. The resulting ion mobilities were shown to be directly correlated with the average lifetimes of ion associations. Moreover, such a trend was demonstrated to contrast with the behavior in pure ionic liquids, wherein ion motion is more closely correlated with structural relaxations of the surrounding medium.

In the present work, we expand upon the results of our 2017 communication by characterizing the ion-transport properties of $pBvIm^+$-$PF_6^-$ polymerized ionic liquids with varying numbers of repeat units, including pure and polymerized ionic liquids (Figure 3.1). [217] Consistent with corresponding ex-

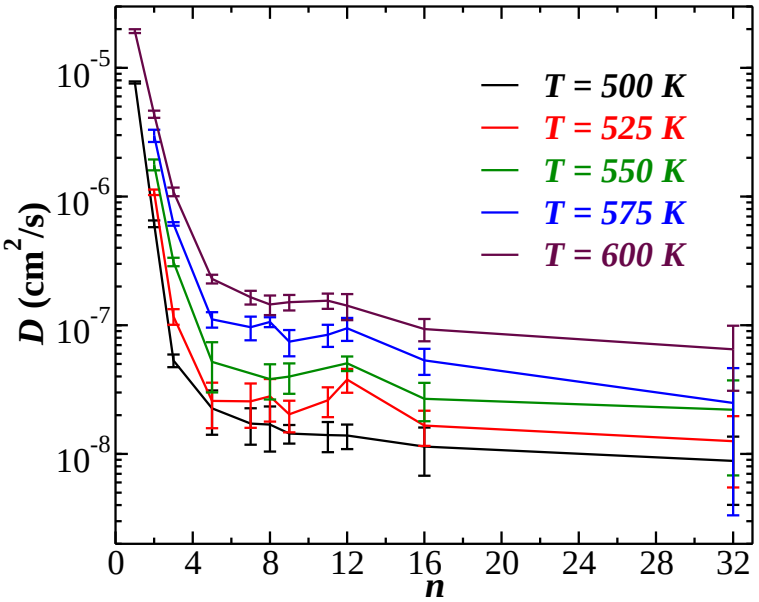


Figure 3.2: Diffusivity of $PF_6^-$ plotted versus the number of repeat units $n$. Reference 147 – Reproduced by permission of the PCCP Owner Societies.

perimental results, our simulations indicate that the ionic diffusivity decreases with increasing molecular weight and plateaus to an almost constant value for longer polymers. At the same time, ion motion is seen to become less correlated with structural relaxation times and more correlated with ion-association lifetimes. Additionally, we characterize ionic and polymer coordination and show that the ions move by a motion which resembles climbing a ladder with four polymeric cations from two different polymers.

## 3.2 Results

### 3.2.1 Ion self-diffusivity

Figure 3.2 shows data, borrowed from reference 147, depicting the trend for diffusivity of $PF_6^-$ with respect to the number of repeat units. It can be seen that the diffusivity drops dramatically when $n$ increases in the range of two to five monomers. However, the diffusivity changes are seen to become much less significant when $n$ increases from seven to 32 monomers. This data is qualitatively consistent with the findings of Fan and coworkers, who reported a similar drop in conductivity for polymerized ionic liquids of up to $n = 10$ [86]. For "long" polymers, lengthening the polymer appears to have less impact upon the transport properties, but what is the cause of this phenomenon?

### 3.2.2 Structural Relaxation Times

We characterized the structural relaxation times, $\tau_C$, as a first step towards probing the mechanisms underlying the decoupling between the ion mobilities and the mechanical properties of polymerized ionic liquids. In Figure 3.3 we display the results for $\tau_C^{-1}$ as a function of $n$ at different temperatures. The general trend of $\tau_C^{-1}$ is seen to resemble the behavior of the diffusivity, viz., increasing the temperature is seen to lower the relaxation times. The most significant changes are seen to occur in the range between two to five repeat units. Further increase in the number of repeat units is seen to result in a much more gradual increase in $\tau_C$.

In Figure 3.4(a), the ionic diffusivities $D$ for different polymerized ionic

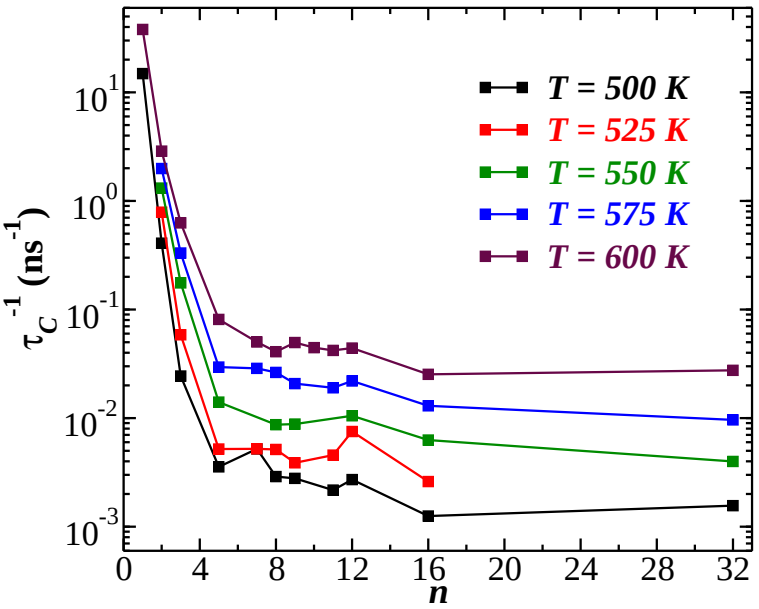


Figure 3.3: Ion-association structural relaxation frequency $\tau_C^{-1}$ as a function of $n$. Data for $n = 1$ and 32 taken from Reference 217. Reference 147 – Reproduced by permission of the PCCP Owner Societies.

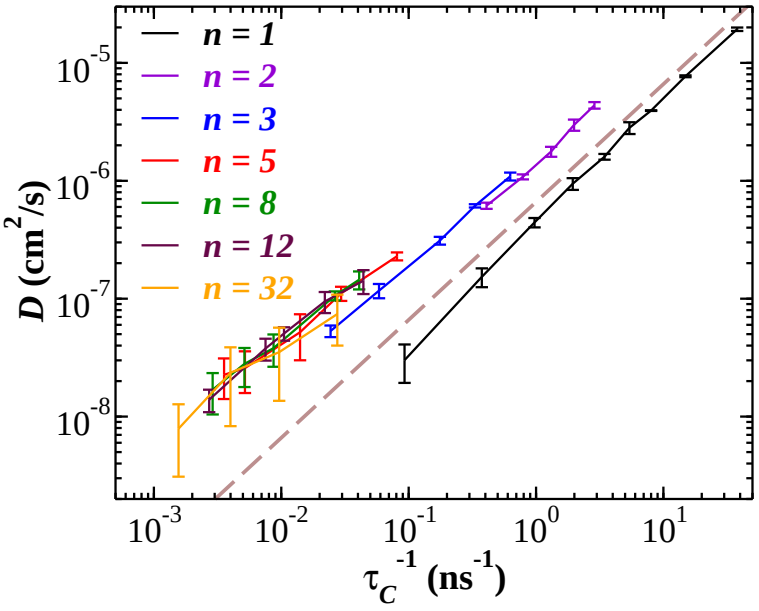


Figure 3.4: $D$ as a function of $\tau_C^{-1}$, demonstrating the "super-ionic" behavior of polymerized ionic liquids ($D \propto \tau_C^{-\alpha}$ with $\alpha < 1$) compared to "ionic" behavior exhibited by pure ionic liquids ($D \propto \tau_C^{-1}$). Reference 147 – Reproduced by permission of the PCCP Owner Societies.

liquids are shown explicitly as a function of the frequency of ion-association structural relaxation events, or $\tau_C^{-1}$. There is an excellent correlation between our results with the experimental results of Fan et al. [86]. Specifically, the ionic mobilities in ionic liquids are seen to exhibit an "ionic" behavior wherein $D \propto \tau_C^{-1}$. Such a result was also demonstrated more exhaustively in simulations by Zhang and Maginn by considering a variety of pure ionic liquids [352]. In contrast, the polymerized ionic liquids are seen to exhibit a "super-ionic" behavior $D \propto \tau_C^{-\alpha}$, in which $\alpha < 1$. While not readily apparent from the data points themselves, the exponents underlying the fit for polymerized ionic liquids were seen to transition from $\alpha \simeq 0.93$ for short polymers ($n = 2$) to $\alpha \simeq 0.75$ for longer polymers ($n = 16, 32$). This suggests that there is a gradual transition from the "ionic" behavior to "super-ionic" behavior with an increase in the number of repeat units.

This only leaves us to argue that the ion-association structural relaxation is a good measure of the "true" structural relaxation time, allowing us to reach conclusions regarding the decoupling behavior of these polymerized ionic liquid systems. Fortunately, in our earlier study, [217] by explicit comparison to decay of the intermediate scattering function $S(q, t)$, we demonstrated that the time scale extracted from the relaxation of ion associations, $\tau_C$, corresponds to the *true* structural relaxation time for the system. Furthermore, for both pure and polymerized ionic liquids, $\tau_C$ was found to follow a nearly universal dependence on the temperature normalized as $T/T_g$.

Based on such results and other examples in literature [55, 354], fig-

ure 3.4 confirms that the ionic mobilities of polymerized ionic liquids are indeed "decoupled" from the structural relaxation times in such systems. Such a decoupling is seen to manifest as a gradual transition from an "ionic" behavior of $D \propto \tau_C^{-1}$ for $n = 1$ to a "super-ionic" behavior of $D \propto \tau_C^{-\alpha}$ ($\alpha < 1$), for $n > 1$. However, for $n > 5$, the dependence of diffusivity on structural relaxation times is seen to approach almost universal behavior — a feature also consistent with the experimental observations. [86]

### 3.2.3 Mechanisms Underlying Ion Motion

In the preceding section, we presented results examining the correlation between diffusivity and structural relaxation times, and demonstrated a "decoupling" similar to that observed in experiments. In this section, we seek to identify the mechanisms underlying such a decoupling by characterizing different aspects of ion coordination and motion as a function of molecular weight in polymerized ionic liquids.

A number of prior studies of salt-doped polymer electrolytes, such as poly(ethylene-oxide), have concluded that ion diffusion in such systems occurs primarily through ion hopping *along* the polymer backbone [28,29,33,77,227]. In our earlier work, [216] we presented results which suggested the existence of a similar mechanism in polymerized ionic liquids, but with ion coordination characteristics reflecting electrostatics and chemical interactions specific to polymerized ionic liquids. Explicitly, for $n = 32$, we demonstrated that ion diffusion manifests from a hopping mechanism, with the most probable

coordination state of $PF_6^-$ involving *four* associated $Im^+$ from *two* distinct polymers. [216] For the present study, we analyzed the coordination states of $PF_6^-$ ions with $Im^+$ as a function of molecular weight to compare directly to these results, and also to understand the relationship between these configurations and the dynamics of ion hopping for varying polymer lengths.

In analyzing coordination states, we employed three key metrics: ionic, inter-polymeric, and intra-polymer ionic coordination numbers. The *ionic* coordination number $N_c$ identifies the number of $Im^+$ within a 6.5 Å cutoff of a given $PF_6^-$. The *polymer* coordination number refers to the number of polymers containing associated $Im^+$ monomers, which lie within the 6.5 Å cutoff of a given $PF_6^-$. Finally, the *intra-polymer ionic* coordination number $N_{cp}$ considers only the number of $Im^+$ monomers that are coordinated with a given $PF_6^-$, *from the same polymer*.

In Figure 3.5, the peak in the $N_c$ distribution is seen to occur at $N_c = 4$, matching the results presented in Mogurampelly et al. for a polymerized ionic liquid of 32 repeat units [216]. More interestingly, this result is seen to be invariant among different polymer lengths, suggesting that the high probability of coordination between an anion and four cations likely represents an inherent coordination feature of the anion and cation of the ionic liquids considered in this work.

Figure 3.6 displays the distribution of the number of distinct polymers, $N_p$, involved in the coordination between an anion and cations. From the peaks in the distributions, it can be deduced that the coordination state of

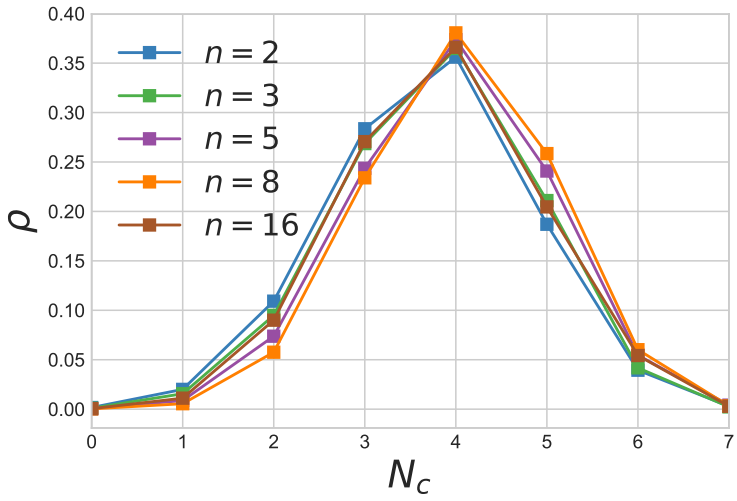


Figure 3.5: Probability distribution of *ionic* coordination states for various number of repeat units. Reference 147 – Reproduced by permission of the PCCP Owner Societies.

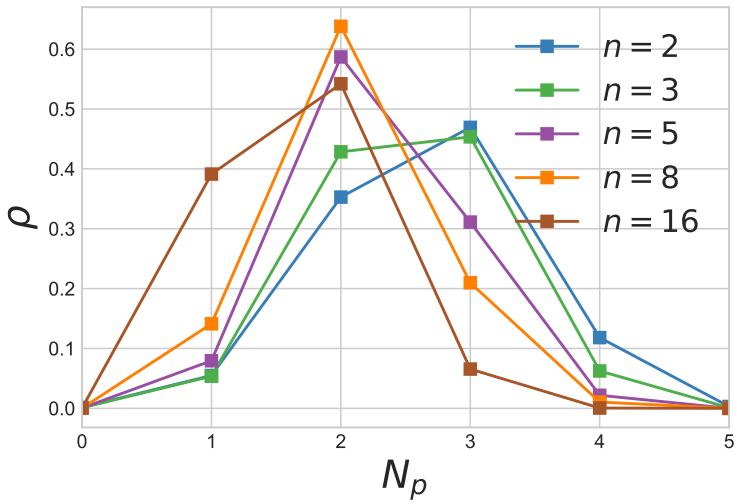


Figure 3.6: Probability distribution of *polymer* coordination states for various number of repeat units. Reference 147 – Reproduced by permission of the PCCP Owner Societies.

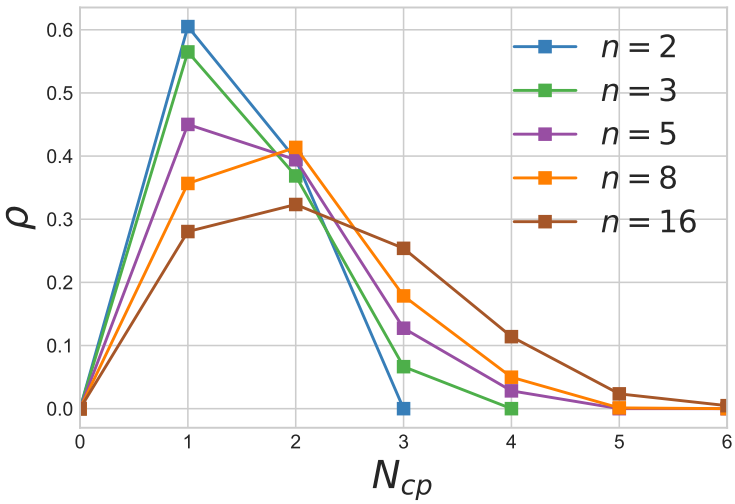


Figure 3.7: Probability distribution of *intra-polymer ionic* coordination states for various number of repeat units. Reference 147 – Reproduced by permission of the PCCP Owner Societies.

anions involve a larger number of polymers for short polymerized ionic liquids. In contrast, for long polymers, the most probable coordination state (the peak in the $N_p$ distribution) shifts to $N_p = 2$, and becomes invariant with the molecular weight of the polymerized ionic liquids for $n \gtrsim 5$.

Complementing these results, in Figure 3.7, we quantify the distribution of $N_{cp}$, representing the number of ionic associations with the same polymer molecule. For polymerized ionic liquids of seven or more repeat units, the peak of this distribution is seen to occur at $N_{cp} = 2$.

The discussion presented above relies primarily on the peak values of the equilibrium distributions and does not provide any insights into the influence of such coordination states on the ion mobilities. Moreover, it can be

seen that significant contributions also arise from other coordination states, such as $N_c = 3, 5$; $N_p = 1$ (particularly for long polymers); and $N_{cp} = 1, 3$ etc. A true understanding of the impact of such states on ion mobility requires a more detailed characterization of the diffusivity of ions with varying degrees of coordination. Since bulk diffusion occurs on a longer timescale than that which is characteristic of ionic association and dissociation, we could not effectively analyze the direct influence of discrete association states upon the ion self-diffusivity. As an alternative, the coordination states ($N_c$, $N_p$, and $N_{cp}$) for each $PF_6^-$ were averaged over the entire simulation and $PF_6^-$ with similar values were binned together. We then computed the diffusivity of each group of $PF_6^-$ using the mean-squared displacement for the corresponding binned ion group.

Figure 3.8 shows the trend for diffusivity versus average ionic coordination. It reveals that $PF_6^-$ diffusivity is optimized with an optimal average ionic configuration between *three* and *four* $Im^+$. This is a somewhat surprising result, as one might guess that a $PF_6^-$ that is associated with fewer ions would be faster moving. It is also interesting to note that this is true, regardless of the number of repeat units contained in the polymer.

Taken in aggregate, a pattern emerges in figure 3.9 whereby $PF_6^-$ diffusivity increases with increasing average polymer coordination number. We do see, within specific materials, that there is an optimal coordination number where diffusivity is maximized. This highlights the role of polymer length, itself, on diffusivity, manifesting as a higher diffusivity for smaller species, who

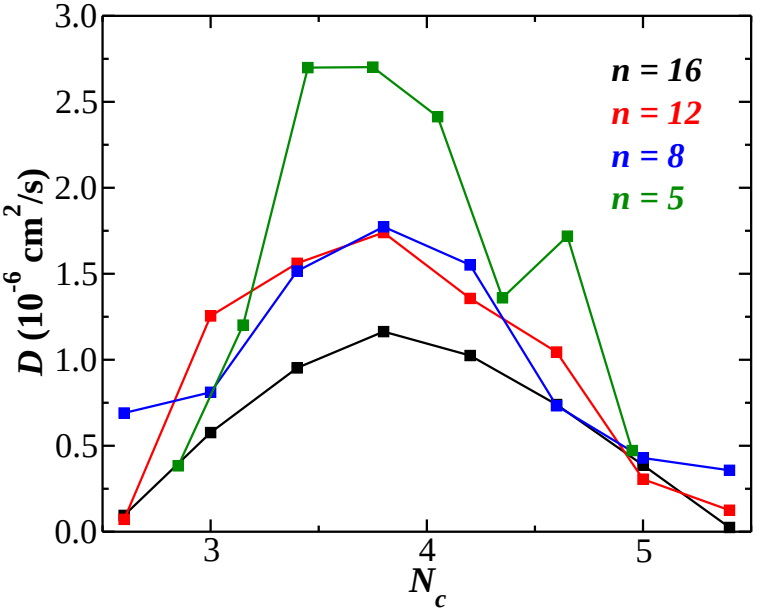


Figure 3.8: Diffusivity of groups of $PF_6^-$ ions that are coordinated with a similar number of *ions* across the entire simulation. Reference 147 – Reproduced by permission of the PCCP Owner Societies.

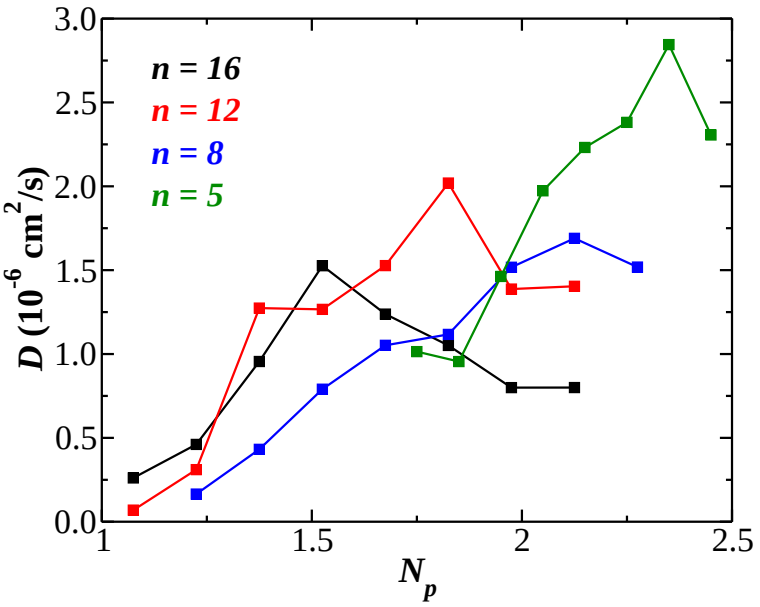


Figure 3.9: Diffusivity of groups of $PF_6^-$ ions that are coordinated with a similar number of *polymers* across the entire simulation. Reference 147 – Reproduced by permission of the PCCP Owner Societies.

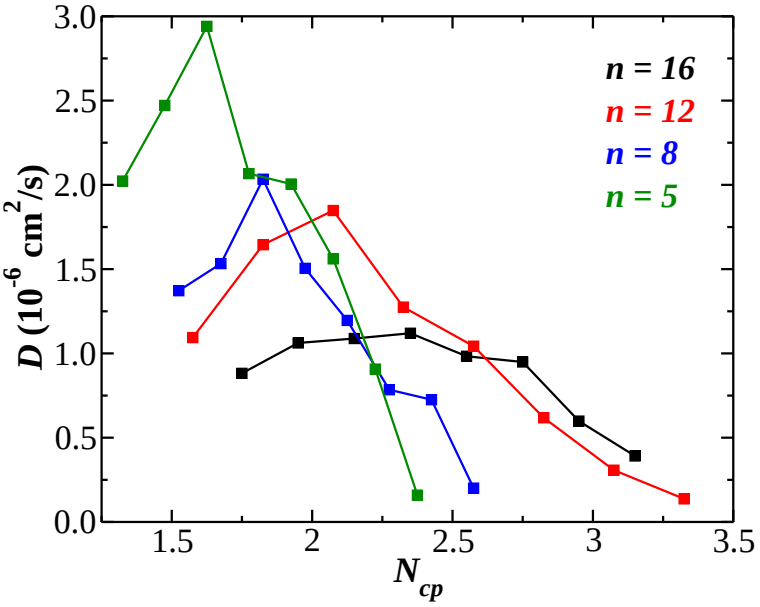


Figure 3.10: Diffusivity of groups of $PF_6^-$ ions that are coordinated with a similar number of *ions from the same polymer* across the entire simulation. Reference 147 – Reproduced by permission of the PCCP Owner Societies.

also tend to show increased polymer coordination. It is fair, however, to say that high-polymer-coordination environments favor higher conductivity than low-polymer-coordination environments for a given number of repeat units.

In the inverse manner, diffusivity generally decreases with increasing intra-polymer ionic coordination number, as shown in figure 3.10. Taken together, the results of Figures 3.5-3.10 demonstrate that, for longer polymerized ionic liquids, the state of $N_c = 4$, $N_p = 2$, and $N_{cp} = 2$ are the most likely to occur, and are effective at facilitating ion motion. For smaller polymerized ionic liquids, the peaks in the distribution of $N_{cp}$ are seen occur at smaller values, representative of the smaller population of intra-polymer $Im^+$ groups

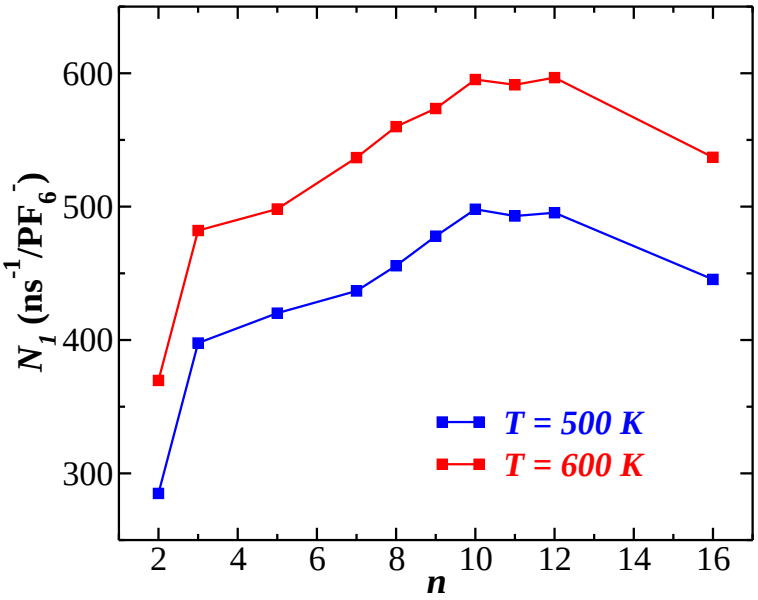


Figure 3.11: Frequency of type 1 hopping events, normalized by $PF_6^-$. Reference 147 – Reproduced by permission of the PCCP Owner Societies.

available for coordination.

As a final step in resolving the mechanisms underlying ion motion in polymerized ionic liquids, we quantified the different kinds of hopping motion underlying ion transport. Figure 3.11 shows that the frequency of type 1 hopping events generally increases with increasing number of repeat units. Considering that as the number of monomers increases, the probability distribution for intra-polymer ionic coordination shifts higher (see figure 3.7), there is no surprise embedded in this result. In an earlier work, we claimed that type 1 hopping played a dominant role in facilitating ion transport, i.e. around 99% of hopping events were categorized as intramolecular events. [217] This occurred as a result of the restrictive definition for intermolecular, type

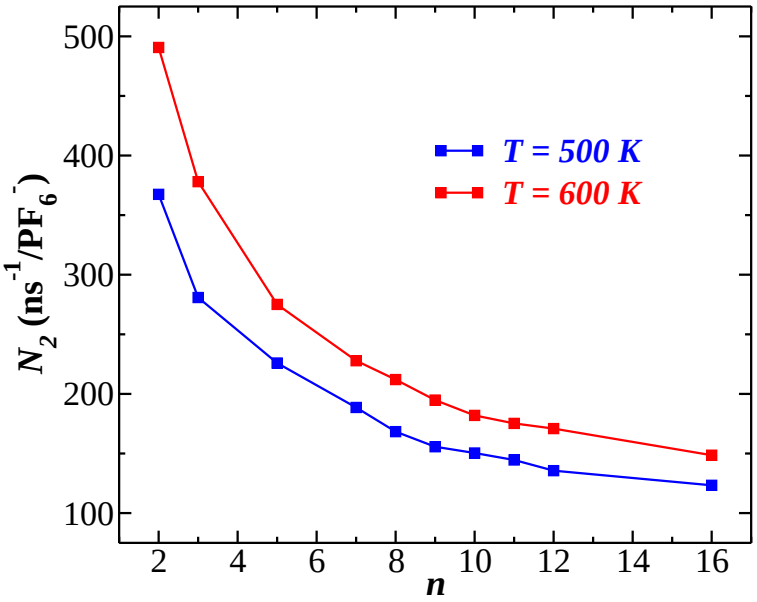


Figure 3.12: Frequency of type 2 hopping events, normalized by $PF_6^-$. Reference 147 – Reproduced by permission of the PCCP Owner Societies.

2, hopping.

Figure 3.12 reveals that with a more expansive, yet still faithful, definition for type 2 hopping, we have a higher fraction of hopping events categorized as type 2. More interestingly, there is a monotonic trend of decreasing type 2 hopping frequency with increasing number of repeat units. Once again, this fits intuitive expectations about ion transport in environments with systematically fewer polymers, decreasing the probability of an ion locating new molecules or vacating old ones. It is interesting to note that, even for higher monomer counts, we don't see any deviation from the trend, suggesting that this measure could be related to the trends observed in $PF_6^-$ diffusivity.

Taken together, the results of Figures 3.5-3.12 help us to formulate a

nanoscale understanding of ion motion in ionic liquids and polymerized ionic liquids. They also reveal the explicit differences in the mechanisms underlying these different materials. Specifically, ion motion in pBvIm$^+$-PF$_6^-$ polymerized ionic liquids involves a coordination state of *four* Im$^+$ from *two* different polymers, with *two* Im$^+$ belonging to each participating polymer. For smaller polymerized ionic liquids, higher and more variable polymer coordination numbers are seen, likely influenced by the more limited possibility for intramolecular coordination, in addition to the lower densities and higher free volumes in smaller linker systems. Complementary dynamic analysis demonstrated that ion motion in ionic liquids and small molecule polymerized ionic liquids involve mostly type 2 hopping between distinct polymers. In contrast, in long polymerized ionic liquids, ion motion primarily involves type 1 hopping, which preserves the identities of the associated polymers. The latter is akin to an ion motion which "climbs the ladder" between two polymer molecules via type 1 hopping along *two* associated polymers.

The above observations provide insights regarding the origin of decoupling between mobilities and structural relaxations observed in long polymerized ionic liquids. Explicitly, the observation that intermolecular hopping involving multiple polymer chains underlies ion motion in small molecule polymerized ionic liquids is consistent with the structural relaxation dynamics of the medium, i.e. of the polymer chains surrounding the associated ions, being of importance for such system [86, 352]. In contrast, for long molecule polymerized ionic liquids, intramolecular hopping involving identical polymer

chains were seen to play a role. For such motion, it can be envisioned that the structural relaxations of the surrounding medium are less important in influencing the ion motion.

For ion transport dominated by intramolecular hopping, the ion mobilities can be expected to be correlated more strongly to the average lifetimes of anion-cation associations instead of the structural relaxation times in such systems. Indeed, in our earlier work [217], for polymerized ionic liquids of $n = 32$, it was demonstrated that average ion-association lifetime, $\tau_S$, provides a better characterization of the timescales underlying ionic mobilities in polymerized ionic liquids. More explicitly, it was shown that the $D \propto \tau_S^{-1}$ (for $n = 32$) over the entire range of temperatures investigated therein. Below, we present the dependence of the average ion-association lifetimes on the number of repeat units to explicitly probe the transition of this correlation from short to long polymerized ionic liquids.

In Figure 3.13, we display the results for ion-dissociation relaxation frequency, $\tau_S^{-1}$ as a function of the number of repeat units. Broadly, the trends for $\tau_S^{-1}$ are seen to resemble the behaviors observed in the context of ionic diffusivity and the structural relaxation frequency. Specifically, in increasing the length of the polymerized ionic liquid, the most significant changes in $\tau_S^{-1}$ are seen to occur in the range between one to five repeat units, and further increase in monomer count is seen to result in a much a more gradual decrease in $\tau_S^{-1}$. Such results are not surprising, since systems in which the matrix exhibits faster dynamics are expected to facilitate more dissociation events.

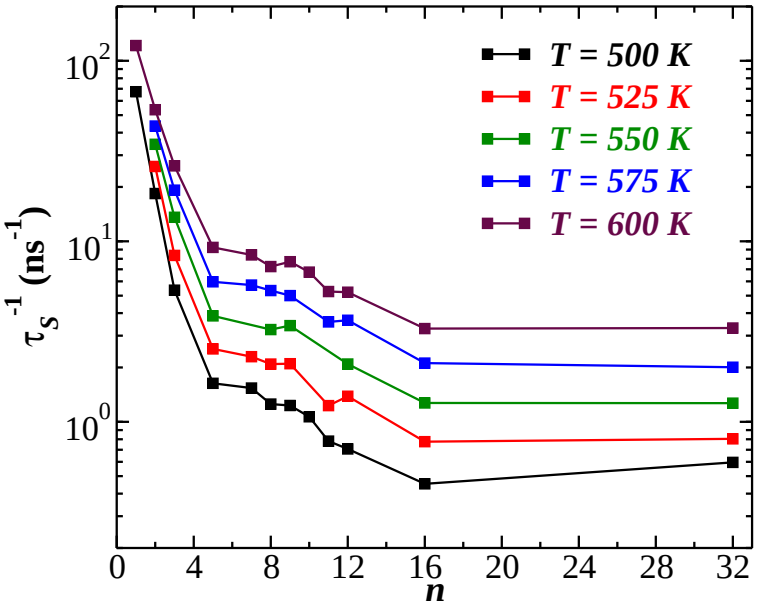


Figure 3.13: Ion-dissociation relaxation frequency $\tau_S^{-1}$ as a function of number of repeat units. Reference 147 – Reproduced by permission of the PCCP Owner Societies.

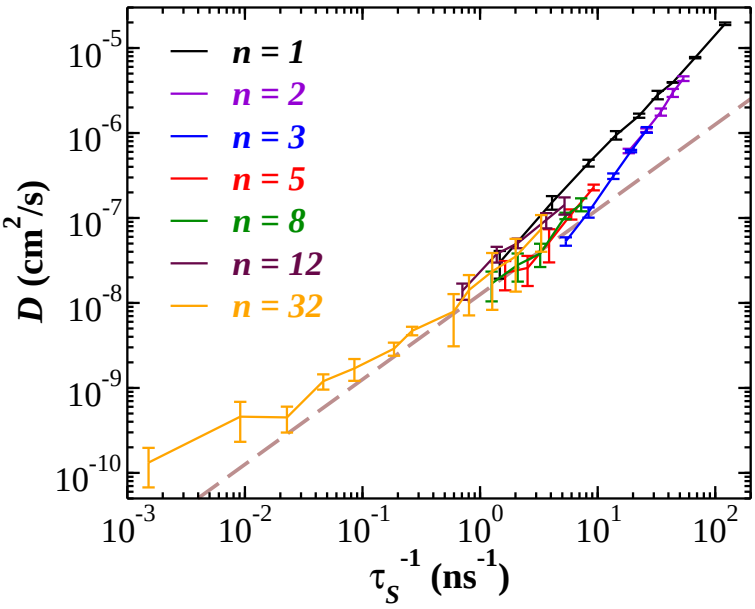


Figure 3.14: $PF_6^-$ diffusivity as a function of ion-dissociation relaxation frequency $\tau_S^{-1}$. Reference 147 – Reproduced by permission of the PCCP Owner Societies.

In Figure 3.14, we depict a quantitative comparison of the correlation between the diffusivities and ion-dissociation relaxation frequency, $\tau_S^{-1}$. Within the representation of $D \propto \tau_S^{-\beta}$, it is seen that $PF_6^-$ diffusivities indeed transition from $\beta > 1$ for short polymerized ionic liquids to $\beta \simeq 1$ for long polymerized ionic liquids. The non-monotonic trend in exponent between $n = 1$ and 3 may be due to a lower rate of back-reactions in pure-ionic-liquid systems compared with short polymerized-ionic-liquid systems. These results confirm the transition to intramolecular anion hopping as the dominant mode of ion transport in polymerized-ionic-liquid membranes, and identify the molecular mechanism underlying the decoupling of the ionic mobilities from structural relaxations.

## 3.3 Conclusions

In this chapter, we used atomistic molecular dynamics simulations to investigate $PF_6^-$ diffusion in poly(1-butyl-3-vinylimidazolium-$PF_6^-$) polymerized ionic liquids with varying number of repeat units. $PF_6^-$ diffusivity was observed to decrease with an increase in the length of the polymerized ionic liquid. For short polymerized ionic liquids, we observed consistency with previously reported linear relationships between diffusivity and structural relaxation time for pure ionic liquids [217, 255, 257, 352]. For longer polymerized ionic liquids, we observed deviations from such a linear relationship with a behavior mirroring experimental observations.

We explored the nature of ion hopping, and demonstrated that the

frequency of intramolecular (type 1) hopping events increases, and the frequency of intermolecular (type 2) hopping events decreases monotonically as the number of repeat units increase. This observation supports the traditional perspective of ion hopping within polymer-electrolyte and polymerized-ionic-liquid systems, which highlights the importance of ion hopping along a polymer backbone in diffusion processes. Analysis of coordination states suggested that the highest mobility ions move via a "ladder mechanism," involving *two* polymers, each with one, two, or three $Im^+$ ions associating with a given $PF_6^-$. In support of such a mechanism, the $PF_6^-$ diffusivity was seen to transition to an inverse correlation with the average lifetime of ion pairs as the number of repeat units increases.

# Chapter 4

# Identifying variation of ion-transport mechanisms in polymerized ionic liquids with different polymerized cation chemistry

## 4.1 Introduction

Lithium-ion batteries continue to be a popular thrust of research for portable power storage and energy solutions [202, 289, 303].[1] A particular focus of the efforts in this context has been on the design of polymer materials which can simultaneously provide the mechanical strength and charge transport properties desired in electrolytes for such applications [2, 62, 180, 326]. However, liquid and neutral-polymer electrolyte materials consisting of simultaneously mobile anions and cations exhibit performance-hampering charge polarization as a result of the coordinated diffusion of counterions and subsequent buildup of anions near the anode [140, 197, 198]. In such a context, single-ion conductors, materials in which either the anions or cations are covalently attached in a macromolecule, have been proposed as a solution. In

[1] Adapted with permission from Jordan R. Keith, Santosh Mogurampelly, Bill K. Wheatle, and Venkat Ganesan. Influence of side chain linker length on ion-transport properties of polymeric ionic liquids. *J. Poly. Sci. Part B: Polymer Physics*, 55(23):1718-1723, 2017. My contributions include designing and performing the research, contributing new analytic tools, analyzing data, and writing the article. Copyright 2017 John Wiley and Sons.

such materials, the coordinated diffusion of the ion pairs is significantly reduced, and as a result, the charge polarization effects are virtually eliminated, resulting in transference numbers close to unity [153, 177, 193, 204, 300].

Ionic liquids are a class of materials which have attracted significant attention in view of their excellent chemical stability, low volatility and toxicity, and desirable compatibility with various polar and ionic media [9, 115, 231]. Due to such features, polymerized ionic liquids have emerged as popular single-ion conducting materials. Early work by Ohno demonstrated that improvements could be made on the conductivity of polymerized ionic liquids by swapping the anionic and cationic moieties, and by doping the polymerized ionic liquids with salts containing large, plasticizing ions [230]. Comprehensive reviews have summarized the progress made since then for polymerized ionic liquids as polyelectrolyte materials for batteries and other applications [112, 209], and we refer the interested reader to such sources for a discussion of the accompanying developments.

A number of different physicochemical parameters have been examined to understand (and optimize) the transport properties of polymerized ionic liquids [168, 179, 341]. The motivation for the present study comes from a set of (superficially) conflicting experimental reports pertaining to the influence of the length of the side chain of ionic liquids upon the transport properties of polymerized ionic liquids. Specifically, for polymerized 1-vinyl-3-*alkyl*imidazolium, Salas-de la Cruz and coworkers reported a decrease in conductivity with increasing length of the Group 1 alkyl side chain in

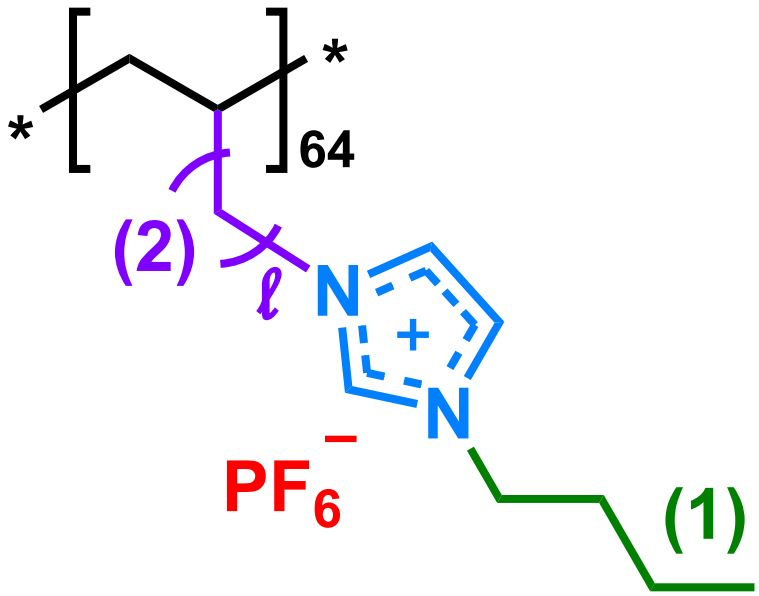


Figure 4.1: Schematic of polymer used in this study. Reprinted with permission from reference 148. Copyright 2017 John Wiley and Sons.

Figure 4.1 [253]. In contrast, Choi and coworkers reported increasing ionic conductivity with increasing Group 2 alkyl length (Figure 4.1) for a similar imidazolium-based polymerized ionic liquid [60, 61]. Together, such observations have raised the question [73], "what are the mechanisms underlying the influence of the linker side-chain length on the transport properties of polymerized ionic liquids?"

Herein, we report the results of atomistic computer simulations which were used to study the structure and mechanisms underlying the effect of Group-2-linker length ($l$) on the transport of non-polymerized ions. We quantify the structural organization in such systems through the radial distributions and the average intermolecular separation between cationic groups. Inspired

by our recent findings in the context of ion-transport mechanisms in polymerized ionic liquids [217], we employ an analysis tool for identifying ionic association/dissociation processes to elucidate the connection between the intermolecular ion-hopping mechanism and the $PF_6^-$ diffusion, and thereby identify the origins underlying the influence of side chain linker length.

In a 2017 article, we studied the transport properties of $PF_6^-$ counterions in poly(1-butyl-3-vinylimidazolium) electrolyte membranes (which corresponds to the case of $l = 0$ in our notation of Figure 4.1) [217]. The polymers were constructed and packed randomly into a simulation box containing eight polyILs of 64 monomers each, along with 512 $PF_6^-$ counterions [206]. We begin our discussion of results by presenting the focal result of this article; namely, the diffusivity of $PF_6^-$ ions as a function of linker size and temperature. We then discuss structural features using the radial distribution function. This is followed by a brief discussion of the ion-association relaxation times. The central ideas of this chapter are contained in the next discussion, which systematically explored ion hopping, intermolecular hopping distance, and ion-dissociation relaxation time. Together, these results support our earlier conclusions regarding the role of ion-dissociation relaxation time (or frequency) as a controlling timescale for ion transport in polymerized ionic liquids.

All simulations in the present work were conducted in the constant pressure/temperature (NPT) ensemble, adjusting temperature every 100 fs and pressure every 1 ps using a Nosé-Hoover thermostat and the Parrinello-Rahman barostat [207, 238, 279, 314], and employed periodic boundary condi-

tions with fixed linear momentum, zeroing the center of mass every 100 fs. All simulations were conducted with a timestep of 1 fs. Identical polymers containing 64 repeat units were constructed using Gaussview. We heated the final configuration from from 0 K to 1,000 K. We then conducted the NPT simulation for 2 ns at 1,000 K and 1 atm on the resulting configuration. We packed eight polymer molecules and the balance (512) of $PF_6^-$ ions randomly into a simulation box with cubic edges of 120 Å using the Packmol software package [206].

We applied the minimization process to the PACKMOL output configuration using the same tolerances. We heated the resulting configuration for 100 ps from 0 K to 1,000 K using the NVE simulation, followed by a 2 ns constant pressure/temperature simulation at 1,000 K and 1 atm on the resulting configuration. We followed this with a 100 ps cooling the resulting configuration to 600 K. To complete equilibration, we applied the NPT simulation at 600 K and 1 atm for 84 ns. The length of production simulations (data collected for analysis) was 30 ns for all temperatures (600 K, 550 K, and 500 K). We cooled each resulting configuration to 550 K and equilibrated the system using constant temperature/pressure for 22 ns. Likewise, once production was complete at 550 K, the final configuration was cooled to 500 K and equilibrated using the constant temperature/pressure simulation for another 22 ns.

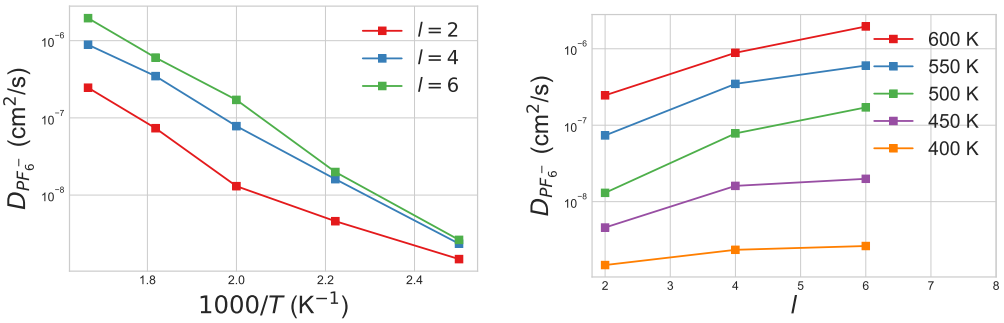


(a) $PF_6^-$ diffusivity as a function of $1000/T$ (b) $PF_6^-$ diffusivity as a function of linker length $l$.

Figure 4.2: Summary of $PF_6^-$ diffusivity for polymerized ionic liquids of different linker sizes $l$. Adapted with permission from reference 148. Copyright 2017 John Wiley and Sons.

## 4.2 Results

Figure 4.2 shows that, at a specified temperature, diffusivity increases with linker length, matching the experimental results of Choi and coworkers [60, 61]. This is shown in two ways. First, temperature-dependence reveals Arhennius behavior, and it is clear from the graph of linker-dependence in figure 4.2(b) that $PF_6^-$ diffusivity increases with increasing linker length.

Structural characteristics such as aggregate sizes and scattering profile have been widely used in prior studies to understand the mechanisms underlying transport phenomena in polymer electrolyte and single-ion conducting materials [24,42,120,121,151,184,184,193,234]. Figure 4.3 displays the density-normalized radial distribution functions $g(r)$ for $Im^+$-$PF_6^-$ pairs for the systems considered in the present systems. Specifically, the cation is represented by the center of mass of imidazolium-ring atoms ($Im^+$) owing to the dominant

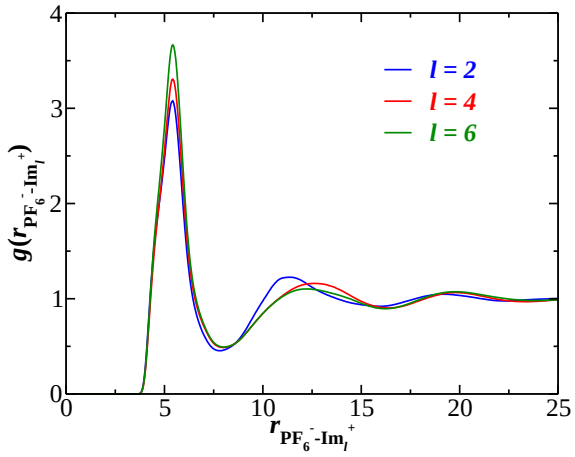


Figure 4.3: Radial distribution function of cation-anion coordination at 500 K for polymerized ionic liquids of varying linker length. Reprinted with permission from reference 148. Copyright 2017 John Wiley and Sons.

share of positive charge, while the anion is represented by its full center of mass. The strongest electrostatic interactions exist between $PF_6^-$ and $Im^+$, justifying incorporation of the ring atoms into the cationic center of mass. A sharp and consistent peak is seen for all linker sizes at an interionic distance of 5.5 Å. This suggests that the cation-anion local structure, with respect to the distance characterizing the first peak, is not influenced by the size of the linker groups in the polymerized ionic liquid. However, the most notable difference can be found in the intensity of the first peak, which is seen to increase monotonically with the size of the linker. Such trends are indicative of a stronger interaction between the cation and anion for larger linker sizes, and can be understood to be a result of the weaker impact of backbone related constraints hindering the ion pair coordinations.

A second peak is seen in $g(r)$ at a distance of 12.5 Å for $l = 4$ and 6, but is seen to be shifted to 11-11.5 Å for $l = 2$. Such trends are consistent with our results for $l = 0$ reported in Mogurampelly et al. [217], wherein it was shown that relative to pure (non-polymerized) ionic liquid, the polymerization of the ionic liquid monomer leads to a closer cation-anion second peak. It may be envisioned that systems with longer linker chains exhibit a behavior closer to non-polymerized ionic liquids due to the accompanying reduction in backbone-related constraints. The extent of second-coordination shell and corresponding peak value may indicate slightly increased ionic displacements with linker length. However, since the first peak is stronger, it is not clear whether the combined structural features revealed by $g(r)$ could explain the effect of linker length on ionic diffusivities. Overall, the above results indicate that, at the level of equilibrium cation-anion coordination behaviors, there are no *specific signatures* which rationalize the enhanced $PF_6^-$ diffusivities observed for longer linker systems.

In a 2017 work from our group [217], we used atomistic-molecular-dynamics simulations to demonstrate that ion transport in polymerized ionic liquids occur through a mechanism involving intra- and inter-molecular ion hopping through the formation and breaking of ion-associations. As a consequence, the ion mobilities in polymerized ionic liquids were shown to be inversely correlated to the average lifetimes of the cation-anion associations. Such results were shown to be in contrast with the behavior in pure ionic liquids, wherein the structural relaxation times served as the critical parameter

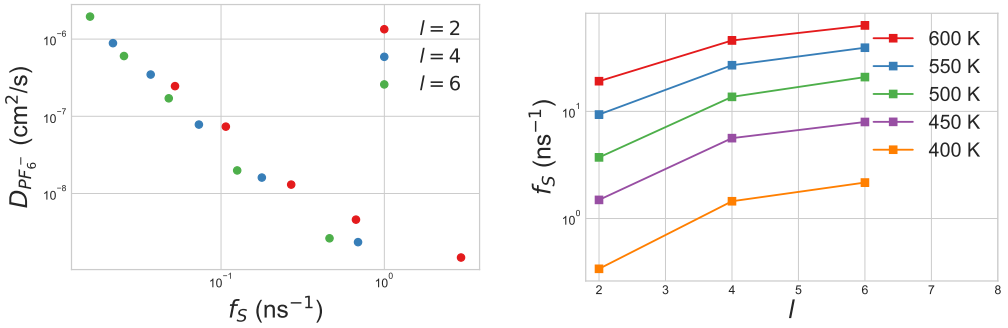


(a) $PF_6^-$ diffusivity as a function of ion-dissociation relaxation frequency $f_S$.

(b) Ion-dissociation relaxation frequency $f_S$ versus linker length $l$.

Figure 4.4: Response of ion-dissociation relaxation frequency to changes in polymerized ionic liquid linker length. Adapted with permission from reference 148. Copyright 2017 John Wiley and Sons.

underlying ion mobilities [1, 217, 256]. Motivated by such earlier findings, in the present work, we sought to characterize whether the linker-size-dependent ion diffusivities are correlated to the respective average lifetimes of the ion associations, and if so, the manner by which the linker size influences the latter time scales.

In Figure 4.4(a), we present results for the ion diffusivities as a function of ion-dissociation relaxation frequency $f_S$, obtained from fitting the decay to the stretched exponential function, as described in chapter 2. We observe that the ion diffusivities in different polymerized ionic liquid linker systems can indeed be collapsed onto an approximately universal function when plotted in such a representation. Such results are consistent with the conclusions of our previous work [217]. This also suggests that the mechanisms underlying the results displayed in Figure 4.2(a) are likely tied to the influence of the linker

on the average lifetimes of the ion-pairs. Such reasoning is confirmed in the results of Figure 4.4(b), which explicitly displays the inverse average lifetimes of the ion-pairs $f_S = \tau_S^{-1}$ as a function of the linker length and temperature. Therein, it can be seen that with increasing linker length, there is a reduction in average lifetimes of the ion-associations $\tau_S$, a result which mirrors the behavior observed for the ion diffusivities in figure 4.2(b).

Since the ion pair lifetimes are expected to be influenced by the number and rate of inter/intramolecular hopping events, we turn our attention to the latter characteristics and the influence of linker size upon such features [217]. For such an objective, we use a 1 ps time interval to collect the association variable $h(t)$, which changes from null to unity (or unity to null) when the $PF_6^-$ ion becomes associated (dissociated) with a $Im^+$. We identified two categories of hopping events: intramolecular and intermolecular. Intramolecular hopping events characterize hopping motion of a $PF_6^-$ ion from monomer to monomer on the same polymer. In contrast, intermolecular hopping events represent $PF_6^-$ hopping among monomers of different polymers.

In Figure 4.5 we present results depicting the number of intra- (denoted as $N_1$) and intermolecular ($N_2$) hopping events as a function of the linker length and temperature. We observe that polymerized ionic liquids possessing longer linker segments exhibit a larger number of intermolecular hopping events $N_2$, and a smaller number of intramolecular events $N_1$. Moreover, it can be seen that the total number of hopping events ($N_1 + N_2$) increases with increasing linker length. Together, the results indicate that the transition to longer linker

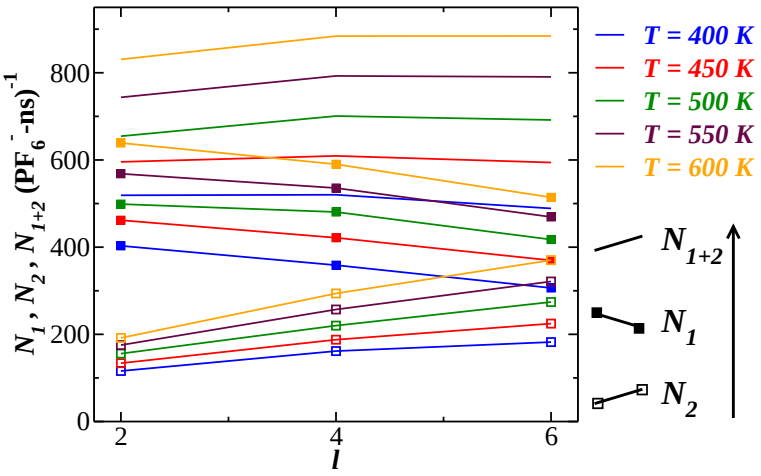


Figure 4.5: Frequency of intra (solid symbols, $N_1$), inter (open symbols, $N_2$) and total (no symbols) molecular hopping events per $PF_6^-$ per ns for polymerized ionic liquids of varying linker length. Reprinted with permission from reference 148. Copyright 2017 John Wiley and Sons.

segments leads to a larger number of intermolecular-ion-hopping events, which lowers the average lifetimes of the ion associations and leads to higher ion mobilities.

As a final step in the understanding of the ion mobility characteristics, we seek to identify the origin of the linker size's influence on the intermolecular hopping events. In this regard, we were inspired by the works of Annapureddy [5] and Salas-de la Cruz [253], which pointed to the intermolecular separation distance of polymerized-ionic groups as an important length scale in ionic liquids. To characterize such a measure, we compiled the average intermolecular-nearest-neighbor distance between cationic centers-of-mass, $d_p$. The results are presented in Figure 4.6, wherein it can be seen that an increase in the linker size leads to a reduction in the intermolecular distance between

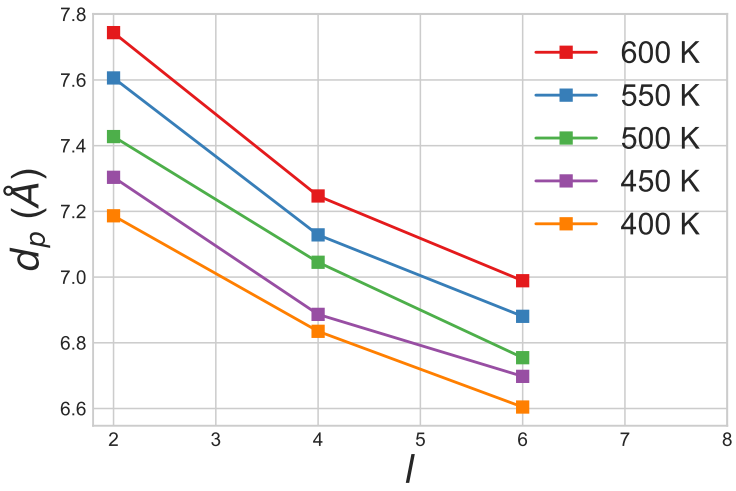


Figure 4.6: Average minimum intermolecular distance $d_p$ between $Im^+$ as a function of the linker size $l$ and temperature. Adapted with permission from reference 148. Copyright 2017 John Wiley and Sons.

cationic $Im^+$ groups, $d_p$.

Some clarification may be helpful with regard to the the definition of the intermolecular cationic distance $d_p$, and the intermolecular backbone distance $d_b$. The value $d_p$ is defined as average intermolecular-nearest-neighbor distance between Group-2-linked nitrogen atoms. For every $Im^+$, there is another $Im^+$ from a *different* polymer molecule that is closest to it. The distance between these two atoms is averaged over all $Im^+$ for all saved frames to determine $d_p$.

The above results indicate that the influence of linker size on the intermolecular hopping events can be traced back to the role of the linkers in modulating $d_p$. More explicitly, an increase in the linker size of polymerized ionic

liquids leads to more proximally located intermolecular cationic groups, which increases the frequency of intermolecular hopping events and the associated rate of ion pair hopping events. Such characteristics manifest macroscopically as enhanced $PF_6^-$ mobilities (and conductivities).

We propose that our above finding is consistent with the (apparently) conflicting experimental observations of Salas-de la Cruz et al., who reported a decrease in conductivity with increasing length of the Group 1 alkyl side chain in Figure 4.1 [253]. Our results showed a closer approach of cationic groups due to the increased length and flexibility of the Group-2 linker segment. In contrast, extending the Group 1 alkyl chain, such as in the work of Salas-de la Cruz, is more likely to reduce the possibilities for cation rearrangement and increase the corresponding intercationic distances. Therefore, for situations where the Group-1 side chain length is increased, we expect the propensity for intermolecular hopping to be lowered, and the corresponding rates of ion pair hopping events to become slower. In turn, such characteristics are expected to manifest in lower ion mobilities as noted in the experiments [253].

## 4.3 Conclusions

In summary, this study probed the effects and mechanisms underlying changes in monomer linker length on the transport properties of polymerized ionic liquids using atomistic simulations. Our simulation results were consistent with experimental observations that an increase in the linker length leads to a corresponding enhancement in anion mobilities. We rationalized

our results and related experimental observations by demonstrating that ion motion in such systems proceeds primarily through intra- and intermolecular hopping. Moreover, an increase in the linker length was shown to increase the propensity for intermolecular ion hopping through the influence of the former upon the intermolecular cationic distances. The results of our study highlight the intermolecular cationic distances as a novel physicochemical parameter, which can be tuned to influence the ion-transport characteristics of polymerized-ionic-liquid membranes.

# Chapter 5

# Analyzing the influence of varying mobile-anion chemistry on ion transport in polymerized ionic liquids

## 5.1 Introduction

Polymerized ionic liquids have attracted significant attention in the pursuit of polymer electrolytes possessing an optimal combination of mechanical strength, conductivity and transference number [229, 247, 276].[1] These macromolecules carry ionic liquid species as repeat units, combining the attractive properties of ionic liquids with the improved mechanical properties and architectural richness of polymeric materials. Moreover, unlike other classes of single-ion conductors, polymerized ionic liquids typically possess lower glass-transition temperatures even at high charge densities due to the weaker electrostatic ion-pair interactions characteristic of ionic liquids [209, 276].

A number of experimental and simulation studies have probed the dynamical properties of *ionic liquids*, and have identified the molecular param-

[1] Adapted with permission from Jordan R. Keith, Nathan J. Rebello, Benjamin J. Cowen, and Venkat Ganesan. Influence of Counterion Structure on Conductivity of Polymerized Ionic Liquids. *ACS Macro Letters*, 8:387-392, 2019. My contributions include designing and performing the research, contributing new analytic tools, analyzing data, and writing the article. 

eters underlying such characteristics. For instance, the diffusion coefficient of the ions have been found to decrease with an increase in the size, conformational flexibility and the shape of the ions [157, 293, 312, 313]. Other studies have demonstrated that the magnitude and directionality of the interaction energy of the ion pairs plays an important role in determining the transport properties [262, 291, 292, 313]. Recently, Maginn and coworkers considered the dynamical properties of a wide variety of ionic liquids and demonstrated that the diffusivities of the ions obeys a universal correlation to the inverse of ion pair/cage timescales [352].

In contrast to the status above in the context of ionic liquids, a comparable understanding of the dynamical properties of polymerized ionic liquids does not exist. Among the different observations reported in polymerized ionic liquids, significant interest has arisen in a specific finding termed as "decoupling" between ionic conductivity and glass transition or segmental dynamics. Explicitly, such a terminology has been used to refer to the property in which the dc conductivity of the polymerized ionic liquid exceeds that of its ionic liquid counterpart at their respective calorimetric glass-transition temperature [86, 87, 101, 113, 217, 323, 324].

Motivated by such experimental observations, in a series of studies from 2017-2018, we examined the mechanisms underlying ion transport in polymerized ionic liquids using atomistic molecular dynamics [147, 148, 215, 217]. Therein, we demonstrated that $PF_6^-$ anions exhibited a delocalized coordination involving multiple cations from distinct polymer chains. Further, trans-

port in polymerized ionic liquids was shown to occur through a combination of intra- and intermolecular ion hopping, involving the formation and breaking of ion associations between the anions and polymerized cationic monomers bonded to different polymer chains. Based on an analysis of the accompanying time scales, we rationalized the phenomena of "decoupling" as a consequence of such ion hopping motion which was distinct from those observed in ionic liquids.

Despite the insights arising from the studies described above, a number of issues regarding the mechanisms and conductivity properties of polymerized ionic liquids remain to be resolved. Among these, there is still less clarity on the influence of the physicochemical characteristics of the counterion on transport properties. For instance, Ye and Elabd showed that ionic conductivity of polymerized ionic liquids are influenced by both the size and symmetry of the anion and the dissociation energy of the ion pair [341]. In a different study, Sangoro, Runt and coworkers investigated the influence of different counterions on ion transport and observed that smaller sized counterions exhibit a larger degree of decoupling [134].

More recently, Winey and coworkers chose a trisaminocyclopropenium polycation, which is "electron-rich with a highly delocalized charge," to promote ion hopping, and demonstrated a 4-6 order-of-magnitude increase in dc ionic conductivity of the polymerized ionic liquid over the ionic liquid at their respective glass-transition temperatures [113]. Simmons and coworkers followed with coarse-grained simulations that revealed size-sensitivity and im-

proved decoupling in percolated networks of ionic aggregates [58].

Other studies have also considered the influence of ion pair properties on the glass transition temperature of polymerized ionic liquids. For instance, Colby and coworkers suggested that the glass-transition temperature of a polymerized ionic liquid exhibits a direct correlation with the ion-pair volumes of such materials [60]. Subsequent work by Sokolov and coworkers expanded such a model to include effects such as chain stiffness and dielectric constant of the polymer [21].

In this work, we seek to shed light on the influence of the physicochemical properties of the counterion on the its transport properties in polymerized ionic liquids. Specifically, we use atomistic simulations to probe the transport properties of 1-butyl-3-vinylimidazolium ($pBvIm^+$) with eight different anions: tetrachloroaluminate ($AlCl_4^-$), tetrafluoroborate ($BF_4^-$), $Br^-$, $Cl^-$, pentafluoroethyl sulfate ($PfO^-$), bispentafluoroethyl-sulfonylimide ($PFSI^-$), trifluoromethyl sulfate ($TfO^-$), and bistrifluoromethyl-sulfonylimide ($TFSI^-$). This list encompasses the bulk of computationally probed ionic-liquid anions with well-established inter- and intra-molecular interaction parameters [47, 72, 188, 317].

Within such a group are subsets of spherically symmetric and linear molecules spanning a wide range of sizes. The linear ions can be further grouped into two canonical ionic-liquid chemical moieties: sulfates and sulfonylimides. By choosing a variety of counterions with differing sizes, symmetries and chemical characteristics, we seek to identify the parameters in-

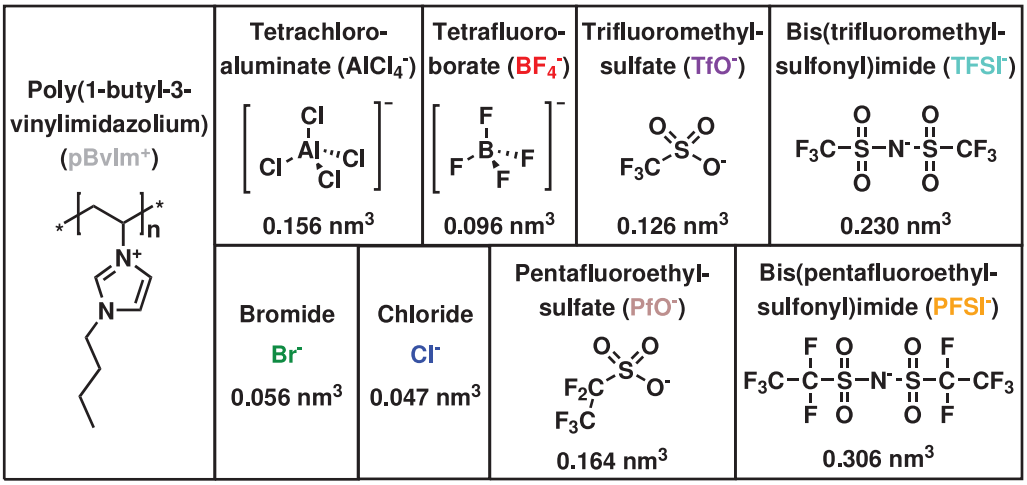


Figure 5.1: The polymerized ionic liquid monomer ($pBvIm^+$) and the eight ionic liquid anions explored in this study. Molecular volumes collected from references 286 and 203 ($pBvIm^+$), 14 ($TFSI^-$ and $TfO^-$, plus $PfO^-$ and $PFSI^-$ by group contribution), and 141 ($AlCl_4^-$, $BF_4^-$, $Br^-$, $Cl^-$). Reprinted with permission from reference 149. Copyright 2019 American Chemical Society.

fluencing the conductivity characteristics of polymerized ionic liquids and the mechanisms underlying such properties.

Figure 5.1 shows the ions under investigation. Molecular volumes shown in the figure were compiled from a number other sources, with some results, specifically some fluoronated ionic species and the polymer backbone atoms, being derived from group contribution volume estimation [14, 141, 203, 286].

## 5.2 Analysis

### 5.2.1 Association distance and the unbiased cutoff radius

The "center" of the cations was taken to be the nitrogen labeled NA2 (polymerized ionic liquid) and iNA2 (ionic liquid). Likewise, we chose a single atom within each anion to represent its center: Al ($AlCl_4^-$), B ($BF_4^-$), Br ($Br^-$), Cl ($Cl^-$), SN ($PfO^-$), NP ($PFSI^-$), ST ($TfO^-$), and NF ($TFSI^-$). These atom identifiers, and all other atom identifiers, can be located in Figure 5.2. For the spherically symmetric species and the linear asymmetric $TfO^-$ and $PfO^-$, the choices could be naturally tied to the distributed charge geometry, focusing attention on the region of concentrated negative charge. For $TFSI^-$ and $PFSI^-$, although the nitrogen does not reflect a charge-centered atom, it was selected to ensure that only one atom represented each anion, and that the proposed center would not reside where the association distance could be nonphysically close to zero.

All hydrogen atoms in the $BmIm^+$ and $pBvIm^+$ are left out of figure 5.2 to improve its clarity. Hydrogen atoms are named to mirror the carbon atom to which they are connected. For example, the hydrogen atoms bonded to CA are named HA. Likewise, those bonded to iCA are named iHA. All anion atoms are explicitly labeled, and are color-coded to match their respective data throughout the chapter.

The cutoff distance is a critical quantity in a number of our analysis methods, including the intermittent ion-association auto-correlation function

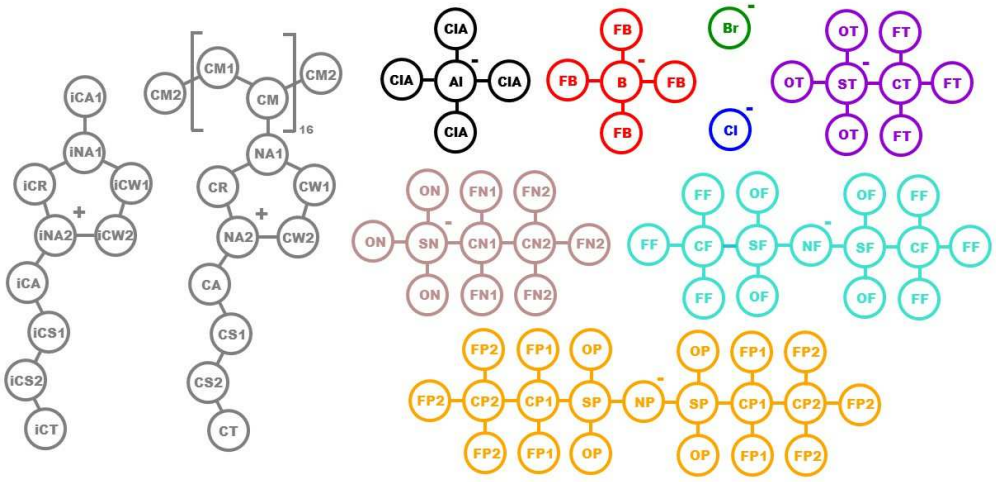


Figure 5.2: Mapping for all ions and polymers included in this study. The positive- or negative-charged label indicates the cation or anion center atom chosen to represent the ion in coordination and association studies. Hydrogen atoms are left out for improved clarity. Ions are as follows, from upper left to lower right: $BmIm^+$ (grey), $pBvIm^+$ (grey), $AlCl_4^-$ (black), $BF_4^-$ (red), $Br^-$ (green), $TfO^-$ (violet), $Cl^-$ (blue), $PfO^-$ (brown), $TFSI^-$ (turquoise), and $PFSI^-$ (orange). Reprinted with permission from reference 149. Copyright 2019 American Chemical Society.

($C(t)$), continuous ion-association auto-correlation function ($S(t)$), coordination profile, and ion hopping frequencies.

Previously, we utilized a constant, arbitrarily chosen cutoff for the single anion type investigated in atomistic molecular dynamics simulations of polymerized ionic liquids, $PF_6^-$ [147, 148, 217]. Now, confronted with varying shape and dimensional characteristics for each ion, a consistent and universal definition must be created. We settled on a formulation using the radial distribution function $g(r)$.

The choice is the distance at which $g(r) = 1$ on the negative slope of the first coordination peak. We will refer to such a distance as the radius of ionic *association*, which should not be confused with the radius for ion *pairing*. Ion pairing distance is better represented by the radius at which the average coordination number reaches 1.0.

Figure 5.3 shows these distances, along with the radius of the maximum in the first peak of the $g(r)$. For the spherical ions and $TFSI^-$, the maximum peak falls beyond the ion-pair distance. This suggests that multiple anions can be closely *associated* to a single cation. This is an important distinction, as we are purposefully using *associated* rather than *bound* to avoid implying that ions require higher energy to escape association. This detail will emerge later in our analysis.

To conclude this discussion, the maximum peaks for $PfO^-$, $TfO^-$, and $PFSI^-$ lie inside of the respective ion-pair cutoff, implying that not all cations

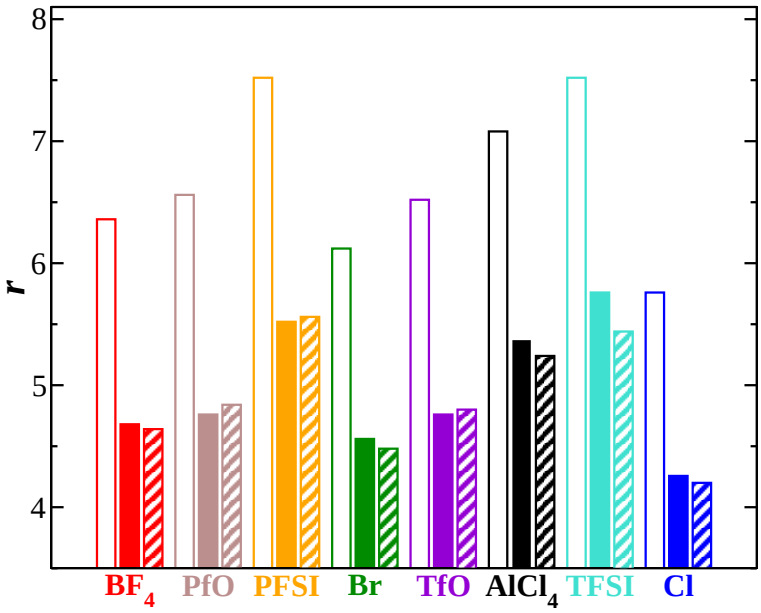


Figure 5.3: Open symbols are cutoff distance based on the entire first peak of the radial distribution function $g(r)$. Solid filled symbols represent the radius at which the first maximum in the radial distribution function is observed. The patterned symbols show the radius at which the average coordination number is 1.0 (ion-pair cutoff distance). The ions are presented left to right in order of counductivty/dynamics-decoupling extent. Reprinted with permission from reference 149. Copyright 2019 American Chemical Society.

have a closely associated counterpart. It is worth noting the disparity between the first-peak radius and the ion-pair radius in $TFSI^-$, and to a lesser extent, $AlCl_4^-$. These two species emerge as key, highly decoupled species, and we devote some attention to analyzing the underlying origins. Finally, the overall trends in the solid-filled and pattern-filled in Figure 5.3 follow the trend of the association cutoff distance (open symbols). $PFSI^-$ and $TFSI^-$ have similar distances, as do $PfO^-$ and $TfO^-$. $AlCl_4^-$ falls between these two sets, while the remaining spherical species lie below the rest, with the distances directly proportional to the ionic radius.

### 5.2.2 Determining glass-transition temperature

We determined the glass-transition temperatures for all of the polymerized-ionic-liquid and ionic-liquid materials evaluated in this study. We used the volumetric expansion method by quantifying density as a function of temperature. For ionic liquids, fast structural relaxation allows the materials to equilibrate quickly, thus enabling the use of a rapid cooling rate of 5 K/ns. Beginning with a well-equilibrated configuration at 450 K, we continuously and linearly cooled the sample to 100 K for 100 ns of simulation time. We used a constant temperature/pressure plus integrator to run the simulations, but we forced the temperature to change step-wise to maintain the cooling rate.

Figure 5.4 shows the result of the volumetric expansion method of calculating glass-transition temperature for the ionic liquid and polymerized

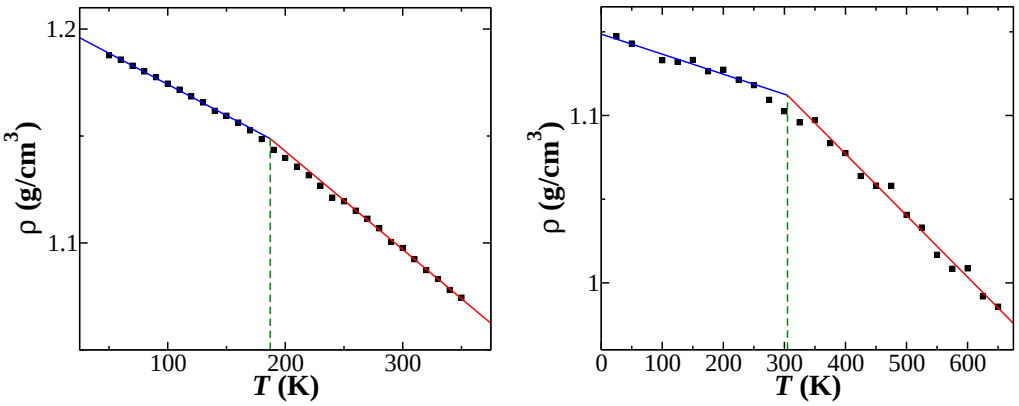


(a) Ionic liquid $BmIm^+$-$Cl^-$. (b) Polymnerized ionic liquid $pBvIm^+$-$Cl^-$.

Figure 5.4: Example plots of volumetric expansion results for quantifying glass-transition temperature. Reprinted with permission from reference 149. Copyright 2019 American Chemical Society.

ionic liquid materials containing $Cl^-$. These plots appear to be quite successful at capturing the transition point, with its hallmark "kink" and corresponding non-equilibrium free volume above the curve at low temperatures. Figure 5.4(a) also contains the fitting lines for both high- (red) and low-temperature (blue) regions of the density curve. The green dotted line on each graph draws the reader's attention to the intersection point of the two fitting lines. The value of temperature at these intersections represents glass-transition temperature. Ionic liquid glass-transition temperatures are reported in Table 5.1, column 2.

The glass-transition temperatures for polymerized ionic liquids were more difficult to extract. Polymerized ionic liquids relax at a much slower rate, causing uncertainty in the values of density extracted from rapid cooling simulations, such as the ones executed for the ionic liquid materials. Fur-

| anion | $T_{gIL}$ | $T_{gpolyIL}$ |
|---|---|---|
| $AlCl_4^-$ | 213 | 231 |
| $BF_4^-$ | 205 | 185 |
| $Br^-$ | 239 | 222 |
| $Cl^-$ | 187 | 305 |
| $PfO^-$ | 211 | 227 |
| $PFSI^-$ | 219 | 232 |
| $TfO^-$ | 215 | 237 |
| $TFSI^-$ | 218 | 260 |

Table 5.1: Values of glass-transition temperature ($T_g$) extracted from the intersection of lines fit above and below $T_g$ on density versus temperature plots. For ionic liquid (IL) and polymerized ionic liquid (polyIL) containing the noted anion.

thermore, the range of possible values for glass-transition temperature was extensive upon initial inspection.

Many early attempts were made to characterize glass-transition temperatures using prior knowledge of experimental values for these materials. Glass-transition temperatures are known from experiment for five of the eight polymerized ionic liquids tested in this study. An empirical fit between the molecular volume of the ion pair and glass-transition temperature, proposed by Bocharova et al., provided an estimate of the unknown glass-transition temperatures [21]. The empirical formula is as follows,

$$\frac{1}{T_{g0}} = \left(A + \frac{B}{V_m^{1/3}} + CV_m^{2/3}\right)^{-1} - \frac{K}{V_m}, \tag{5.1}$$

where $T_{g0}$ represents the glass-transition temperature of an infinitely long polymer.

This equation includes the term containing a fourth adjustable parame-

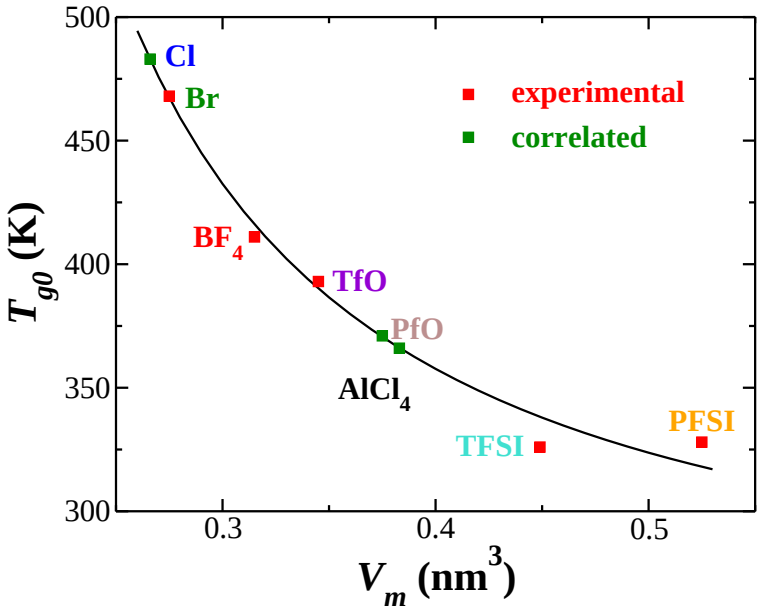


Figure 5.5: Experimental and empirically derived infinite-length-polymer $T_g$ for all polymerized ionic liquids tested in this study. Reprinted with permission from reference 149. Copyright 2019 American Chemical Society.

ter ($K$), which reflects the influence of variable molecular weight, as described by Bocharova et al., who cited Ueberreiter and Kanig [21, 316]. Figure 5.5 summarizes this information, and a number of sources are credited with these experimental results, while differing values are averaged to the value shown on this plot [111, 134, 224]. Molecular volume measurements were compiled from a number other sources, with some results, specifically for some fluoronated ionic species and the polymerized-ionic-liquid backbone atoms, being derived from group contribution volume estimating [14, 141, 203, 286].

Given that such values represent the dynamics of infinitely long polymers, it is reasonable to assume that the lower molecular weight tested in this study will lead to lower glass-transition temperature. Our search space initially included 250 K to 600 K, depending on the material and the expected value of glass-transition temperature. We tried the same procedure used with success on the ionic liquids for these ranges at cooling rates of 5 K/ns, 1 K/ns, 0.4 K/ns. In all cases, we failed to isolate a repeatably identifiable transition.

The force field parameters utilized in this study are not validated against experimental properties such as density in the polymerized ionic liquids. Nor are the molecular volumes, derived from experiment, necessarily representative of such values in the simulation environment. Thus, we cannot be certain that these materials will follow the same trends identified in real materials. This makes it crucial to extract glass-transition temperature from simulation. In a final attempt to extract glass-transition temperature, we used constant pressure/temperature simulations with 100 ns of equilibration time

and 50 ns of production data collection to compute the average density at over intervals of 25 K from 25 to 650 K.

Figure 5.4(b) shows the results of this procedure for the pBvIm$^+$-Cl$^-$ polymerized ionic liquid. We are encouraged by the obvious change in slope that occurs near the glass-transition temperature for each material. Values were extracted using the same procedure described for ionic liquids and are included in column 3 of Table 5.1 for the reader's convenience. These values are surprisingly low, given the experimental values shown previously. We speculate that the use of empirically charge scaled force fields to be a potential origin for these discrepancies.

### 5.2.3 Mobility

In polymerized-ionic-liquid systems, the mobility of the polymerized counterions is expected to be small relative to the free counterions. Hence, the conductivities are approximated as proportional to the product of the concentration of charge carriers and the diffusivity of the nonpolymerized counterions. To render a comparison of the transport properties of different polymerized ionic liquid systems, in figure 5.6 we display the results for the Nernst-Einstein conductivity as a function of the inverse glass-transition-normalized temperature ($T_g/T$).

Since we probed the same range of temperatures for the different systems, the ranges of normalized temperatures do not generally overlap for different materials. Based on the results displayed, at a specified $T_g/T$ the following

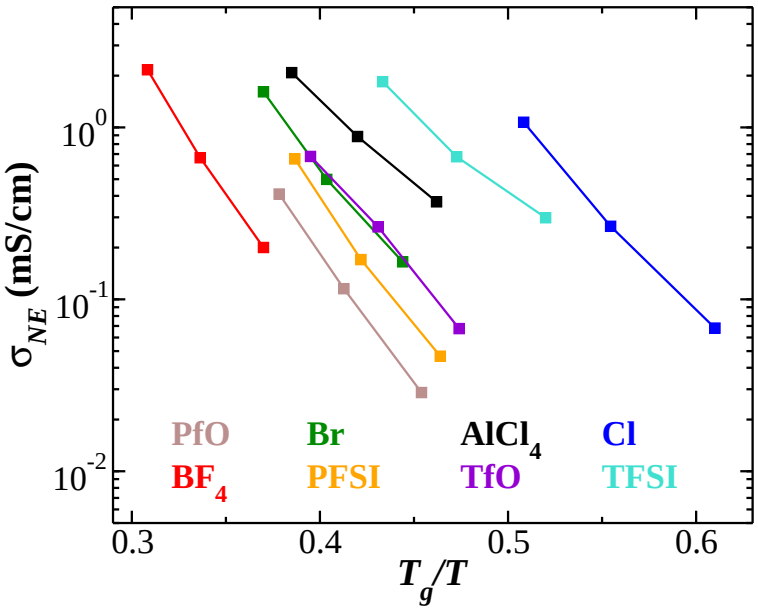


Figure 5.6: Nernst-Einstein conductivity of polymerized ionic liquids plotted against $T_g$/T, the inverse glass-transition-normalized temperature. Reprinted with permission from reference 149. Copyright 2019 American Chemical Society.

order is observed for the highest to lowest ion mobilities in these polymerized ionic liquids: $BF_4^-$< $PfO^-$< $PFSI^-$< $Br^-$< $TfO^-$< $AlCl_4^-$< $TFSI^-$< $Cl^-$. Further, since the polymeric backbone and the cation was maintained the same, the differences in the ion mobilities at the same $T_g/T$ can be construed as a measure of the extent of decoupling between ion mobility and segmental dynamics.

Are the ion mobilities/conductivities of different polymerized ionic liquids correlated with the counterion size? As discussed in the introduction, a number of studies in the context of ionic liquids and polymerized ionic liquids have suggested that counterion size is a critical parameter which influences ion mobilities [157, 293, 312, 313]. Explicitly, in accord with intuitive expectations, such studies have reported that smaller ions are expected to have higher mobilities [134]. More recently, coarse-grained simulations by Simmons et al. reported that small free ions exhibit increased extent of decoupling from polymer segmental dynamics [58].

To probe whether our results agree with such expectations, we display a histogram of three distinct size measures in Figure 5.7, with ions organized from left to right by increasing magnitude of mobilities at a specified $T_g/T$ as deduced from Figure 5.6. The values from the open symbols were derived from ion volumes reported by a variety of experimental sources [14, 141, 203, 286], assuming a spherical shape. Considering the potential impact of shape on coordination behavior, two other coordination distances are also included in the plot as a surrogate for the size of the ion. From the results displayed, it is

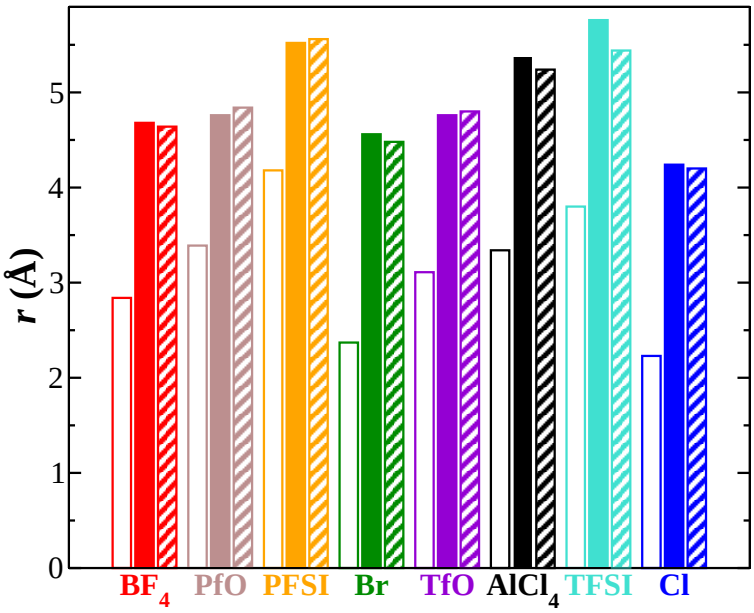


Figure 5.7: Histogram showing various measures of ion size of the least- to most-decoupled ions in this study (left to right). Empty bars represent hypothetical spherical radii, computed from molecular volumes reported in literature. [14, 141, 203, 286] Solid-filled symbols show the distance corresponding to the first maximum in $g(r)$. Finally, the pattern-filled symbols show the distance at which the average ionic coordination number reaches 1.0. Reprinted with permission from reference 149. Copyright 2019 American Chemical Society.

| anion | $IL_{300K}$ | $IL_{350K}$ | $IL_{400K}$ | $IL_{450K}$ |
|---|---|---|---|---|
| $AlCl_4^-$ | 1.0001 | 0.99306 | 0.99522 | 1.0017 |
| $BF_4^-$ | 0.99083 | 0.99944 | 1.0012 | 0.99948 |
| $Br^-$ | 1.002 | 1.0023 | 1.008 | 0.98866 |
| $Cl^-$ | 0.84264 | 1.0032 | 1.0013 | 0.99114 |
| $PfO^-$ | 0.99112 | 1.0009 | 1.0099 | 1.0039 |
| $PFSI^-$ | 0.9977 | 0.99911 | 1.0018 | 0.99632 |
| $TfO^-$ | 0.99934 | 1.0051 | 0.99344 | 0.99445 |
| $TFSI^-$ | 0.99082 | 0.99036 | 0.99914 | 0.99711 |

Table 5.2: $\beta$ linearity parameter for anions in ionic liquids with varying counterion.

clearly seen that ion volume correlation, and even coordination distances, are insufficient as unique parameters to explain the ion mobilities in polymerized-ionic-liquid systems.

Are the ion mobilities correlated to the counterion size within the specific ion classes? To address this question, we classify the ions into three categories based on their physiochemical characteristics, viz., spherically symmetric ions ($AlCl_4^-$, $BF_4^-$, $Br^-$, $Cl^-$), sulfates ($PfO^-$, $TfO^-$), and sulfonylimides ($PFSI^-$, $TFSI^-$). We observe that the extent of ion mobilities following order: 1) spherical ions: $BF_4^- > Br^- < \mathbf{AlCl_4^-} > Cl^-$, 2) sulfates: $PfO^- < TfO^-$ , and 3) sulfonylimides: $PFSI^- < TFSI^-$. With the exception of $AlCl_4^-$ (bold for emphasis), which is part of the spherical class, the rest of the ions appear to follow the expected trend with their respective classes. $AlCl_4^-$ is the largest spherical ion but has a higher ion mobility than both $BF_4^-$ and $Br^-$.

Tables 5.2 and 5.3 shows the quality of the results reported in this work. All $\beta$ fall within 20% of unity. Excluding $BmIm^+$-$Cl^-$ at 300 K, all linearity

| anion | $polyIL_{500K}$ | $polyIL_{550K}$ | $polyIL_{600K}$ |
|---|---|---|---|
| $AlCl_4^-$ | 0.99213 | 0.99961 | 0.97382 |
| $BF_4^-$ | 0.94208 | 0.9949 | 1.0099 |
| $Br^-$ | 1.0083 | 1.0038 | 0.93964 |
| $Cl^-$ | 0.9827 | 0.95703 | 0.99264 |
| $PfO^-$ | 0.95254 | 0.92745 | 0.99193 |
| $PFSI^-$ | 0.99227 | 0.95673 | 0.99454 |
| $TfO^-$ | 0.98079 | 1.0033 | 0.98691 |
| $TFSI^-$ | 0.97983 | 0.97015 | 0.99516 |

Table 5.3: $\beta$ linearity parameter for anions in ionic liquids and polymerized ionic liquids with varying counterion.

| anion | $IL_{300K}$ | $IL_{350K}$ | $IL_{400K}$ | $IL_{450K}$ |
|---|---|---|---|---|
| $AlCl_4^-$ | 1.0025 | 1.0077 | 0.99371 | 1.0091 |
| $BF_4^-$ | 0.98842 | 0.9935 | 0.99377 | 0.99482 |
| $Br^-$ | 0.97428 | 0.99276 | 1.0047 | 1.0027 |
| $Cl^-$ | 1.0107 | 0.99394 | 0.99972 | 1.0042 |
| $PfO^-$ | 1.0094 | 0.98953 | 0.99833 | 1.0035 |
| $PFSI^-$ | 1.0029 | 0.99805 | 1.0076 | 1.001 |
| $TfO^-$ | 1.0001 | 0.99097 | 0.99747 | 0.99289 |
| $TFSI^-$ | 1.0027 | 0.97626 | 1.0083 | 1.0058 |

Table 5.4: $\beta$ linearity parameter for cations in ionic liquids with varying counterion.

parameters fall within 10% of unity. Further excepting $pBvIm^+$-$PfO^-$ at 550 K, all values are within 5% of unity.

Table 5.4 shows that $\beta$ for the cation mean-squared displacements are even better behaved, all falling within 3% of unity. Excepting two cases ($BF_{4\,300K}^-$ and $Br^-{}_{300K}$), the rest fall within 1% of unity. Figure 5.8 shows the diffusivities of the $BmIm^+$ cations for each system and temperature.

Figure 5.9 summarizes anion diffusivities for all ionic-liquid and polymerized-

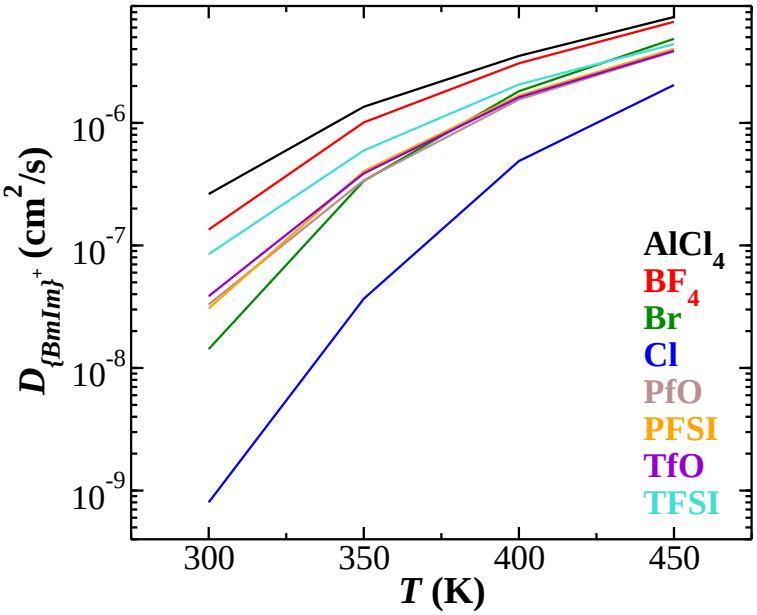


Figure 5.8: $BmIm^+$ diffusivity for ionic liquid with varying counterion.

ionic-liquid systems and temperatures. A few salient features emerge from this figure. First, anions in ionic liquids show a markedly steeper decline in the logarithm of diffusivity than their polymerized ionic liquid counterparts. Additionally, the negative concavity of the ionic-liquid anion diffusivity curve suggests that probing lower temperatures would reveal increasingly steep declines for all species. For polymerized-ionic-liquid anions, the linearity in Figure 5.9 is striking, but no direct comparisons with ionic liquids are possible due to the difficulty of accessing dynamical properties for these systems at low temperatures.

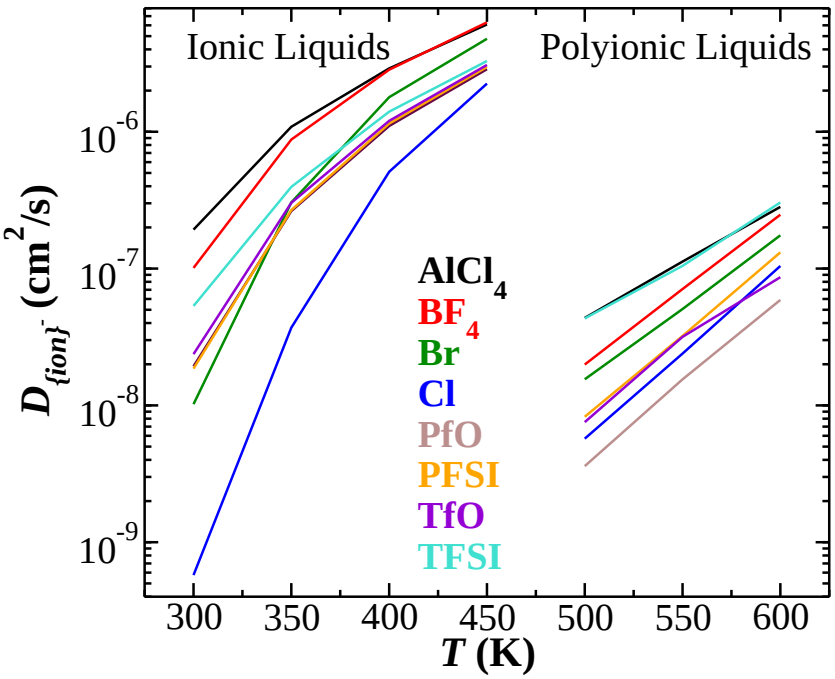


Figure 5.9: Anion diffusivity for all ionic liquids and polymerized ionic liquids in the counterion study. Reprinted with permission from reference 149. Copyright 2019 American Chemical Society.

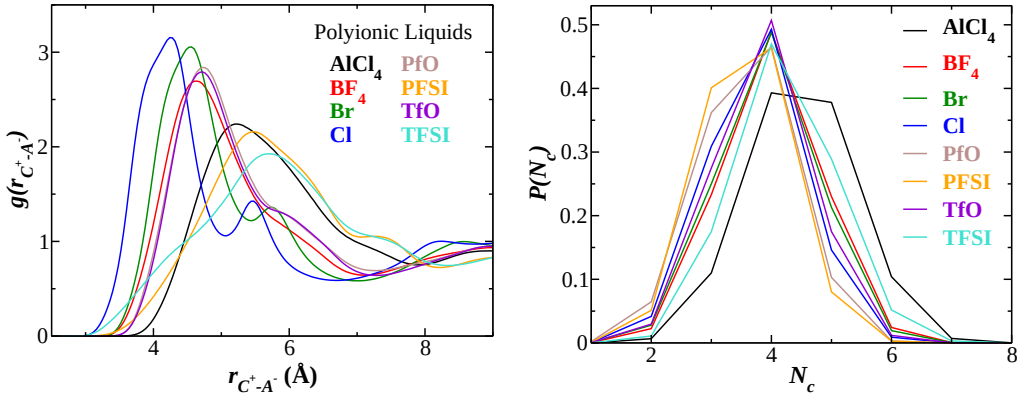


(a) pBvIm$^+$-anion radial distribution function $g(r)$ for all ions in this study.

(b) Ionic coordination number ($N_c$) distribution for all ions.

Figure 5.10: Structure properties for polymerized ionic liquids with varying counterion. Reprinted with permission from reference 149. Copyright 2019 American Chemical Society.

### 5.2.4 Structure and association

To understand the origins underlying the results for $AlCl_4^-$, we consider the cation-anion radial distribution functions $g(r)$, displayed in Figure 5.10(a). Therein, it is seen that among the spherical ions, $AlCl_4^-$ (black line) exhibits a much weaker extent (relative to the other spherical anions' blue, green, and red lines) of coordination with the cations. To substantiate such results, we also display Figure 5.10(b), the probability distribution of the number of cations coordinated with the anion.

It is seen that while $BF_4^-$, $Br^-$ and $Cl^-$ exhibit a sharply peaked distribution at $N_c = 4$, $AlCl_4^-$ exhibits a much broader distribution, with almost equal probability of coordination with four and five cations. Such results confirm the delocalized coordination exhibited by $AlCl_4^-$ anion in contrast to the

other spherical anions.

Together, the above results indicate that within classes of ions which share the same physical or chemical characteristics, ion sizes do indeed serve as a useful measure to identify the relative values of ion mobilities. However, based on the results for $AlCl_4^-$ within the spherical class of ions, it is clear that such a correlation is not necessarily sufficient to identify the order of ion mobilities. Indeed, it is seen that for $AlCl_4^-$, the delocalized coordination between the anion and the cations is sufficient to overcome the influence of size relative to $BF_4^-$ and $Br^-$. However, $Cl^-$, which exhibits the strongest peak in the coordination with the cation, exhibits the fastest ion mobility — a consequence of its size. With respect to the other classes of ions (sulfates and sulfonylimides), we observe that while there are differences in the coordination behavior (Figure 5.10), such differences are much less pronounced, thereby rationalizing the stronger influence of the ion sizes on their mobilities.

### 5.2.5 Ion-association relaxation

Are there universal correlations underlying the transport properties of different polymerized-ionic-liquid systems? As discussed in the introduction, Maginn and coworkers have used molecular dynamics simulations to quantify the Nernst-Einstein conductivities, and demonstrated that such transport properties exhibit a universal correlation to the ion-pair/ion-cage relaxation time of the system [352]. We studied ion mobilities in polymerized-ionic-liquid systems [147,148,215,217], and demonstrated that, due to the ion hopping na-

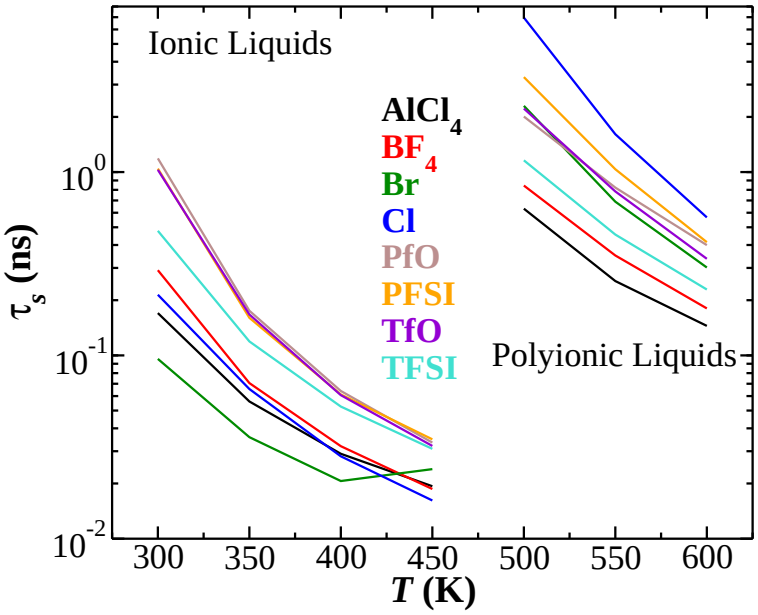


Figure 5.11: Average lifetime of ion pairs versus temperature when varying counterion. Reprinted with permission from reference 149. Copyright 2019 American Chemical Society.

ture of the motion in such systems, the correlation between the ion diffusivities and the ion-pair lifetimes were different from the functional form observed in the corresponding ionic liquid systems. However, since all of our earlier studies pertained to only the case of $PF_6^-$ anion, an interrogation of universality, if any, of correlations in ion mobilities of polymerized ionic liquids and the corresponding ion pair relaxation times could not be probed.

In the present study, we undertook an effort to probe whether the Nernst-Einstein conductivities of polymerized-ionic-liquid systems with different counterions exhibit a correlation with the ion-pair association timescales. Such a timescale quantifies the rate at which the ions enter and exit the local

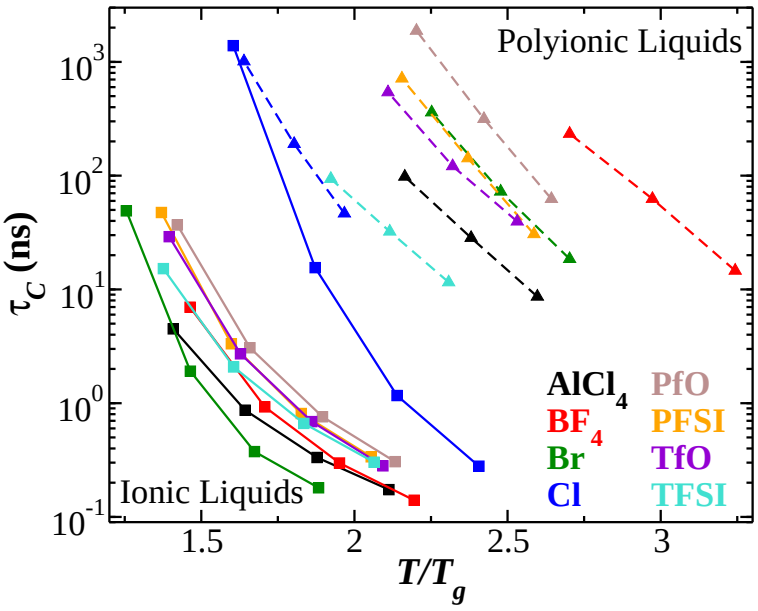


Figure 5.12: The ion-association structural relaxation time compared against $T/T_g$ , for ionic liquids (solid lines with square symbols) and polymerized ionic liquids (dashed lines with upward triangle symbols). Reprinted with permission from reference 149. Copyright 2019 American Chemical Society.

coordination environment, i.e. ion hopping, and is expected to be influenced by the size, symmetry and the charge delocalization of the ions [352]. In figure 5.11, the average lifetime of ion-association pairs is plotted on a logarithm scale versus temperature for all ionic liquids and polymerized ionic liquids. While $\tau_C$ for the halide ions showed much higher relaxation times compared with the other ions, they show low values for $\tau_S$. We are not able to explain the result for $Br^-$ at 450 K, and suggest ignoring this outlier for the purpose of evaluating trends.

How does the $\tau_C$ behave when normalized with respect to polymer dy-

namics using $T/T_g$? Figure 5.12 reveals ionic liquid curves with positive concavity, showing $\tau_C$ increases more steeply as the temperature approaches $T_g$. The pBvIm$^+$-Cl$^-$ and BmIm$^+$-Cl$^-$ lines appear poised to cross, whereas these curves crossed within our temperature range for diffusivity and conductivity. This could be indicative of decoupling between conductivity and polymer dynamics in the Cl$^-$ polymerized ionic liquid. Comparing polymer results across $T/T_g$ for these relaxation times, we note the following order of decoupling in ion and polymer dynamics: $BF_4^- < PfO^- < Br^- \approx PFSI^- < TfO^- < AlCl_4^- < TFSI^- < Cl^-$. This is consistent with the results obtained in diffusivity and ideal conductivity.

In comparing the results for the ideal conductivity and $\tau_C$, we observe that the trends are very similar. Explicitly, among the spherical ions, Cl$^-$ is seen to exhibit the smallest relaxation times and the order of relaxation times ($BF_4^- > Br^- < \mathbf{AlCl_4^-} > Cl^-$) mirror the results seen for the conductivities. Similarly, the relaxation times within the other classes of ions are also in accord with the order seen in the Nernst-Einstein conductivities.

Inspired by the correlation demonstrated between the conductivties and the ion pair lifetime for ionic liquids [352], we display the conductivities as a function of $\tau_C$ in figure 5.13. It is seen that these quantities indeed exhibit a universal correlation for different polymerized-ionic-liquid systems. Such a result is remarkable considering the different classes of polymerized-ionic-liquid systems considered and the differences noted in terms of their size and charge delocalization characteristics. Moreover, considering that a similar universal

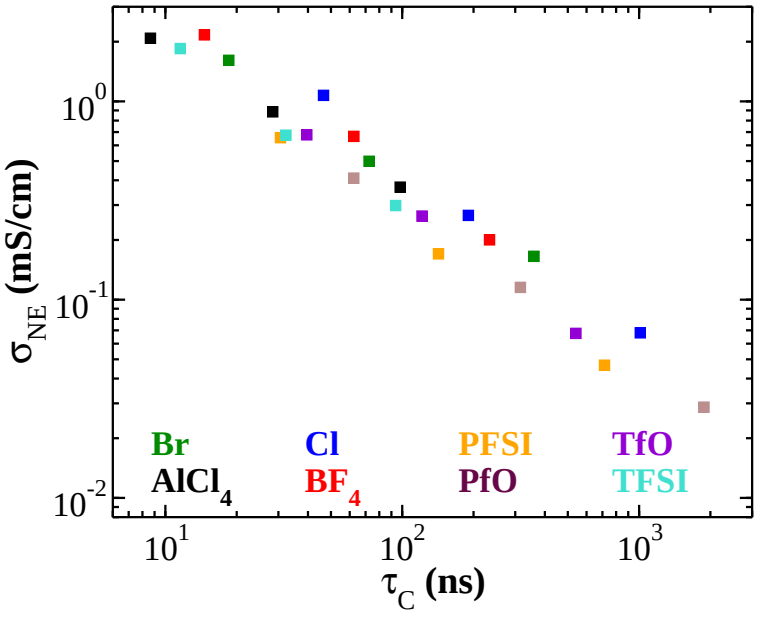


Figure 5.13: Nernst-Einstein conductivity versus ion-association structural relaxation time ($\tau_C$) of polymerized ionic liquids to demonstrate a universal relationship among various counterions. Reprinted with permission from reference 149. Copyright 2019 American Chemical Society.

correlation also holds in ionic liquids, this result suggests that consideration of the factors influencing mobilities in ionic liquids would serve to provide an indication of the trends expected in polymerized ionic liquids.

## 5.3 Conclusion

In summary, the results of the atomistic molecular dynamics simulations support findings from earlier simulation and experimental studies, while also uncovering new insights on local structure and ion hopping in polymerized ionic liquids. Our results reinforce ion size as a key influence on conductivity within the respective physicochemical ion classes of polymerized ionic liquids, while noting that large ions with delocalized charge can outperform some smaller ions. Despite such complex effects, our results indicated that the conductivities of the different systems exhibit a universal correlation to the ion-association structural relaxation time of the polymerized ionic liquid. Further studies should seek to expand the scope of these findings, and elucidate a more detailed understanding of the amalgamated influences of ion and polymer chemistry, $T_g$, polymer segmental dynamics, and ion hopping frequency on ion mobility in polymerized ionic liquids.

# Chapter 6

# Characterizing the impact of backbone versus pendant architecture on ion transport in polymerized ionic liquids

## 6.1 Introduction

Electrolytes employed in lithium-ion batteries require a shear modulus beyond a critical value to maintain interfacial stability and prevent dendrite formation [221, 278]. In this context, interest has arisen recently in polymeric materials that possess sufficient mechanical strength with good ion conduction [39, 85, 125, 210, 237, 259, 310]. Generally, however, ionic conductivity of polymers is inversely correlated to their mechanical strength. Decoupling ion transport from polymer dynamics still represents an outstanding challenge to transitioning such materials to lithium-ion batteries [83].

In the above context, single-ion conductors and polymerized ionic liquids have attracted interest as a means to surmount another performance challenge; namely, increased ion-transport selectivity, i.e. lithium-transference number in lithium-ion batteries [82, 103, 202, 350]. By rendering one of the ions immobile, such materials reduce the correlated motion of the anions and cations, and thereby mitigate the effects of concentration polarization in lithium-ion batteries. In this context, polymerized ionic liquids combine

advantages of ionic liquids, namely chemical stability and low volatility, with those of single-ion conductors, including selective ion transport and improved mechanical strength [348]. Interestingly, recent studies have revealed that ion transport in such materials exhibits reduced coupling to polymer segmental dynamics [58, 114, 149, 217]. While such findings have triggered a flurry of research activity, a number of fundamental issues relating to the role of polymer architecture, molecular weight, ion chemistries etc. remain to be clarified.

In a recent set of studies, we undertook atomistic computer simulations of polymerized ionic liquids to identify the mechanisms underlying ion transport in such systems. Our first study considered pBvIm$^+$-PF$_6^-$ polymerized ionic liquid, in which the ion-transport mechanism was traced to ion hopping among transient association states involving, most often, four cations (Im$^+$) and two polymers [217]. In subsequent reports, we studied a number of related issues including the influence of molecular weight of the polymerized ionic liquid [147], varying Im$^+$-linker lengths [148] of pendant polymerized ionic liquids, and role of counterion chemistry [149] on the mechanisms of ion transport and the correlations between anion mobility and the underlying relaxation time scales.

While the above studies have contributed insights on the properties of polymerized ionic liquids, it is not evident if the ion-transport mechanisms deduced in our work extend to other polymerized-ionic-liquid architectures. Recently, backbone-embedded polymerized ionic liquids are garnering attention for their superior ion-transport properties [39, 85]. Segalman and cowork-

ers reported a 10-fold-increase in $T_g$-independent conductivity for a backbone polymerized ionic liquid compared to a chemically similar pendant polymerized ionic liquid [85]. Miller and coworkers reported similar observations in a gel-polymer electrolyte [39]. It was speculated that the increased conductivity was due to ionic percolation, which has been shown to raise conductivity and induce decoupling [58, 120, 122, 308].

Motivated by the above reports, in this study, we use atomistic molecular dynamics simulations to probe the ion-transport properties and mechanisms in a set of backbone polymerized ionic liquids. The simulation methodology, is presented first, followed by details on the conceptual and mathematical bases for quantifying ion association and transport. Results are presented and discussed, with special attention devoted to the differences seen among backbone polymerized ionic liquids in the context of coordination and ion-hopping measures. Ultimately, despite these differences, the diffusivity of backbone polymerized ionic liquids is shown to be correlated to similar relaxation time scales identified in our previous studies.

## 6.2 Simulation Details

Molecular dynamics simulations were run on systems of 16 polymers and 256 bistrifluoromethylsulfonylimide ($TFSI^-$) using the LAMMPS software package [206, 243]. Molecular dynamics was carried out in the isothermal-isobaric ensemble using the equations of motion of Shinoda et al. [279], which combine the Nosé-Hoover thermostat [207] and Parinello-Rahman barostat

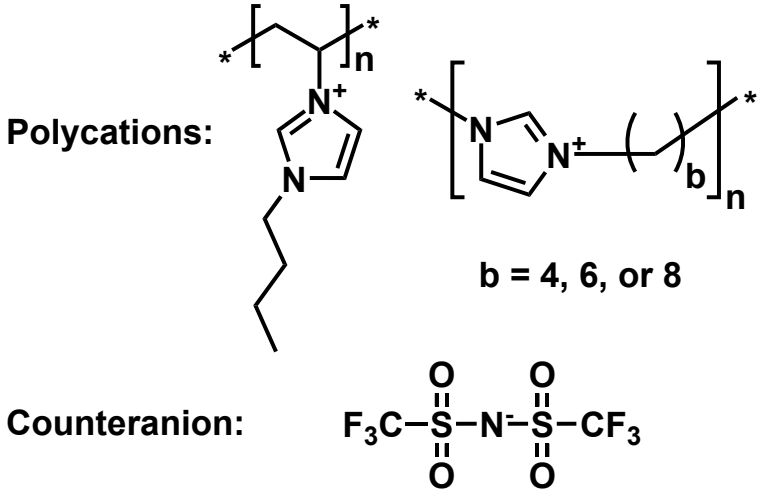


Figure 6.1: Chemical compositions of polymerized ionic liquids in this study: $n = 16$.

[238] with a time-integration scheme closely following that of Tuckerman et al. [314] using a 1.0 fs timestep.

This study covers three backbone-embedded, imidazolium-based polymerized ionic liquids with four, six, and eight methylene spacer units ($b = 4,\ 6,$ and 8, see figure 6.1). A pendant polymerized ionic liquid, poly(1-butyl-3-vinylimidazolium) ($pBvIm^+$), is also evaluated within certain analysis frameworks, based on trajectories obtained in an earlier study [149]. We utilized the all-atom optimized potential for liquid simulations (OPLS) force field [145] and the work of Sambasivarao and Acevedo [254] to collect potential-energy parameters.

We note that accurate modeling of ionic liquids and polymerized ionic liquids require the use of polarizable force fields. However, such methodolo-

gies are computationally expensive for ionic liquids, and become even more magnified for atomistic modeling of polymerized ionic liquids because of their slow relaxation timescales. As an alternative, it has been suggested that charge transfer phenomena can be qualitatively captured as an "average effective description of polarization" [79] by using constant scaled partial charges. This technique purportedly reproduces structural and dynamic properties for isotropic ionic liquids [19, 54, 183, 294, 351, 352]. Motivated by such developments, we have adapted a similar approach for polymerized ionic liquids by borrowing vacuum-phase partial charges from the compilation of Sambasivarao and Acevedo [254], and then scaling by a factor of 0.8 for evaluating the Coulombic potential energy.

Our previous studies on polymerized ionic liquids were effected at temperatures of 500-600 K [147–149,217]. However, in the context of the backbone polymerized ionic liquids we investigated, our preliminary results indicated extremely low ion mobilities in such a range of temperatures. As such, we were forced to probe higher temperatures of 750-850 K to reach the diffusive regime within reasonable limits for atomistic molecular dynamics simulations. We speculate that the quantitative discrepancies in mobility between experiments and simulations result from the lack of explicit polarization in the potential field, and/or from the use of generic force field parameters from the OPLS database, which are not optimized for use with these specific polymerized ionic liquids. Furthermore, to account for the departure from earlier simulation results, we highlight the use of unfitted partial charges, which diverged

from the methods our earlier studies, where we fit partial charges from the electrostatic potential of a monomer or dimer [147–149,217]. Since addressing these various effects requires a much more concerted effort, and since qualitative trends are not expected to be influenced by these differences, we opted to probe, within the context of the adopted force fields, the mechanisms of ion transport in backbone polymerized ionic liquids.

## 6.3 Results and Discussion

In Figure 6.2, we display the $TFSI^-$ self-diffusivity as a function of temperature and spacer length. As discussed earlier, the diffusivities were exceedingly low within the range of temperatures probed in the experiments, forcing us to probe high temperatures of 750-850 K to extract meaningful ion mobilities. Two trends are evident in the displayed results. First, as expected, the ion mobilities are seen to increase with an increase in temperature. More pertinently, we observe that the anion diffusivities decrease with increasing backbone spacer length. For the rest of this article, we focus on the latter result and seek to identify the ion coordination and transport mechanisms underlying such trends.

In Figures 6.3(a)-(c), we display the results for the coordination features in the backbone systems as a function of the backbone spacer length and compare with the results for a pendant polymerized ionic liquid system (labeled as $p = 6$). Figure 6.3(a) considers the ionic coordination characteristics corresponding to the number of cations ($N_I$) to which an anion is coordinated.

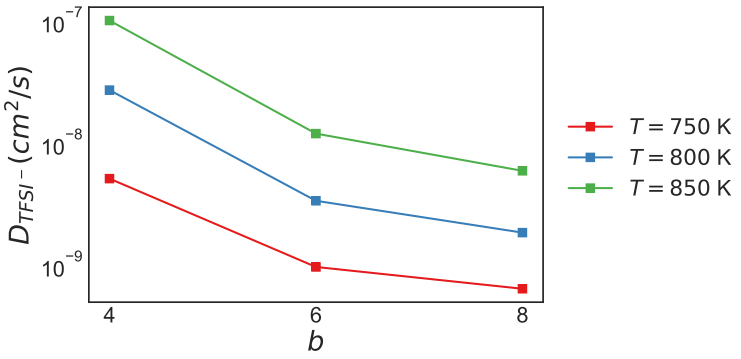


Figure 6.2: $TFSI^-$ self-diffusivity as a function of spacer length, $b = 4, 6, 8$.

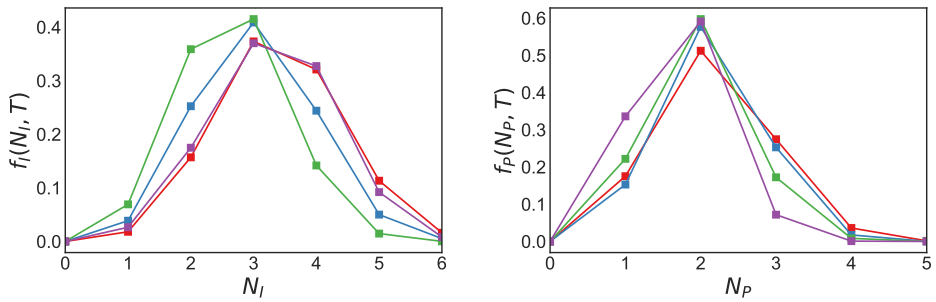


(a) Ionic coordination.

(b) Polymer coordination.

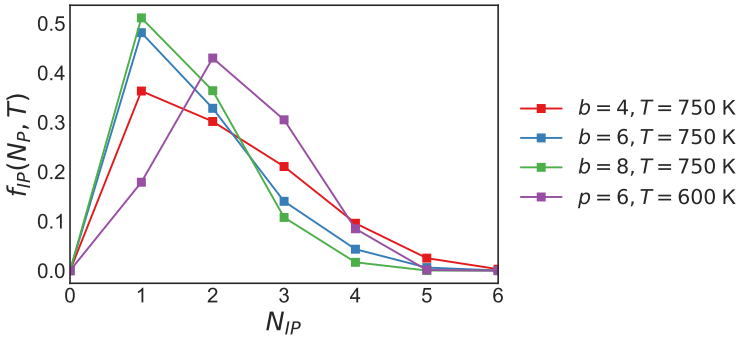


(c) Intrapolymeric ionic coordination.

Figure 6.3: Relative probability of $TFSI^-$- $Im^+$ ($N_I$), polymer ($N_P$), or intrapolymeric $Im^+$ ($N_{IP}$) coordination number at temperature $T$ for backbone polymerized ionic liquids and pendant polymerized ionic liquid $pBvIm^+$-$TFSI^-$.

The results presented therein reveal that, for $b = 8$, there is a pronounced peak in $N_I$ at two and three coordinated ions. As we transition to $b = 6$, coordination is displaced from $N_I = 1, 2$ to $N_I = 4, 5$, with $N_I = 3$ remaining the most probable state. We speculate that the shift in the distribution with respect to $N_I$ arises from two effects: 1) the reduction of methylene units per monomer, and 2) a simultaneous increase in the overall density. These two effects bring ionic groups closer together, increasing the probability for higher $N_I$ states. The result for $b = 4$ lies at even higher $N_I$, and almost overlaps the distribution observed for the pendant polymerized ionic liquid. Such an observation is surprising since the pendant polymerized ionic liquid has an additional two methylene units per monomer, and also exhibits lower density. By the reasoning advanced when rationalizing the transition from $b = 8$ to 6, such factors should suggest that the distribution of $N_I$ should shift *lower*. While we do not have a conclusive explanation of the result for pendant systems, we speculate that morphological features such as the organization of polymerized ionic liquids in ionic domains may underlie such an observation [58, 120, 122, 308].

The polymer-coordination ($N_P$) distribution displayed in Figure 6.3(b) is seen to be relatively insensitive to the backbone spacing. In contrast, the intrapolymeric ionic coordination number ($N_{IP}$, Figure 6.3(c)) displays the starkest contrast between the backbone and pendant cases, with the maximal probability state as *one* $\mathrm{Im}^+$ for the backbone polymerized ionic liquids, compared with *two* for the pendant polymerized ionic liquid. The backbone polymerized ionic liquid $b = 4$ has a lower probability for $N_{IP} = 1$, and a

probability distribution that is noticeably smeared to higher $N_{IP}$, while the $b = 6$ and 8 cases have a higher maximum probability peak at $N_{IP} = 1$ and have quite similar distribution shapes. Comparison between $b = 6$ and 8 reveals that the decrease in $N_I$ likely results from decreasing density, since the probability distribution for $N_{IP}$ does not change considerably, i.e. the same number of monomers from the same polymer tend to associate with a given $TFSI^-$. However, longer distances between adjacent monomers, resulting from adding methylene units, may play a substantial role in lowering $N_I$ from $b = 4$ to 6. For the pendant polymerized ionic liquid, the peak at $N_{IP} = 2$ suggests that paired intramolecular cations are prevalent.

The results for the intrapolymeric ionic coordination number suggest a possible explanation for the dependence of ionic mobility on the backbone spacing. Specifically, in our previous studies [147,217], we have established the importance of the intramolecular mode of ion hopping (type 1) in polymerized ionic liquids in influencing the ion mobilities. By comparing the results in Figure 6.3(c) for the pendant and backbone polymers, one may hypothesize that the coordination characteristics in pendant systems, involving pairs of monomers from the same chain, lends itself to a larger extent of intramolecular hopping (type 1). In contrast, the peak at $N_{IP} = 1$ for backbone polymerized ionic liquids is likely consistent with limited type 1 hopping frequency, and thereby increased participation of type 2 hopping, potentially leading to an increase in the ion-association timescales and lower anion mobilities. Further, among the different backbone systems, we observe that the distribution of $N_{IP}$

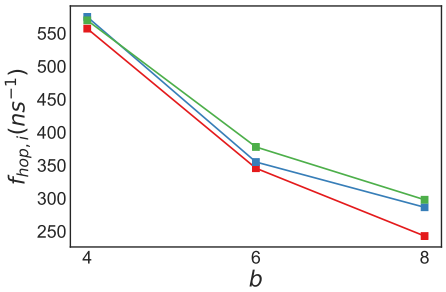


(a) Type 1 hopping frequency.

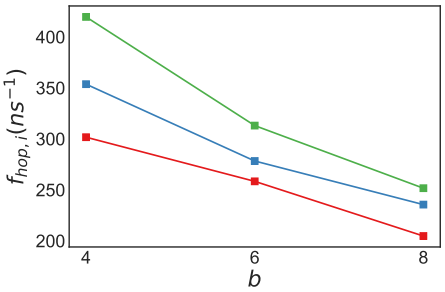


(b) Type 2 hopping frequency.

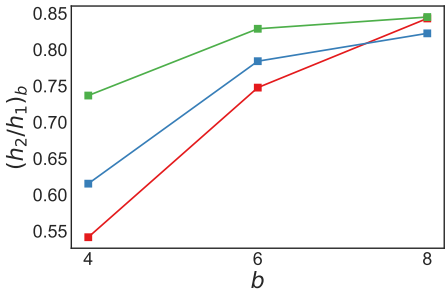


(c) Type 2 to type 1 hopping ratio: backbone spacer.

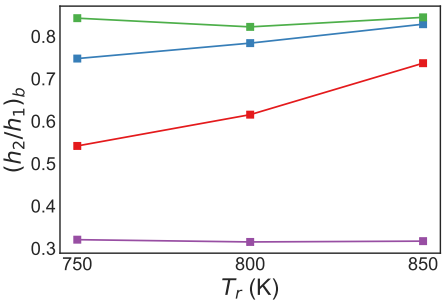


(d) Type 2 to type 1 hopping ratio: temperature.

Figure 6.4: Ion-hopping behavior for backbone polymerized ionic liquids and pendant polymerized ionic liquid pBvIm$^+$-TFSI$^-$. (a)-(c) Legend matches figure 6.2: $b = 4$ (red), $b = 6$ (blue), $b = 8$ (green). (d) Legend matches figure 6.3: $b = 4$ (red), $b = 6$ (blue), $b = 8$ (green), $p = 6$ (purple). $T_r = T$ for backbone cases, $T_r = T + 250$ K for pendant polymerized ionic liquid.

for smaller backbone spacings ($b = 4$) exhibits a larger extent of coordination involving pairs of cations ($N_{IP} = 2$), and are therefore likely to display a larger degree of intramolecular hopping and therefore faster ion mobilities.

In Figure 6.4(a)-(d), we present results confirming our above proposal and hypothesis. Specifically, Figures 6.4(a) and (b) display results for the numbers of intra ($h_1$) and intermolecular ($h_2$) hopping events and demonstrate that

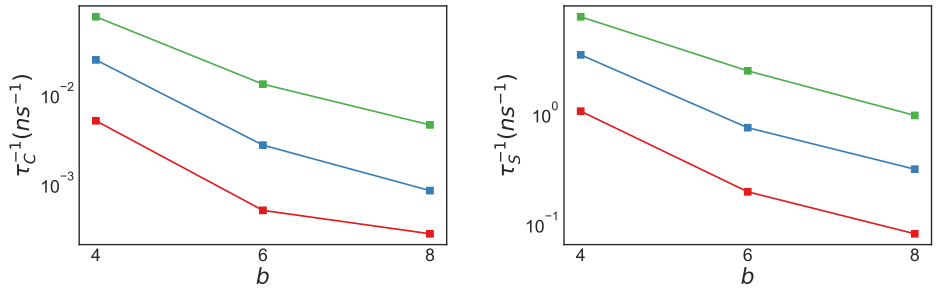


(a) (b)

Figure 6.5: Inverse $TFSI^{-}$-$Im^{+}$ ion-association relaxation time $\tau_C^{-1}$ and lifetime $\tau_S^{-1}$ as a function of spacer length. Legend matches figure 6.2: $b = 4$ (red), $b = 6$ (blue), $b = 8$ (green).

shorter spacer lengths yield higher type 1 *and* type 2 hopping frequencies in backbone polymerized ionic liquids. In Figures 6.4(c) and (d), we explicitly compare the ratio $h_2/h_1$, which reveals that, for backbone polymerized ionic liquids with longer spacers, type 2 hopping contributes more to hopping dynamics. This relative "type 2 participation" rate is also seen to be higher for all of the backbone polymerized ionic liquids when compared with the pendant polymerized ionic liquid in figure 6.4(d), which is also consistent with the intrapolymeric ionic coordination trends in figure 6.3(c).

While the preceding discussion and results demonstrate the influence of intrapolymeric ion coordination on the ion-hopping mechanisms, it still leaves open the question of whether such differences reflect in the relaxation dynamics of ion-associations. To address this, in Figure 6.5(a)-(b), we display the relaxation times $\tau_C$ and $\tau_S$ (equation 2.27) as a function of the backbone spacing. In accord with our expectations, we observe an increase in $\tau_C$ and

$\tau_S$ with increasing spacer length. Such results confirm that the decreased propensity for intramolecular hopping does indeed translate to increased time scales for ion association/dissociation.

In our previous studies, we showed that the ion mobilities of polymerized-ionic-liquid systems exhibit a direct correlation to the ion-association relaxation time scales. Such a correlation was similar to the one observed in the ionic liquid counterparts, and was shown to extend to comparisons involving polymerized ionic liquids with different counterions [149]. Considering the differences in instantaneous coordination and ion hopping in backbone systems, do we still observe a correlation between diffusivity and the ion-association times?

In Figure 6.6 we display the results for the diffusivity as a function of the relaxation time scales $\tau_C$ and $\tau_S$. Therein, we observe that, for the backbone polymerized ionic liquids, a correlation exists between the diffusivity and *both* $\tau_C$ and $\tau_S$. Together, these results demonstrate that the ion-association relaxation time scales, which in-turn are influenced by the relative extent of intra- and intermolecular hopping rates, are responsible for the backbone-spacing dependence of anion mobilities.

## 6.4 Conclusion

In this study, we investigated a set of backbone-embedded polymerized ionic liquids to probe ion-transport mechanisms. The diffusivity of the free anion was seen to decrease when the number of methylene units in the back-

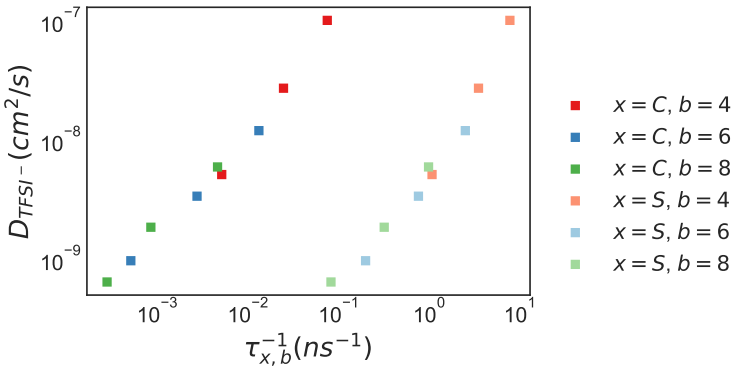


Figure 6.6: Diffusivity in relation to inverse ion-association relaxation time $\tau_C^{-1}$ and lifetime $\tau_S^{-1}$.

bone spacer is increased. In comparing backbone polymerized ionic liquids with their pendant counterparts, significant differences were observed in the intrapolymeric ion coordination characteristics. Such differences were shown to shift the ion-transport mechanisms in backbone polymerized ionic liquids to one in which intermolecular hopping played a more significant role relative to intramolecular hopping. As a result, the ion-association time scales were shown to become larger (slower) for backbone systems, and increased with increasing backbone spacing. However, despite the differences that emerge in coordination and hopping, a correlation exists between $TFSI^-$ self-diffusivity and both ion-association relaxation time $\tau_C$ and the lifetime $\tau_S$. The correlation of diffusivity and $\tau_S$ underscores the importance of managing interaction strength between ionic groups to influence ion-hopping frequency and optimize ion transport in backbone polymerized ionic liquids.

# Chapter 7

# Extending principles of ion motion in polymerized ionic liquids to polymerized zwitterions for battery electrolytes

## 7.1 Introduction

Zwitterions (ZIs) are small molecule ampholytes, or covalently bonded cations and anions, of zero net charge [139]. Their ionic properties and hydrophilicity have made them targets for use in organic electronics, catalysis, battery electrolytes, surfactants, drug-delivery, and anti-fouling coatings, among other applications [71, 139, 270, 357]. ZI-incoporated polymers (polyZIs) have also been investigated as novel materials for chromatography, drug-delivery, self-assembled microstructures, and battery electrolytes [52, 117, 118, 135, 159, 163, 181, 185, 186, 190, 191, 233, 274, 280, 281, 334, 355].

ZI-containing ionogels have shown promise in eliminating the trade-off between mechanical strength and conductivity through non-covalent crosslinking and ion-dissociation [67, 181, 299, 302, 305]. The addition of ZIs to electrolyte formulations also purportedly improves cycling performance, and energy density by increasing Coulombic efficiencies for lithium plating/stripping reactions [46, 339]. Strong dipole effects, induced by charge separation, have

been shown to enable the formation of ZI-salt complexes up to stoichiometric ratios [48, 49, 117, 281, 332]. Furthermore, tuning the interaction strengths between lithium, the counterion, and the ZI groups, have been shown to influence conducting ion concentration, lithium-transference number, and ionic conductivity [45, 46, 49, 67, 102, 185, 191, 295, 297, 298, 345].

A few studies have sought to clarify the fundamental mechanisms underlying ion transport in polyZIs [48, 49, 117, 118, 191]. In this context, a study reported by Ohno and coworkers highlighted a surprising impact of polymer architecture on ionic conductivity [233]. Specifically, they reported ionic conductivity for salt-polyZI blends of lithium bistrifluoromethylsulfonylimide ($Li^+$-$TFSI^-$) with polyZIs composed of imidazolium cationic and triflate-like anionic moieties, arranged in a pendant configuration from the backbone as follows: anion-cation (motif B) and cation-anion (motif C). The ionic conductivity of motif C (figure 7.1, 1) was reported to be of the order $10^{-8}$ S/cm in comparison to a conductivity of $10^{-5}$ S/cm for that of motif B (figure 7.1, 2). Such observations raise the question, "why do polyZIs, with opposite architecture but similar chemical functionality, produce such different conductivities?" We credit the naming convention for motifs B and C to Laschewsky, from a recent review of polyZIs [163].

The work reported in this chapter is motivated by the above-discussed work of Ohno and coworkers. Specifically, we use atomistic molecular dynamics (MD) simulations to probe the ion mobilities, and the underlying structural features, in motifs B and C at various concentrations of $Li^+$-$TFSI^-$ to under-

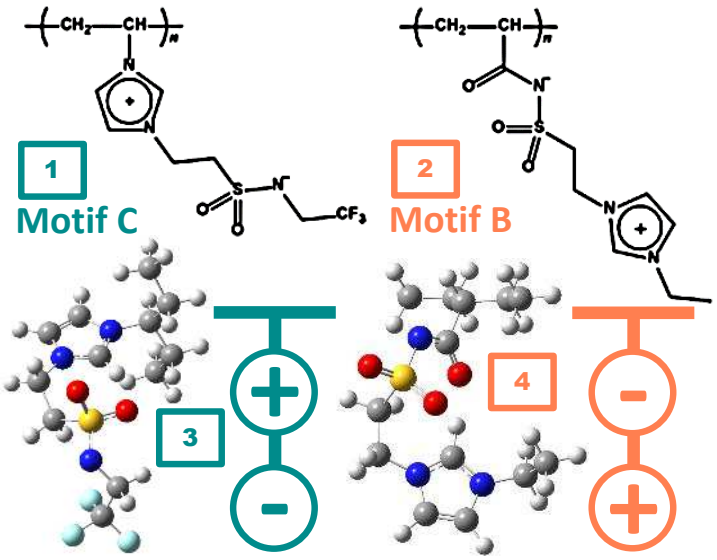


Figure 7.1: Polymer motifs B (2, 4) and C (1, 3) with matching optimized structures from Gaussian16, reference 99. Atom color scheme: Carbon (gray), Fluorine (light blue), Hydrogen (white), Nitrogen (blue), Oxygen (red), and Sulfur (yellow). Image components 1 and 2 adapted and transformed under Creative Commons Attribution 3.0 Unported (CC BY 3.0) License: Hiroyuki Ohno, Masahiro Yoshizawa-Fujita, and Yuki Kohno, "Design and properties of functional zwitterions derived from ionic liquids," Figure 9.

stand the origins of the differences noted in their conductivities. Within such a context, we also seek to clarify the ion-transport mechanisms in salt-doped polyZIs and examine parallels to the physics identified in our recent studies of polymerized ionic liquids [103, 147–149, 213, 215, 217]. We begin by documenting general elements of the simulation and analysis methodology, but much of the detailed coverage can be found in chapter 2. We cover numerous results, including the conductivity, diffusivity, and the radial distribution functions. The latter analysis is used to justify the high mobility of $TFSI^-$ over architecturally comparable $Li^+$. This is followed by reported ion-association relaxation times, and conclusive proof for an alternative ion-transport mechanism for counterions to backbone-adjacent ZI moieties.

### 7.1.1 Simulation and analysis methodology

Shao et al. performed the most extensive set of MD investigations to date on ZI/salt solubility and association phenomena [271–273, 275]. They used the optimized potential for liquid simulations (OPLS), which we deploy in the current context, and has appeared in recent studies on ionic liquids and polymerized ionic liquids [144, 147–149, 217].

Dommert et al. produced a seminal review on polarization phenomena in MD simulations of ionic liquids [79]. Therein, they documented evidence of charge transfer due to orbital overlap, leading to an effective reduction in partial charges. A reduced constant partial charge yields an "average effective description of polarization" [79] that acceptibly reproduces structural

and dynamic properties in ionic liquids [19, 54, 183, 294, 351, 352]. Julian and Jarrold dispelled long-standing objections to the existence of internal charge-separation in gas-phase molecules using quantum chemical models [146]. Early studies by Shao et al. used a non-polarizable potential with partial charges developed from the electrostatic potential map of molecules optimized in a polarizable-continuum implicit solvent [272]. But, they did not include the implicit solvent model in later studies, and instead, optimized molecules in the gas phase [273].

The monomers in our present study were optimized in the gas phase at a B3LYP/6-311++G** level of theory using Gaussian16 [99]. The electrostatic potential was mapped at Merz-Singh-Kollman points, and partial charges were computed using Amber Antechamber and scaled by 0.8, a scaling constant used in previous work to mimic charge transfer and capture average polarization effects in ionic liquids [17,149,283,319,320]. Simulation boxes were packed with polymers of motifs B or C [206], along with $Li^+$-$TFSI^-$ salt in systematically varied fractions relative to polyZI monomers ($r$ $mol_{salt}/mol_{ZI}$). All bonded and LJ interaction parameters were compiled from the LigParGen Server [78, 145]. We utilized the LAMMPS software package for all MD simulations [243]. Forces and positions were evaluated every 1.0 fs at 600 K and 1.0 atm (Nosé-Hoover thermostat, Parinello-Rahman barostat), with LJ and Coulombic pair energies evaluated using equation 2.3 up to a 10 Å cutoff [207,238,279,296,314]. Long-range interactions were evaluated using a Van der Waals tail correction (LJ) and the particle-particle particle-mesh solver with a tolerance of $1 \times 10^{-5}$

(Coulombic) [131, 244].

To render a comparison to the experimental results of Ohno discussed in the introduction [233], we compute the ideal, Nernst-Einstein (NE), conductivities. While we would prefer to capture correlated motion in the true dc conductivity, this requires long simulations and is less statistically reliable [96]. Additionally, since the polyZI charged moieties are polymerized and neutral, they are assumed to play a limited role in conductivity, and their self-diffusivities are not reported. Nor are these ionic moieties included in the calculation for ideal conductivity, for the same reason. Hence, we center the subsequent discussion on the diffusivities of the mobile ionic components, $Li^+$ and $TFSI^-$.

In past studies on polymerized ionic liquids, we established correlations between ion-association relaxation timescales and measures of mobility, including diffusivity and conductivity [147–149, 217]. In particular, the ion-association structural relaxation time $\tau_C$ represents the average time required for two ions to permanently separate from each other. Its foundation lies in the intermittent ion-association autocorrelation function $C(t)$, which quantifies the probability as a function of time of two ions, having been associated at time $t_0$, being associated at time $t_0 + t$.

While $\tau_C$ has proven to be a versatile measure of the fundamental diffusion timescale across various polymerized-ionic-liquid platforms, we expect that it will be insufficient to capture the same timescale for some or all of the ions in this study. This prediction is based on the diversity of local coordi-

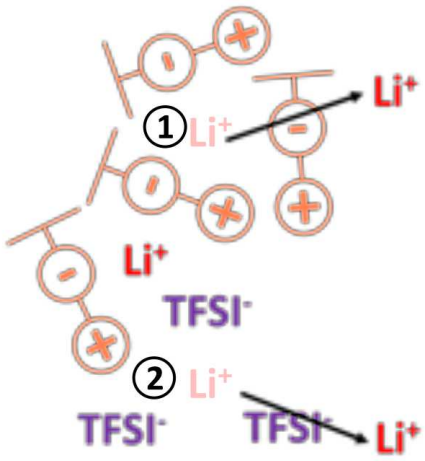


Figure 7.2: Diagram of $Li^+$-$TFSI^-$ in motif B. $Li^+$ is engaged in three coordination states, and two distinct cage relaxation events from starkly different association environments are shown. A similar figure depicting the cage environments of motif C is excluded due to its similarity, but a very similar effect occurs for $TFSI^-$ in that polymer.

nation environments expected in these systems. An illustration in figure 7.2 depicts segregation of ions among environments with i) dense polyZI coordination (1), ii) dense mobile-ion coordination (2), and iii) combined states of varying participation. We craft a "cage relaxation time" to capture an appropriate relaxation timescale for these diverse structures, where ion motion may be due to the combined effect of $ZI^-$ and $TFSI^-$ relaxation from the central $Li^+$ atom, as shown by the arrows for ions 1 and 2. Of particular note, the choice of cage-assignment for $Li^+$ and $TFSI^-$ differs due to the large size discrepancy. Figure 7.2 offers the correct cage definition for $Li^+$: combined coordination with $TFSI^-$ and $ZI^-$. However, because of the small size of $Li^+$, we selected $ZI^-$ as the second coordinating moiety (along with $ZI^+$) to $TFSI^-$. Despite the repelling interaction between $TFSI^-$-$ZI^-$, we expect these ionic moieties to structurally associate via $Li^+$ bridging at longer cutoff distances than the atom-atom interactions underlying oppositely charged coordination.

## 7.2 Results and Discussion

### 7.2.1 Conductivity, diffusivity, and the roles of architecture and interaction strength

Figure 7.3, which plots NE conductivity for motifs B and C as a function of $r$ (number of moles of lithium salt per mole of ZI monomers), shows that the NE conductivity for the B polymer is greater than that of the C polymer. This result is qualitatively consistent with the Ohno experiment discussed in the introduction [233]. At a quantitative level, our simulations indicate a more

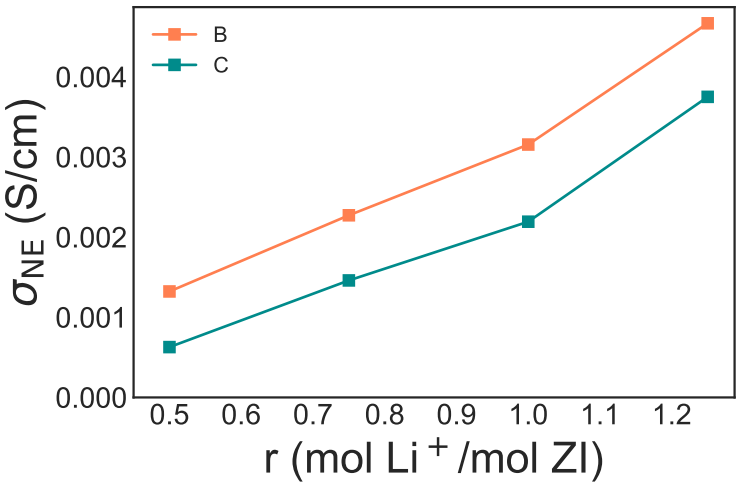


Figure 7.3: Ideal conductivity for motifs B and C at 600 K.

modest difference between the conductivities of the two architectures, compared to the orders-of-magnitude enhancement reported in experiments. We speculate that correlated ionic motion could be an important factor influencing the overall conductivity [103, 215].

We observe that the diffusivities of both $Li^+$ and $TFSI^-$ increase with increasing $r$ in figure 7.4. Such a trend is qualitatively consistent with experiments on polyZIs and for salt-droped polymerized ionic liquids [117], and has been rationalized as a consequence of two factors: i) a reduction in the number of *polymeric coordination centers* for the mobile $Li^+$ and $TFSI^-$ ions; since such polymeric ions (ZIs) possess lower mobilities, coordination of $Li^+$ and $TFSI^-$ ions with such counterions is expected to lower the mobility of the nonpolymerized ions; and, ii) plasticization of the dynamics of the polymer due to the introduction of the small molecule salts [129, 130, 349].

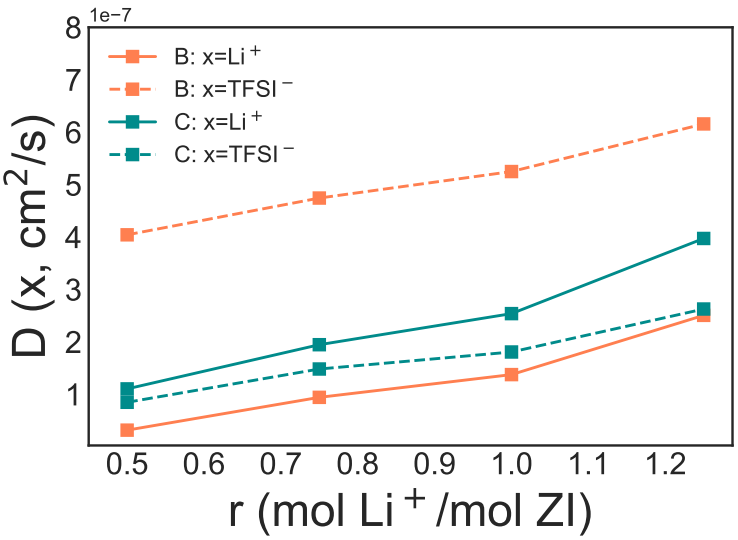


Figure 7.4: Diffusivity of $Li^+$ (solid) and $TFSI^-$ (dashed) for motifs B (orange) and C (blue) at 600 K.

In comparing the diffusivities of the individual ions, we observe that in motif B, $D_{\mathrm{TFSI^-}} > D_{\mathrm{Li^+}}$, whereas in motif C, $D_{\mathrm{Li^+}} > D_{\mathrm{TFSI^-}}$. Such a result can be qualitatively understood based on the position of the oppositely charged ZI moieties relative to the polymer backbone. For each motif, we observe that the species with higher diffusivity is of opposite charge to the ZI moiety that is located at the end of the monomer pendant. Since we expect the ZI groups closest to the backbone to possess lower mobilities than the pendant-end group, $Li^+$/$TFSI^-$ ions that coordinate with the ion closer to the backbone are expected to also possess lower mobilities. When considering only pendant-end group ZI-counterions, $D_{\mathrm{TFSI^-,B}} > D_{\mathrm{Li^+,C}}$. Similarly, for backbone-adjacent ZI-counterions, $D_{\mathrm{TFSI^-,C}} > D_{\mathrm{Li^+,B}}$. From this, we speculate that the mobility of $TFSI^-$ is the most significant contributor to the

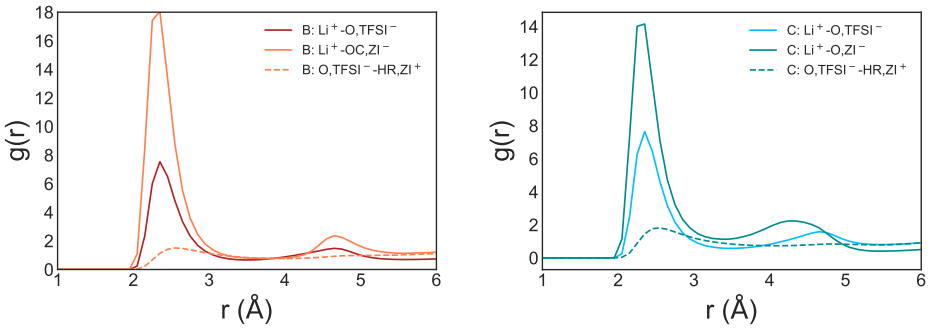


(a) Motif B.

(b) Motif C.

Figure 7.5: Key atomic coordination $g(r)$ curves for various ionic pairs. Specific labeled atomic interactions in the legend are described in section 7.4, along with other important atomic correlations not shown in this figure.

conductivity disparity between the architectures B and C.

The root of this phenomenon is traced back to simple ionic interaction strengths, as quantified using atomic correlation functions. Specifically, figure 7.5 shows the radial distribution functions $g(r)$ for key atomic correlations, which are representative of ionic interaction strengths for the three ion-ion association pairs examined in this study: $Li^+$-$TFSI^-$, $Li^+$-$ZI^-$, and $TFSI^-$-$ZI^+$. We see that the association behavior of $Li^+$ and $TFSI^-$ with the ZI counterions and each other bear no qualitative differences between motifs B and C. The height of the first peak implies the same order of interaction strength for both motifs, from strongest to weakest: $Li^+$-$ZI^-$, $Li^+$-$TFSI^-$, and $TFSI^-$-$ZI^+$.

In our past studies of polymerized ionic liquids, we examined the probabilities of ionic coordination states as a function of coordination number

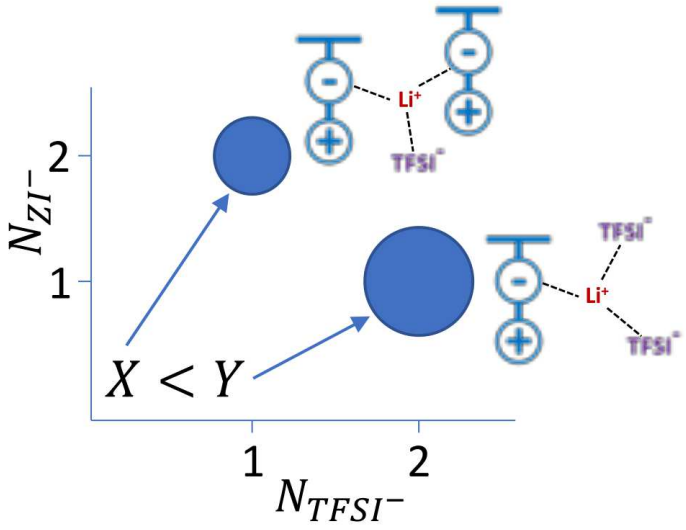


Figure 7.6: Schematic depicting multi-ion coordination states and corresponding probabilities in two-dimensional weighted graphs.

[147–149,217], and identified key aspects of ion-transport mechanisms through such a characterization. Coordination was determined in the present study by direct atomic coordination using cutoff distances informed by the radial distribution functions, such as those displayed in figure 7.5. Due to the multiplicity of ion types engaged in coordination with salt-doped polyZIs, we extend the coordination analysis to two dimensions of variability, with specific reference to coordination involving mobile and polyZI counterions (i.e. $Li^+$ with $TFSI^-$ and $ZI^-$). Figure 7.6 depicts this concept by showing two hypothetical coordination states, $Li^+$ coordinated with two $ZI^-$ and one $TFSI^-$ (state X) or one $ZI^-$ and two $TFSI^-$ (state Y). The size of the circle is used to indicate the relative probability of each state. For instance, in the depicted example, state X is less probable than state Y. For clarity and consistency across all plots,

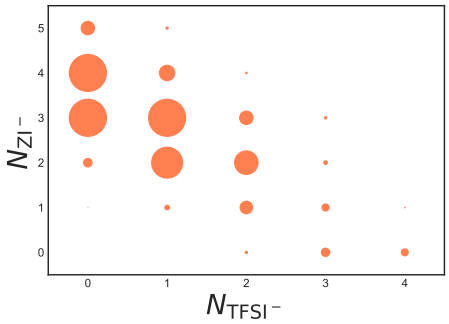


(a) Motif B, $r = 0.5$ molLi$^+$/molZI.

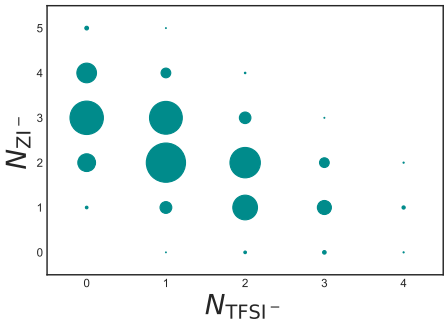


(b) Motif C, $r = 0.5$ molLi$^+$/molZI.

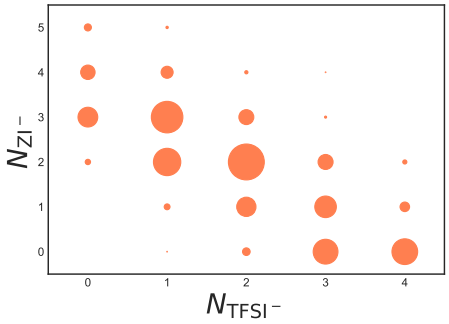


(c) Motif B, $r = 1.25$ molLi$^+$/molZI.

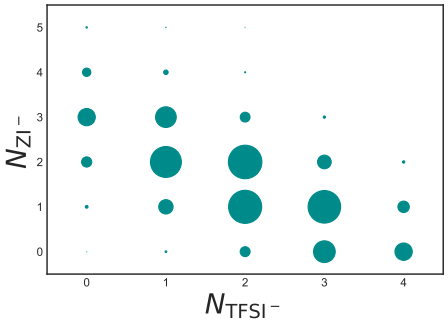


(d) Motif C, $r = 1.25$ molLi$^+$/molZI.

Figure 7.7: Probability of Li$^+$-coordination with TFSI$^-$ and ZI$^-$.

we limit the coordination ranges in the following multi-coordination plots to a maximum of five TFSI$^-$/Li$^+$ and four ZI counterions.

Figure 7.7 shows the two-variable probability distribution of instantaneous Li$^+$-coordination with ZI$^-$ and TFSI$^-$ at $r = 0.5$ mol$_{salt}$/mol$_{ZI}$ and $r = 1.25$ mol$_{salt}$/mol$_{ZI}$. Figures 7.7(a) and (b) show that there are more zero-TFSI$^-$-coordinated Li$^+$ states in motif B, which can be attributed to the orientational exclusion by ZI$^+$ and and the backbone, which bracket ZI$^-$ in the polymer architecture. In motif C, since ZI$^-$ resides at the end of the monomer pendant, we expect Li$^+$ to encounter less structural exclusion, which enables

the enhanced coordination of $Li^+$ with $TFSI^-$.

In figures 7.7(c) and (d), the propensity for $Li^+$ coordination with $ZI^-$, in lieu of $TFSI^-$, in motif B is seen to extend to high-salt-content systems. However, the likelihood of encountering a zero-$ZI^-$-coordinated state actually increases in motif B compared to motif C, which is consistent with the polymer coordination centers "saturating" above $r = 1.0$ $mol_{salt}/mol_{ZI}$. Such results also confirm that the population of higher-mobility $Li^+$ (i.e. $Li^+$associated with $TFSI^-$) grows with increasing salt concentration in both motifs B and C, which supports the monotonic increase of $Li^+$ diffusivity over the same variation.

Does $TFSI^-$ exhibit similar coordination trends, even given its larger size and different shape? First, the results for $TFSI^-$coordination, displayed in figure 7.8, indicate that $TFSI^-$ has a more expansive range of coordination states, including a non-negligible probability of having no coordinated ions (i.e. zero $Li^+$ and $ZI^+$). Additionally, differences between graphs of motifs B and C are more subtle, meaning that structural variations between the two architectures are less pronounced. We attribute such observations to two factors: 1) the low interaction strength between $TFSI^-$ and $ZI^+$, and ii) the bulkiness of $TFSI^-$.

In comparing $TFSI^-$ at low salt concentration in figures 7.8(a) and (b), it has a noticeably higher probability of associating with four or more $ZI^+$ while surrounded by one or fewer $Li^+$ in motif C. This result is complimentary to the $Li^+$-centered data from figure 7.7, since the $ZI^+$ is buried adjacent to the polymer backbone in motif C. Similarly, $TFSI^-$ in motif C associates with more

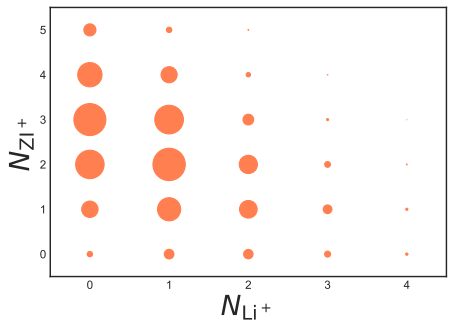


(a) Motif B, $r = 0.5$ molLi$^+$/molZI.

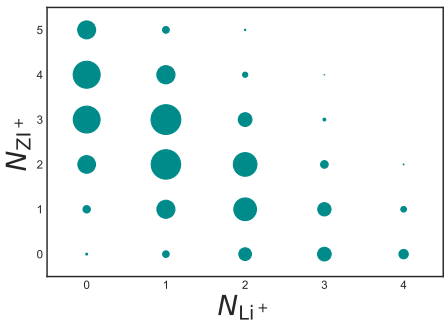


(b) Motif C, $r = 0.5$ molLi$^+$/molZI.

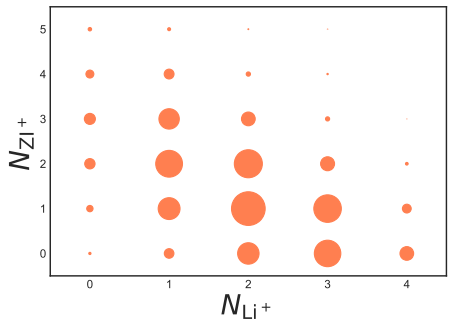


(c) Motif B, $r = 1.25$ molLi$^+$/molZI.

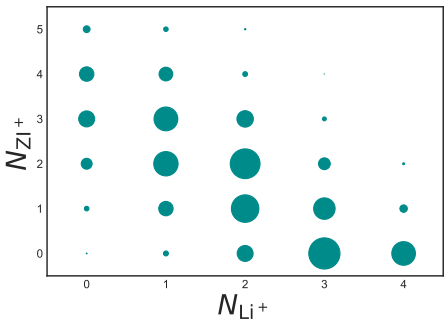


(d) Motif C, $r = 1.25$ molLi$^+$/molZI.

Figure 7.8: Probability of TFSI$^-$-coordination with Li$^+$ and ZI$^+$.

$Li^+$ at low $ZI^+$-coordination numbers and high salt content in figures 7.8(c) and (d), analogous to the saturation effect observed in the $Li^+$-centered data. We have thus shown that each ion, despite differences in size and shape, experience similar coordination phenomena when considering the location of their ZI counterion relative to the polyZI backbone.

### 7.2.2 Cage relaxations and Ion Associations

Can we then explain the high diffusivity of $TFSI^-$ and the low diffusivity of $Li^+$ in motif B, and the reversal seen in motif C, through consideration of relevant time scales? In our past studies on polymerized ionic liquids, which contain only a polymerized pendant cation and a mobile anion, we observed ion hopping via association/dissociation of ion pairs from transient coordination states involving multiple ions and polymers. Recall that $C(t)$ represents the probability that two ions, which were associated at time $t = 0$, are still associated at time $t_0 + t$ [147–149, 217]. Thus, the characteristic timescale of decay extracted from this function, $\tau_C$, quantifies the average amount of time required for a pair of ions to become spatially separated (i.e. no reversible engagement). The anion diffusivities of various polymerized-ionic-liquid systems were found to be correlated with $\tau_C$ [149, 217].

Inspired by these findings, and their applicability in a variety of different systems, we extracted $\tau_C$, displayed in figures 7.9(a) and (b), for counterions $Li^+$ and $TFSI^-$ relative to the backbone-adjacent and pendant-end ZI moieties: $ZI^-$ and $ZI^+$, respectively. Just as in diffusivity, the interaction

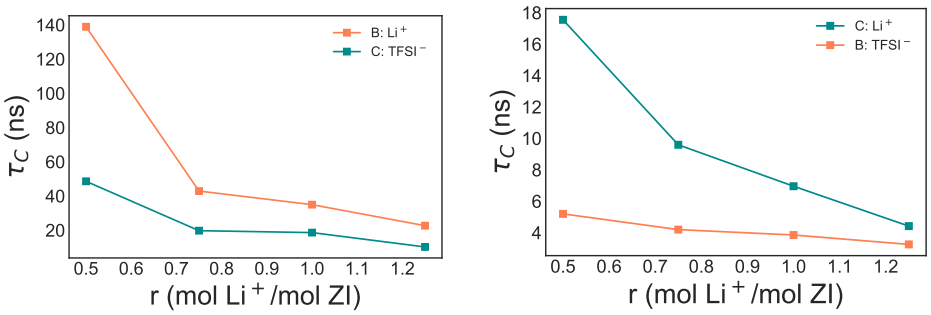


(a) Backbone-adjacent, $\tau_C$.

(b) Pendant-end, $\tau_C$.

Figure 7.9: $\tau_C$ for $Li^+$ and $TFSI^-$ relative to each positional ZI-counterion (backbone-adjacent and pendant-end).

strengths obtained from $g(r)$ support these results, with $TFSI^-$ demonstrating faster relaxation times across all salt concentrations for backbone-adjacent and pendant-end arrangements. The curves in figure 7.9(b) (pendant-end moieties) bear qualitative consistency with the shape and rate of change of diffusivity in figure 7.4. Conversely, backbone-adjacent ions appear to have timescales that are too long. We speculate that such behavior is consistent with the population of highly ZI-coordinated ions (orientational exclusion effect), which have very long timescales for pair relaxation. But we need quantitative proof that $\tau_C$ does not capture the underlying diffusion timescale for these backbone-adjacent counterions to confirm our hypothesis.

We offer such proof in figure 7.10, which shows the diffusivity plotted as a function of $\tau_C$. The triangle symbols, representing the curves for counterions $Li^+$ and $TFSI^-$ of pendant-end ZI moieties, appear to fall in a general correlation. However, the square symbols, for counterions to backbone-adjacent ZI

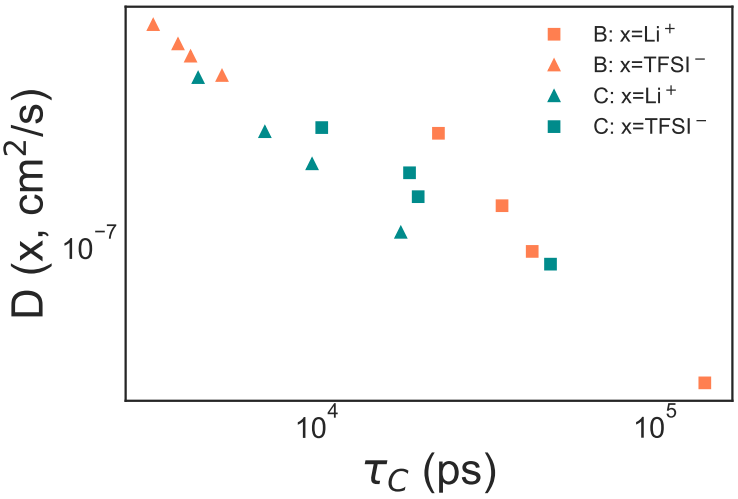


Figure 7.10: Diffusivity versus ion-association timescale $\tau_C$.

moieties, clearly lie at timescales that are too high to follow the same trend. The cage relaxation time, proposed earlier, produces a reduced timescale due to the influence of two factors: i) all ions (not just highly ZI-coordinated ions) contribute equally, and ii) fractional dissociation removes the influence of the longest lasting ion pairs.

We begin in figure 7.11(a) by showing $\tau_{cage}$, similar to $\tau_C$ in figure 7.9(a), for the counterions of backbone-adjacent ZI moieties. These curves are radically different than their $\tau_C$ counterparts, especially showing much lower timescales, as sought and predicted. By replacing $\tau_C$ with $\tau_{cage}$ for these ions, the physical basis of our hypothesis appears to be confirmed. Figure 7.11(b) incorporates diffusivity versus $\tau_{cage}$ for the square symbols (backbone-adjacent ZI counterions). We then see that a generalized trend emerges across all counterion/motif combinations.

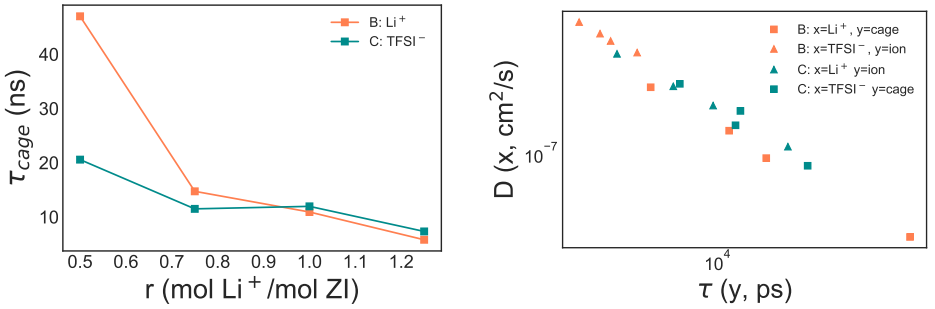


(a) $\tau_{cage}$ for $Li^+$ and $TFSI^-$ relative to each backbone-adjacent ZI-counterion.

(b) $TFSI^-$ and $Li^+$ diffusivity correlated across ion-association and cage relaxation timescales.

Figure 7.11: Investigations into the applicability of the cage relaxation timescale.

We return to the coordination probabilities to rationalize the above observation. The bracketing of the backbone-adjacent ZI moiety by the ZI counterion and the backbone reduces the degrees of translational freedom for certain mobile counterions that are "trapped" in coordination with these ZI moieties. This leads to a general reduction in the relaxation timescale underlying diffusion for the affected species. This effect stems from the same organizational exclusion effect identified in the coordination plots, while the saturation effect, from the same analysis, reveals the presence of non-ZI-coordinated ions, which are expected to have higher mobility. This population of ions lowers the diffusion timescale below the naively computed ion/ZI-counterion structural relaxation time. Thus, the cage relaxation time emerges as an alternative timescale for diffusion of the counterions to these buried ZI moieties.

To summarize our findings presented in this section: the characteristic timescale for $Li^+$ or $TFSI^-$ diffusion is shown to depend upon the *location of*

*their ZI-counterion* relative to the polymer backbone. When the polymerized counterion is adjacent to the backbone, the cage relaxation time $\tau_{cage}$ serves as the underlying diffusion timescale. The cage formulation amplifies the contribution of the lightly-ZI-coordinated ions into the timescale average, capturing the influence of fast cage relaxations on mobility. For the opposite configuration, the ZI ion located at the end of the pendant, local coordination is more homogeneous and has lower association counts. This homogeneity returns the simple ion-association relaxation time to the fundamental diffusion timescale. As a result, the physics of ion mobility aligns with that of polymerized ionic liquids from past studies [149].

With respect to the results presented in Figure 7.4, $TFSI^-$ diffuses faster than $Li^+$ in motif B because the relaxation time of $TFSI^-$-$ZI^+$ associations is lower than the relaxation time of $TFSI^-/ZI^-$-cages for $Li^+$. Even with fast-relaxing $Li^+$-$TFSI^-$ complexes, the diffusivity is depressed by the slow relaxation of high-$ZI^-$-content cages. Conversely, the diffusivity of $Li^+$ in motif C is higher than that of $TFSI^-$ because the relaxation time of $Li^+$-$ZI^-$ association is lower than that of $ZI^+/ZI^-$-cages for $TFSI^-$. This stems from the slow relaxation of the polymer backbone and the pendant-end $ZI^-$, which limits $TFSI^-$ mobility despite the still-weak $TFSI^-$-$ZI^+$ interactions.

## 7.3 Conclusion

In summary, we used atomistic computer simulations to probe the influence of macromolecular architecture on ion diffusivities and underlying time

scales in salt-doped polyZIs. Our results indicate that ion diffusivity is faster in polyZIs of architectural motifs B ($TFSI^-$) or C ($Li^+$) when the ZI counterion is located at the end of the pendant. The underlying timescale for transport of those respective ions was shown to be the ion-association relaxation time $\tau_C$ for $Li^+$-$ZI^-$ and $TFSI^-$-$ZI^+$ pairs. In contrast, the slower ion, whose ZI counterion is adjacent to the backbone, has a different underlying timescale, since these ion-ZI association pairs relax too slowly to predict mobility relative to that of the pendant-end counterparts. The cage relaxation timescale increases the contribution of low-ZI-coordinated ions to the average relaxation time by equally weighting the contribution of each ion, rather than each pair of associations.

Ultimately, materials of motif B, despite the higher conductivity reported in experiment, may not provide the ideal platform for designing lithium-ion batteries due to the lower $Li^+$ ion mobilities. Our results suggest that optimization efforts for $Li^+$ transport might target the reduction of $Li^+$-$ZI^-$ interaction strength of motif C to improve $Li^+$ diffusivity and ionic conductivity.

## 7.4 Coordination and ionic relaxation analyses

### 7.4.1 Local coordination

Local coordination behaviors of $Li^+$ and $TFSI^-$ ions assist in quantifying interaction strengths among ionic components. Such information is succinctly captured by the radial distribution function. The strongest $g(r)$ peaks are chosen and shown in figure 7.5. The corresponding atomic interactions are

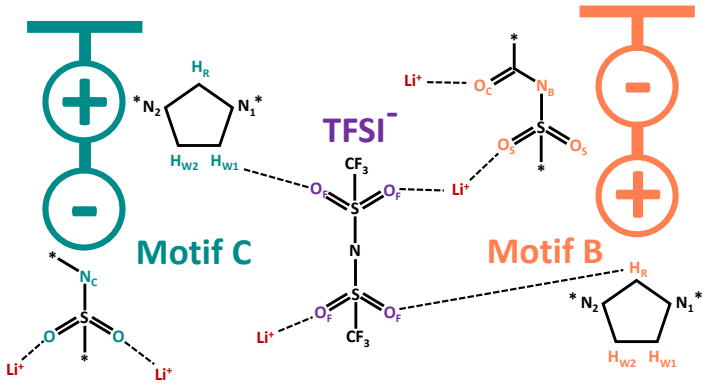


Figure 7.12: Four ionic moieties of interest in this study: $Li^+$ (red), $TFSI^-$ (purple), and motifs B (orange) and C (blue). Preferred associations shown by dotted lines.

identified with dotted lines in figure 7.12 and summarized below. Consider sets of whole-molecule identifiers for $Li^+$ and $TFSI^-$, $m_1 = m_2 = \{1...N\}$, while, unit-specific polyZI moieties are given assignments $u_1 = u_2 = \{1...M\}$ for cations and anions, respectively. Three ion-association pairs are relevant for this work:

1. $p_1 = (m_1, u_2)$ ($Li^+$-$ZI^-$)
2. $p_2 = (m_2, u_1)$ ($TFSI^-$-$ZI^+$)
3. $p_3 = (m_1, m_2)$ ($Li^+$-$TFSI^-$).

To develop a method of identifying association pairs, we turn to the atomic $g(r)$ presented in the first subsection of results. The following guidelines establish coordination pairs in the current framework.

1. $p_1$, $Li^+$-$ZI^-$: $Li^+$ interacts through the sulfonamide oxygen ($O_S$) and nitrogen ($N_{B/C}$) atoms in each motif, and the oxygen possesses the higher peak. The acyl oxygen ($O_C$) of motif C provides an extra association point for that system. Approach of $Li^+$ within 3.0 Å of any of the above atoms signals $Li^+$-$ZI^-$ coordination.

2. $p_2$, $TFSI^-$-$ZI^+$: Imidazolium hydrogen $H_R/H_{W1/W2}$ interact with $TFSI^-$ oxygen $O_F$. Approach of $O_F$ with 3.5 Å of any imidazolium hydrogen signals coordination of the respective $TFSI^-$ and $ZI^+$.

3. $p_3$, $Li^+$-$TFSI^-$: $Li^+$ interacts negligibly with nitrogen and fluorine atoms in $TFSI^-$, but strongly with oxygen atoms ($O_F$). Approach of $Li^+$ within 3.0 Å of any $O_F$ signals coordination of the respective ions.

The $g(r)$ results highlight the weakness of $TFSI^-$-$ZI^+$interactions compared to their $Li^+$-$ZI^-$ counterparts.

### 7.4.2 Definitions and development of cage relaxation time

In order to quantify cage relaxation time $\tau_{cage}$, we must first define a cage and describe when it has "dissolved." First, we assume that a cage is best described by the closest large components in "association" with a mobile ion. We make this generalized distinction for the following reason. Polymer components, specifically $ZI^+$ and $ZI^-$ groups, are considered as cage restraints for $TFSI^-$ and prevent displacement beyond the cage boundary. $Li^+$, because of its small size, cannot be considered in such a manner. However, $Li^+$ cage

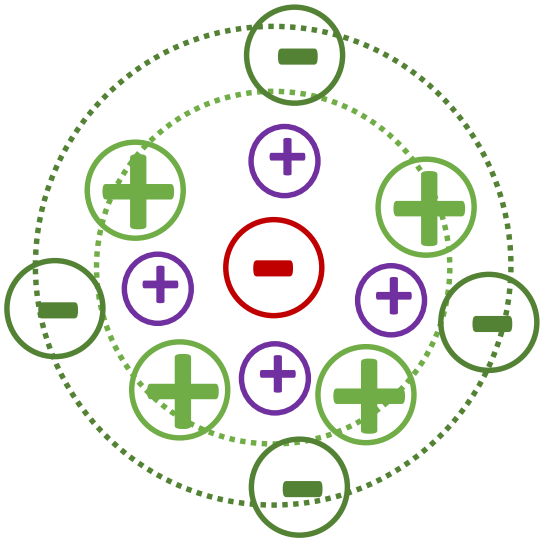

Figure 7.13: Diagram of eight associated ZI cations (dark green) and anions (light green) inside of their respective association shell relative to the central $TFSI^-$. The $Li^+$ (purple) are bridging ions to the ZI anions, but are not explicitly considered in cage definition.

relaxation is assumed to be controlled by $ZI^-$ and $TFSI^-$ itself, allowing us to construct cages using previous association rules. Figure 7.13 shows the key elements of the $TFSI^-$ cage for clarity. We selected the natural ion-association cutoff distance for $TFSI^-$-$ZI^+$ (inner dotted line), and an artificial "cutoff" distance of 5.5 Å for association with $ZI^-$, based on trial and error testing of the fractional cage decay.

For $TFSI^-$ cages, the value of $f_{cut}$ is chosen to be 1/3, while for $Li^+$ cages, it is chosen to be 1/2. What do these numbers mean, in a physical sense? For cage dissolution of $TFSI^-$,

1. Three or fewer ions: all ions must dissociate,
2. Four to six ions: all except one ion must dissociate,
3. Seven to nine ions: all except two ions must dissociate, etc...

A similar analysis can be conducted on the $Li^+$ value. These choices can be generally understood to mean that $Li^+$-cages, formed by direct association of ionic species, break up "earlier" than $TFSI^-$- -cages, whose indirect components may relax away sooner than the cage structure has truly relaxed.

# Chapter 8

# Prospects for the future of the field

## 8.1 Mesoscale modeling using hydrodynamic models to probe complex systems

While atomistic molecular dynamics is a powerful technique, it is length- and time-scale-limited due to the computational expense of explicitly modeling each atom. The Ganesan research group and others have used mesoscale models, including single-chain in mean field simulations [68, 267], to model the phase separation of block-copolymers. The details of this method are available from a large number of studies [68–70, 74, 75, 223, 240]. For charged-polymer systems, additional care must be taken to incorporate electrostatic energies [172,246,321], which is not trivial in application. The accuracy of such methods may suffer if local dielectric fields are not solved self-consistently, but this approach greatly increases the computational expense of the method.

We propose that the hydrodynamic modeling method, dissipative particle dynamics, could serve as an alternative to this and other mean-field approaches. In this section, the fundamentals of dissipative particle dynamics are presented, particularly as it relates to modeling specific chemical features in phase-separating mixtures. We conclude with a list of open questions and continuing research objectives.

### 8.1.1 Background on dissipative particle dynamics

Hoogerbrugge and Koelman introduced dissipative particle dynamics (DPD) as a hydrodynamic simulation method to combine molecular dynamic and lattice-gas automata methodology, retaining advantages and shedding disadvantages from each approach [132,154]. DPD was shown to be fully isotropic and Galilean invariant, while being capable of modeling complex fluids and geometries at small length- and large time-scales. Español and Warren (1995), followed by Groot and Warren (1997), established DPD as a model with proper statistical mechanics, specifically in the canonical ensemble, or constant number of particles, volume, and temperature (NVT) [84, 116]. From this framework, DPD simulations produce a Gibbs-Boltzmann distribution at equilibrium, allowing for the use of standard thermodynamic relations in calculating quantities such as temperature and pressure [116].

While ordinary NVT molecular dynamics methods simulate systems in the canonical ensemble, DPD preserves hydrodynamics, which has been shown to anneal defects into ordered mesophases [109]. Specifically, without hydrodynamic movement, a system undergoing phase separation can become frozen in a local minimum-energy configuration. Hydrodynamic movement eliminates topological defects, accessing the global energy-minimum configuration and proper equilibrium structural morphology [109].

The dissipative-particle-dynamics approach uses the following set of

equations to evaluate forces on off-lattice particles.

$$\overrightarrow{f} = \left(F^C + F^D + F^R\right)\overrightarrow{r_{ij}} \tag{8.1}$$

The force exerted in the direction of a pairwise unit displacement vector between two particles ($\overrightarrow{r_{ij}}$) manifests as the sum of a conservative ($F^C$), dissipative ($F^D$), and random ($F^R$) contribution of the forms below.

$$F^C = a_{ij} w(r) \tag{8.2}$$

$$F^D = -\gamma w^2(r)\left(\hat{r_{ij}} \cdot \overrightarrow{v_{ij}}\right) \tag{8.3}$$

$$F^R = \sigma w(r) \alpha \Delta t^{-1/2} \tag{8.4}$$

The parameter $a_{ij}$ is the maximum repulsion between particles $i$ and $j$ and the weighting function $w(r)$ is a dimensionless, non-negative function that disappears outside of the cutoff radius $r_c$.

$$w(r) = 1 - r/r_c \tag{8.5}$$

The variable $\alpha$ is a Gaussian-distributed random variable with zero mean and unit variance and $\Delta t$ is the time step of the simulation. Groot and Warren note that the use of this $\Delta t^{-1/2}$ factor precisely generates the step-size dependence of the random force [116]. Español and Warren derived the associated Fokker-Planck equation,

$$\partial_t \rho \equiv \mathcal{L}_C \rho + \mathcal{L}_D \rho, \tag{8.6}$$

where $\mathcal{L}_C$ and $\mathcal{L}_D$ are the conservative- and dissipative-Louiville operators, as defined by Español and Warren [84]. The canonical ensemble is the solution

to $\mathcal{L}_C\rho_{eq} = 0$, where $\rho_{eq}$ is the equilibrium density. Therefore, to achieve statistical mechanics corresponding to the canonical ensemble, $\mathcal{L}_D\rho_{eq} = 0$ emerges as a requirement. Thus, we obtain the fluctuation/dissipation theorem for DPD, which is consistent in form with that of Brownian motion [84],

$$\sigma = \left(2k_BT\gamma\right)^{1/2}. \tag{8.7}$$

The squared weighting function of equation 8.3 likewise emerges from this constraint. Equation 8.7 establishes the temperature in terms of the relative magnitudes of the random and dissipative interactions. Finally, Español and Warren establish a physical basis of the time step, showing that increasing time step leads to increasing departure from equilibrium results [84].

Groot and Warren built upon these insights by analyzing the thermodynamic basis of the model. Therein, they developed a simple scaling relation, which establishes a link between the maximum-repulsion parameter $a_{ij}$ and the Flory-Huggins $\chi$-parameter [116]. This permits DPD simulations to investigate chemical-specific interactions, opening the door for a range of new applications of DPD methodology. They also pioneered the use of a modified velocity-Verlet algorithm to advance the set of positions and velocities, known as the Groot-Warren velocity Verlet (GW-VV) algorithm. This integration scheme includes a simple modification upon classic molecular dynamics velocity Verlet (MD-VV), but is dependent upon proper selection of the tuning parameter $\lambda$, which alters the step change in velocity before evaluating the forces [116].

Velocity Verlet schemes, including MD-VV, GW-VV, and so-called DPD-VV (includes dissipative force correction) have been scrutinized and compared with self-consistent (SC) methods for performance and accuracy [18, 235, 318]. Alternative integrator schemes, including operator splitting and MD-VV with Andersen thermostating, have also been developed and tested against DPD-VV and SC benchmarks for model systems [190, 228, 277]. In particular, the so-called Shardlow-splitting algorithm (SSA) has gained traction, and was extended by Lísal et al. for use in constant-temperature DPD simulations with unequal-mass particles [182].

### 8.1.2 Future work and open questions

At a fundamental level, this methodology has not been deployed to predict the morphologies of polymerized-ionic-liquid block-copolymers. Therefore, the first step is to validate such a model against experimental morphologies by constructing a phase diagram and comparing it to studies such as that of Gao et al. [105], which shows a simple phase diagram distinguishing qualitative phases, including isotropic solution, hexagonal, lamellar, and solid, with respect to ionic-liquid concentration. Along with qualitative agreement in shape formation, one might also be interested in validating domain sizes, such as lamellar domain width or cylindrical domain diameter, which could be important measures for quantifying conductivity-morphology relationships.

Ganesan provides some context for the open questions related to ion transport in phase-separated materials [103]. In particular, the relationship

between conductivity and morphology, mentioned above, is largely unexplored, with a few notable exceptions [211,340,342]. For example, Sanoja et al. studied the effect of lamellar domain spacing on conductivity in a polystyrene-(polymerized-ionic-liquid) block-copolymer [258]. In a 2015 review on this topic, Meek and Elabd provide some commentary on polymerized-ionic-liquid block-copolymer synthesis [210], which is worth reviewing for those interested in exploring this topic.

Understanding of the role of morphology in ion-transport phenomena is largely missing for polymerized-ionic-liquid copolymer materials. Therefore, we may ultimately aim to convert the morphological result from dissipative particle dynamics into an atomistic or transport-fitted coarse-grained framework. Work from our group, to be published soon after this dissertation, has explored this topic in some detail. One of the key challenges in this approach is finding the right length scale for the full simulation. We must balance the speed or computational requirement of the simulation with the need to probe large enough domain sizes in phase-separated materials.

There also needs to be a quantum leap forward in the availability and quality of analysis techniques for non-isotropic, phase-separated systems. Our upcoming publication on this topic uses concepts pioneered by Sethuraman et al. [266,267] to analyze structure and ion transport in biphasic block-copolymer systems where ions preferentially segregate into one phase. For example, local dynamic properties were extracted from the mean-squared displacement, residence-time autocrrelation function, and polymer-dihedral autocorrelation

function and segregated into "near the interface," in the "bulk of the salt-rich domain," and "between the bulk and the interface" [266]. In addition, structural properties such as the local radial distribution function and chain-coordination number were employed to provide further insight [266, 267].

We observed ion transport occurring through a "climbing the ladder" mechanism in polymerized ionic liquids in the simulation studies enclosed in this dissertation. It may, therefore, be expected that such behavior continues in phase-separated, block-copolymer morphologies. Our upcoming paper reveals a tendency for ions to move *perpendicular* to the interface, which is consistent with this outcome (since polymer-backbones are expected to be largely aligned perpendicular to the interface). However, we must extend the trajectory far enough to observe ions entering the diffusive regime, which is impossible when we don't see a significant portion of ion motion occurring *parallel* to the interface. Such a result could reveal the transition that must occur for ions, which traditionally move along two polymers, to movement among polymers as the interface blocks motion. Future studies must look toward modeling sufficiently mobile (dynamic and high temperature) ions, so that we can observe the progression of ions to the diffusive regime. This should reveal the additional transition that is likely essential for ions that "collide" with the interface.

The interface itself is another feature of these materials that deserves additional (or different) attention. At present, the interface is viewed as a hard cutoff, such as a plane separating lamellar phases. Dynamic properties

are binned based on distance from that plane, but local densities can vary considerably within the same binned region. Polymers are particularly difficult in this regard due to the constrained nature of the monomers. In our upcoming paper devoted to ion transport in block-copolymer-(polymerized-ionic-liquids), polymer coordination number indicates a heightened tendency to associate with one polymer near the interface. This seems to be due to the low density of the interfacial region, combined with the forced proximity of covalently linked monomers. This behavior might lead to a unique transport mechanism in regions of low polymerized-ionic-liquid-density, which is something that has not been explicitly reviewed in the upcoming paper or other studies.

We feel that the study of these materials could benefit from the use of average-residence properties, similar to the analysis of coordination-binned diffusivities from chapter 3. For example, using the same scheme as that proposed by Sethuraman et al. [266], one could categorize the diffusivity of ions that spend a majority of time in the bulk, transition, and interfacial regions, respectively. Current state-of-the-art approaches might rely on the *starting location of the ion* to bin transport phenomena, but it should be obvious why this approach is non-optimal: an instantaneous state should not determine the long-time behavior of a given ion. This new proposed approach would require large systems with enough ions to create a meaningful pool of classified ions and a high-quality average for the transport property in question.

## 8.2 Review of polymerized ionic liquids in confinement

Polymerized ionic liquids in confinement is one of the most exciting and fresh areas of polymerized-ionic-liquid research. We are tantalized by recent developments that suggest that polymerized-ionic-liquid conductivity may be higher than that of an ionic-liquid counterpart in sufficiently small pores [304]. Specifically, Tarnacka et al. synthesized 1-butyl-3-vinylimidazolium $TFSI^-$ and characterized ion transport using broadband dielectric spectroscopy in porous aluminum oxide substrates. They demonstrated higher conductivity in confined geometries at roughly 250 K or lower temperatures, and even reported higher conductivity for the nanoconfined polymerized ionic liquid compared with that of the monomer at less than 200 K. Results further indicated that smaller pore sizes improved this effect [304].

In 2016, the group of Sangoro pioneered the first broadband dielectric spectroscopy method for measuring ion-transport properties in polymerized ionic liquid thin films [126]. Such innovation is essential for experimental development in this thrust, but at the time of this writing, little progress has been seen using this technique. A study on electrorheological polymerized-ionic-liquid nanocrystals materialzed in 2018, but there is limited overlap between this application and that of polymerized ionic liquids for battery electrolytes [170]. Still, there is much reason for excitement due to the largely unknown nature of ion transport in confined environments, and we suspect that development will ensue in short order. One computational study has been completed on confined polymerized ionic liquids [346]. There are some

aspects of this investigation that we feel could be improved, but it represents a good first attempt.

### 8.2.1 Overview of broadband dielectric spectroscopy

Broadband dielectric spectroscopy (BDS) has become of the most influential analysis methods in experimental investigations of polymerized ionic liquids. It is critical to understand the fundamentals of BDS before analyzing results for complex systems, such as polymerized ionic liquids in confinement. Thus, this section has been included for the convenience of the reader. These details, particularly equations and most collected commentary, come from the seminal book on the subject, edited by Kremer and Schönhals: *Broadband Dielectric Spectroscopy* [158]. BDS allows one to probe molecular fluctuations and charge transport over a wide range of temperatures and frequencies [257]. It does this by inducing charge transfer via a periodic external electric field, which oscillates at the frequency in question.

The periodic electric field can be represented by the equation

$$E(t) = E_0 \exp(-i\omega t). \tag{8.8}$$

The complex dielectric function (permittivity), or complex compliance is governed by

$$\varepsilon(\omega) = \varepsilon'(\omega) - i\varepsilon''(\omega). \tag{8.9}$$

The real part of equation 8.9 is related to the energy stored reversibly during one cycle, while the imaginary part is related to the energy dissipated during

one cycle. Due to the law of energy conservation, these two quantities must be related through the Kramer-Kronig relationship [158].

Development of the model of polarization response relies on linear response theory, which assumes that the time-dependent polarization ($P(t)$) follows the time-dependent electrical field ($E(t)$) linearly. This assumption allows us to construct the following equation,

$$P(t) = p_\infty + \varepsilon_0 \int_{-\infty}^{t} \varepsilon(t - t') \frac{dE(t')}{dt'} dt', \tag{8.10}$$

where $\varepsilon(t))$ is the time-dependent dielectric function and $P_\infty$ covers all contributions related to induced polarization. As an example, for a stepwise change in the electric field,

$$\frac{dE(t)}{dt} = E_0 \delta(t), \tag{8.11}$$

and

$$\varepsilon(t) = \frac{P(t) - P_\infty}{E_0 \varepsilon_0}. \tag{8.12}$$

Thus, $\epsilon(t)$ can be measured as the time dependent response to a stepwise change in electric field. If the periodic electric field disturbance from equation 8.8 is applied, then equation 8.10 is transformed into the following,

$$P(t)(\omega) = \varepsilon_0(\varepsilon^*(\omega) - 1)E(t)(\omega), \tag{8.13}$$

where $\varepsilon^*(\omega)$ is shown in equation 8.9 [158].

Ultimately, analysis of BDS results relies upon artificial, or at least simplified, models to describe polarization relaxation phenomena. The simplest

of such models is the Debye relaxation,

$$\frac{dP(t)}{dt} = -\frac{1}{\tau_D}P(t). \tag{8.14}$$

Equation 8.14 produces exponential decay in the polarization fluctuation autocorrelation function,

$$\Phi(\tau) = \exp\left(-\frac{t}{\tau_D}\right). \tag{8.15}$$

This result is consistent with a homogeneous relaxation process, which is characterized by a single relaxation time. The Debye function for frequency-dependence of $\epsilon^*$ is

$$\varepsilon^*(\omega) = \varepsilon_\infty + \frac{\Delta\varepsilon}{1 + i\omega\tau_D}, \tag{8.16}$$

where $\Delta\varepsilon$ is the dielectric strength. We can see from this equation that there are two parameters of interest: the aforementioned dielectric strength $\Delta\varepsilon$, along with the characteristic Debye relaxation time $\tau_D$.

These values are easily accessible on plots of the real ($\varepsilon'$) or imaginary ($\varepsilon''$) part of the complex dielectric function. At low frequencies, relexation processes are fast enough to respond fully to electric-field variation, leading to a flat response at a high-value plateau in $\varepsilon'$, which is indicated by $\varepsilon_S$ [158]. Upon reaching a frequency that is higher than that of part of the population of dipoles, that part does not fully respond to electric-field variation, leading to a lower dielectric response, and the $\varepsilon'$ falling off the low-frequency plateau. At the frequency $\omega_D$, which is characterized by the inflection point in $\varepsilon'$ and the maximum of $\varepsilon''$, the frequency is consistent with the characteristic timescale

for dielectric relaxation ($\tau_D$ for Debye relaxation)

$$\tau_P = \frac{1}{\omega_P} \tag{8.17}$$

As the frequency quickens, progressively fewer dipoles have time to respond before the electric field is reversed, eventually leading $\varepsilon'$ to the high frequency limit $\varepsilon_\infty$. Thus, the dielectric strength is calculated $\varepsilon_0 = \varepsilon_S - \varepsilon_\infty$, and is the difference between the two plateaus in $\varepsilon'$. It can also be calculated from the area under the relaxation peak in $\varepsilon''$ [158].

The Debye model, due to its simplicity, may not be sufficient to explain the behavior of experimental data. This is particularly true in polymeric materials, where complex relaxation phenomena are seen to occur. One such departure that is common in polymer materials is asymmetric broadening of the imaginary permittivity peak, particularly at low frequency. There are several models that fall into the "non-Debye" category, including the symmetric Cole/Cole and the asymmetric Cole/Davidson functions. We refer the interested reader to Kremer's book for full details on these functions. We will focus the remainder of our discussion on the most often used empirical model function, the Havriliak/Negami (HN) function,

$$\varepsilon^*_{HN}(\omega) = \varepsilon_\infty + \frac{\Delta\varepsilon}{(1 + (i\omega\tau_{HN})^\beta)^\gamma}, \tag{8.18}$$

where $\beta$ and $\gamma$ are shape parameters corresponding to symmetric and asymmetric broadening of the complex dielectric function. Its two fitting parameters make it easier to fit dielectric relaxation data over a wide range of frequencies

and a diverse set of shapes. It has the additional advantage of built-in limiting behavior that is related to the shape parameters in the following ways:

$$\varepsilon_S - \varepsilon'(\omega) \sim \omega^{\beta}; \varepsilon''(\omega) \sim \omega^{\beta} \tag{8.19}$$

for low frequencies and

$$\varepsilon'(\omega) - \varepsilon_\infty \sim \omega^{-\beta\gamma}; \varepsilon''(\omega) \sim \omega^{-\beta\gamma} \tag{8.20}$$

for high frequencies [158].

Turnhout and Wübbenhorst [23] suggest analyzing the derivative form $\partial\varepsilon'/\partial \log \omega$, which looks like the following for a Debye relaxation process:

$$\frac{\partial\varepsilon'}{\partial \log \omega} = -\varepsilon''^2. \tag{8.21}$$

The relaxation peaks are narrower, allowing close peaks to be more easily resolved. Crucially, conductivity contributions play no role in this analysis because the real part is insensitive to frequency for such phenomena. This allows electrode polarization and Maxwell/Wagner effects to be analyzed in greater detail [158]. Many recent advances in polymerized-ionic-liquid research have utilized this technique, especially efforts by Sokolov and coworkers [87]. Researchers pursuing questions in this field should expect an increasing presence of this method in the experimental literature.

Before moving on, we must cover an important relationship, which connects the complex permittivity to two other important functions, which are often cited in polymerized-ionic-liquid research. These function are the

complex modulus $M(\omega)$ and the complex conductivity $\sigma(\omega)$,

$$\varepsilon(\omega) = \frac{1}{M(\omega)} = \frac{\sigma(\omega)}{i\omega\varepsilon_\nu}. \tag{8.22}$$

We could extract the qualitative behavior of these functions from this equation, but unfortunately, we are unable to do justice to this topic within the scope of this introduction. We refer the interested reader to Kremer's book for a complete discussion (chapter 3) on analyzing dielectric spectroscopy results [158]. We will briefly introduce the topics that can be found in the book here.

The first category that they cover encompasses dipolar fluctuations. We already covered some aspects of this analysis, with reference to the model functions. They include extended insight, especially a discussion on model-free analysis techniques. They then discuss patterns for fluctuations of mobile charge carriers, or conducting ions/electrons. Specifically, this involves the use of conductivity and modulus to simplify analysis. In this context, they introduce the Barton/Nakajima/Namikawa (BNN) relationship, which suggests proportionality between the critical frequency and the dc conductivity and has been cited regularly in polymerized-ionic-liquid literature [61, 256]. They also discuss the separation of charges, or charge-polarization phenomena. Explicitly, Maxwell/Wagner/Sillars polarization must be taken into consideration in any material where interfaces and confinement are expected to play a crucial role. For work related to polymerized ionic liquids in confinement, an understanding of the impact of polarization on dielectric response readings is essential for successful interpretation of experimental results.

### 8.2.2 Ionic liquids in confinement: the basis of our current understanding

The subject of ionic liquids in confined geometries has received mountainous support over the past twenty years. At the time of this writing, the structure and dynamics of ionic liquids in confinement have been well-studied, although most researchers would agree that many tantalizing questions remain. Many review articles are now dedicated to various aspects of the subject. Aliaga et al. summarized research related to ionic liquids at solid, liquid, and gas interfaces [4]. Other reviews focused on more specific aspects of confined-ionic-liquid research, such as measurement techniques, features, and computer simulations [12, 138, 156]. Chen et al. reviewed ionic-liquid clustering, especially as it relates to confined ionic liquids [57]. But, Fedorov and Kornyshev produced arguably the most complete review of research related to confined ionic liquids [89]. Any researcher who is looking to enter this field would be wise to consult this reference first. In sum, the prevailing consensus is that there is orientational ordering [10, 37, 50, 104, 136, 164, 166, 187, 287], and that dynamics slow [282], near the interface.

One of the key considerations in confined materials is the strength and nature of interactions with the wall. As of the time of this writing, many wall matrials have been investigated, including silica [20, 92, 242, 250], quartz [251, 252, 325], gold/platinum [11, 123, 174, 236, 327, 356], graphene/carbon-nanotubes [13, 106, 143, 248, 268, 269, 337, 338], liquid/gas interfaces [3, 36, 50, 104, 137, 165, 195, 205, 260], and polymers [93]. Most of these referenced studies

were concerned with structural features of ionic liquids near interfaces, but other studies focused on dynamic features under confinement, including ionic liquids with polymers [263, 265], silica [167, 242], gold/platinum [174], and generic non-chemical interfaces [108]. Research has been especially active in confinement by graphene and carbon-nanotube surfaces, and many molecular dynamics studies have been conducted on this subject [6,90,107,152,201,282]. Many of these studies showed a well-ordered region near the surface with enrichment of the ion countercharged to the surface [90,107,152]. Some analyzed dynamics, finding that center ions move faster than ions near the interface, and overall dynamics is slower in the confined system compared with the bulk system [282].

Other computer simulation studies have played a significant role in shaping our understanding of ionic-liquid ordering near interfaces. Studies on model or non-chemical ionic liquids and surfaces identified ordering near surfaces [88, 91, 108, 142, 241, 242, 335]. There have been many attempts at coarse-grained modeling of such systems [22,156,161], with an exhaustive discussion and reference list from Fedorov and Kornyshev prior to 2014 [89]. They also cover a wide array of atomistic molecular dynamics studies before that year [89], to which we refer the interested reader for in-depth evaluation.

### 8.2.3 Challenges and solutions for simulation research

The choice of materials for a simulation is a crucial decision, so it is important to consider all of the prior work before selection. The properties of

surfaces can vary with chemistry, and interactions will be dependent upon the dispersion, hydrogen-bonding, and electrostatic interactions between the gap material and the interface. Several groups have examined various ionic-liquid materials in silica nanopores with varying degrees of silanization to encourage or discourage hydrogen bonding [92,127,133]. In one key computational study, Pinilla et al. used a generic Lennard-Jones integrated potential (9-3) for ionic liquid between parallel walls of silica [242]. Yu et al. explored ionic liquids confined by alpha-quartz, another common interface material [346]. Freitas et al. examined mica interfaces, and provided complete documentation of the force field parameters used in the study [97], which were based on the INTERFACE force field created by Heinz et al. [124]. Other simulation studies have relied on non-chemical interfaces to simplify the problem [108, 329]. Finally, many computational studies have examined ionic liquid properties when confined to graphene and carbon-nanotube environments [6, 90, 107, 152, 201, 282].

Recent advances in modeling interfacial environments could pave the way for explosive growth in the field. Heinz et al. produced a comprehensive package of energetic potentials and parameters for combined organic and inorganic systems, the INTERFACE force field [124]. They provide an excellent review of force field development in the supporting information package for that work. This force field has been deployed in at least two contexts as of this writing, once for mica and once for quartz [97, 346].

A particular challenge when modeling slab geometries is the accurate summation of Ewald electrostatic energies. Spohr showed that appropriate

long-range corrections are mandatory for simulations of interfacial properties of electrolyte solutions [290]. At the time, existing truncated solutions led to unphysical electrical fields, preventing formation of a "bulk" region in the simulation cell. In 1999, Yeh et al. demonstrated the three-dimensional Ewald technique [343], which is largely agreed to be the standard for these simulations [89, 309].

Another acute challenge is the incorporation of polarizability of electrodes/image forces in molecular models of electrochemical interface, which is nontrivial and is even more computationally expensive than the three-dimensional Ewald technique highlighted previously [89, 189, 306]. This is a problem that we are not equipped to handle with our current approach of using average polarization behavior via constant scaled partial charges. Yu et al. used our method of scaled partial charges, which leads us to question the validity of their approach [346]. Therefore, it may be necessary for future efforts to use polarizable force fields, further hampering development of the field due to large computational burdens for polymeric systems. Fedorov and Kornyshev mention an innovative thermostat, with canonical sampling through velocity rescaling in this context [44]. Researchers may have to embrace innovative techniques to make these problems computationally tractable.

### 8.2.4 Analysis techniques deployed in confinement studies

This class of problems also requires a large berth for analysis approaches. Pinilla et al. demonstrated the use of the density distribution per-

pendicular to the interface [242]. Ion clustering near charged surfaces can indicate oscillatory organization, or simply preferential charge aggregation near the interface, which could influence structure and dynamics. Analysis mimics from the coordination and hopping analyses, conducted in the context of earlier works in polymerized ionic liquids, would also yield potentially informative results [147–149, 217, 346]. Carillo et al. investigated the Z-resolved collective intermediate scattering function $S(q, t, z)$ [51].

The Legendre polynomial ($P_m(\cos(\theta))$), where $m$ is the order of the polynomial, is represented by

$$\langle P_m(\cos(\theta))P_m(\cos(\theta))\rangle = \exp(-m(m+1)D_{rot}t), \tag{8.23}$$

where $D_{rot}$ is the rotational diffusion coefficient. As Schönhals and Kremer explain [158], the only contributing component of the dipole vector is that which is parallel to the outer electric field. Therefore, only the first polynomial is considered for dielectric relaxation:

$$P_1(\cos(\theta)) = \cos(\theta). \tag{8.24}$$

They point out that for optical spectroscopy, including NMR, Raman, and light scattering experiments, measurements are proportional to the second polynomial,

$$P_2(\cos(\theta)) = \frac{1}{2}(3\cos(\theta)^2 - 1). \tag{8.25}$$

Both of these measures have been used in past studies for analyzing the orientational decay of unit bond vectors in ionic liquid confinement, and could

be targets for use in studies on confined polymerized ionic liquids [51, 92, 194, 195, 242, 250].

Weyman et al. examined the probability distribution of species within a channel and identified local mean drift velocities [329]. Density and packing characteristics under confinement and along the confinement axis have also been targets of analysis in the past [133, 242]. Pinilla et al. looked at a unique free energy with an isothermal, reversible change in inter-wall distance [242]. For polymeric confined systems, the dynamic length scale governing glass transition and cooperatively rearranging regions has been posited to be an important consideration [133]. Finally, gauche defects in the side-chains and polymeric backbones could be intersting targets for data collection [92, 250].

### 8.2.5 Future work and open questions

So, what are the open questions that remain at the time of this writing? What diffusion mechanism dominates near the interface, and is it distinct from that which we observe in the bulk of a polymerized ionic liquid? What is the role of surface roughness or curvature on structure and transport? At what length scale does the bulk material contain inherent structural organization, and does this play a role in determining pore sizes for interesting ion-transport and organizational phenomena in polymerized ionic liquids?

For polymerized ionic liquids, what is the effect of the surface, compared with the effect of simple polymer alignment? Since we observed the "climbing the ladder" mechanism in bulk polymerized ionic liquids, could we

see enhanced transport near the interface with pathways oriented parallel to the axis of confinement? Another important question is "how do we distinguish the role of pore size (related to curvature and roughness), especially in experiments where, at best, we can hope for a narrow distribution of pore sizes" [133, 167]? With a distribution of pore sizes leading to varying rates of relaxation and competing polarization effects due to the presence of the interface, one can only hope to extract a mean conductivity from the maximum of the imaginary modulus [304]. This means that researchers may struggle to capture a true conductivity for experimental confined materials. Also, this challenges the simulation researcher by clouding experimental results and making it difficult to reliably compare effects to real systems. Finally, what role does the interface have in determining polymer mobility [51]? And is this an important consideration for ion mobility, or will ion-hopping keep the conductivity high, even for glassy and frozen polymer systems?

Although this section does not offer a complete review of the prior work in this area, we hope that it has been beneficial in revealing some of the fundamental questions that can be explored. We think that this is an exciting area of research that could benefit from a dedicated research strategy, which could enable valuable contributions to the development of next-generation charge-carriage and storage devices.

# Bibliography

[1] A L Agapov and A P Sokolov. Decoupling ionic conductivity from structural relaxation: A way to solid polymer electrolytes? *Macromolecules*, 44(11):4410–4414, 2011.

[2] R C Agrawal and G P Pandey. Solid polymer electrolytes: materials designing and all-solid-state battery applications: an overview. *Journal of Physics D: Applied Physics*, 41(22):223001, 2008.

[3] Cesar Aliaga and Steven Baldelli. Sum Frequency Generation Spectroscopy of Dicyanamide Based Room-Temperature Ionic Liquids. Orientation of the Cation and the Anion at the Gas-liquid Interface. *The Journal of Physical Chemistry B*, 111(33):9733–9740, aug 2007.

[4] Cesar Aliaga, Cherry S Santos, and Steven Baldelli. Surface chemistry of room-temperature ionic liquids. *Physical Chemistry Chemical Physics*, 9(28):3683–3700, 2007.

[5] Harsha V R Annapureddy, Hemant K. Kashyap, Pablo M. De Biase, and Claudio J. Margulis. What is the origin of the prepeak in the x-ray scattering of imidazolium-based room-temperature ionic liquids? *Journal of Physical Chemistry B*, 114(50):16838–16846, 2010.

[6] Santiago Aparicio and Mert Atilhan. Molecular Dynamics Study of Carbon Nanostructures in N-Methylpiperazinium Lactate Ionic Liquid. *The Journal of Physical Chemistry C*, 117(42):22046–22059, oct 2013.

[7] G. B. Appetecchi, G. T. Kim, M. Montanino, M. Carewska, R. Marcilla, D. Mecerreyes, and I. De Meatza. Ternary polymer electrolytes containing pyrrolidinium-based polymeric ionic liquids for lithium batteries. *Journal of Power Sources*, 195(11):3668–3675, 2010.

[8] Michele Aresta and Angela Dibenedetto. Utilisation of CO2 as a chemical feedstock: Opportunities and challenges. *Journal of the Chemical Society. Dalton Transactions*, (28):2975–2992, 2007.

[9] Michel Armand, Frank Endres, Douglas R MacFarlane, Hiroyuki Ohno, and Bruno Scrosati. Ionic-liquid materials for the electrochemical challenges of the future. *Nature Materials*, 8(8):621–629, 2009.

[10] Steven Baldelli. Influence of Water on the Orientation of Cations at the Surface of a Room-Temperature Ionic Liquid: A Sum Frequency Generation Vibrational Spectroscopic Study. *The Journal of Physical Chemistry B*, 107(25):6148–6152, jun 2003.

[11] Steven Baldelli. Surface Structure at the Ionic Liquid-Electrified Metal Interface. *Accounts of Chemical Research*, 41(3):421–431, mar 2008.

[12] Steven Baldelli. Interfacial Structure of Room-Temperature Ionic Liquids at the Solid-Liquid Interface as Probed by Sum Frequency Genera-

tion Spectroscopy. *The Journal of Physical Chemistry Letters*, 4(2):244–252, jan 2013.

[13] Steven Baldelli, Jiming Bao, Wei Wu, and Shin-shem Pei. Sum frequency generation study on the orientation of room-temperature ionic liquid at the graphene–ionic liquid interface. *Chemical Physics Letters*, 516(4):171–173, 2011.

[14] Witali Beichel, Ulrich P. Preiss, Sergey P. Verevkin, Thorsten Koslowski, and Ingo Krossing. Empirical description and prediction of ionic liquids' properties with augmented volume-based thermodynamics. *Journal of Molecular Liquids*, 192:3–8, 2014.

[15] H. J.C. Berendsen, J. P.M. Postma, W. F. Van Gunsteren, A. Dinola, and J. R. Haak. Molecular dynamics with coupling to an external bath. *The Journal of Chemical Physics*, 81(8):3684–3690, 1984.

[16] C. Berthier, W. Gorecki, M. Minier, M. B. Armand, J. M. Chabagno, and P. Rigaud. Microscopic investigation of ionic conductivity in alkali metal salts-poly(ethylene oxide) adducts. *Solid State Ionics*, 11(1):91–95, sep 1983.

[17] B. H. Besler, K. M. Merz, and P. A. Kollman. Atomic charges derived from semiempirical methods. *J. Comput. Chem.*, 11:431–439, 1990.

[18] Gerhard Besold, Ilpo Vattulainen, Mikko Karttunen, and James M Polson. Towards better integrators for dissipative particle dynamics simu-

lations. *Phys. Rev. E*, 62(6):R7611—-R7614, dec 2000.

[19] B. L. Bhargava and S. Balasubramanian. Refined potential model for atomistic simulations of ionic liquid [bmim][PF6]. *The Journal of Chemical Physics*, 127(11):114510, sep 2007.

[20] Jennifer M Black, Mengyang Zhu, Pengfei Zhang, Raymond R Unocic, Daqiang Guo, M Baris Okatan, Sheng Dai, Peter T Cummings, Sergei V Kalinin, Guang Feng, and Nina Balke. Fundamental aspects of electric double layer force-distance measurements at liquid-solid interfaces using atomic force microscopy. *Scientific reports*, 6:32389, sep 2016.

[21] V. Bocharova, Z. Wojnarowska, Peng Fei Cao, Y. Fu, R. Kumar, Bingrui Li, V. N. Novikov, S. Zhao, A. Kisliuk, T. Saito, Jimmy W. Mays, B. G. Sumpter, and A. P. Sokolov. Influence of Chain Rigidity and Dielectric Constant on the Glass Transition Temperature in Polymerized Ionic Liquids. *Journal of Physical Chemistry B*, 121(51):11511–11519, 2017.

[22] Dezso Boda, Douglas Henderson, and Kwong Yu Chan. Monte Carlo study of the capacitance of the double layer in a model molten salt. *Journal of Chemical Physics*, 110(11):5346–5350, 1999.

[23] A Boersma, J van Turnhout, and M Wubbenhorst. Dielectric Characterization of a Thermotropic Liquid Crystalline Copolyesteramide: 1. Relaxation Peak Assignment. *Macromolecules*, 31(21):7453–7460, oct 1998.

[24] Dan S Bolintineanu, Mark J Stevens, and Amalie L Frischknecht. Influence of cation type on ionic aggregates in precise ionomers. *Macromolecules*, 46(13):5381–5392, 2013.

[25] Oleg Borodin. Polarizable force field development and molecular dynamics simulations of ionic liquids. *The Journal of Physical Chemistry B*, 113(33):11463–11478, 2009.

[26] Oleg Borodin, W Gorecki, Grant D Smith, and Michel Armand. Molecular Dynamics Simulation and Pulsed-Field Gradient NMR Studies of Bis ( fluorosulfonyl ) imide ( FSI ) and Bis [( trifluoromethyl ) sulfonyl ] imide ( TFSI ) -Based Ionic Liquids. *Journal of Physical Chemistry B*, 114(20):6786–6798, 2010.

[27] Oleg Borodin and G D Smith. Li+Transport Mechanism in Oligo(Ethylene Oxide)s Compared to Carbonates. *Journal of Solution Chemistry*, 36(6):803–813, 2007.

[28] Oleg Borodin and Grant D. Smith. Molecular Dynamics Simulations of Poly(ethylene oxide)/LiI Melts. 1. Structural and Conformational Properties. *Macromolecules*, 31(23):8396–8406, 1998.

[29] Oleg Borodin and Grant D. Smith. Molecular dynamics simulations of poly(ethylene oxide)/LiI melts. 2. Dynamic properties. *Macromolecules*, 33(6):2273–2283, 2000.

[30] Oleg Borodin and Grant D Smith. Development of Many-Body Polarizable Force Fields for Li-Battery Components: 1. Ether, Alkane, and Carbonate-Based Solvents. *The Journal of Physical Chemistry B*, 110(12):6279–6292, 2006.

[31] Oleg Borodin and Grant D Smith. LiTFSI structure and transport in ethylene carbonate from molecular dynamics simulations. *The journal of physical chemistry. B*, 110(10):4971–4977, 2006.

[32] Oleg Borodin and Grant D Smith. LiTFSI Structure and Transport in Ethylene Carbonate from Molecular Dynamics Simulations. *The Journal of Physical Chemistry B*, 110(10):4971–4977, 2006.

[33] Oleg Borodin and Grant D Smith. Mechanism of Ion Transport in Amorphous Poly(ethylene oxide)/LiTFSI from Molecular Dynamics Simulations. *Macromolecules*, 39(4):1620–1629, 2006.

[34] Oleg Borodin and Grant D Smith. Molecular Dynamics Simulations of Comb-Branched Poly(epoxide ether)-Based Polymer Electrolytes. *Macromolecules*, 40(4):1252–1258, feb 2007.

[35] Oleg Borodin, Grant D. Smith, and Wesley Henderson. Li+ cation environment, transport, and mechanical properties of the LiTFSI doped N-methyl-N-alkylpyrrolidinium+TFSI- Ionic liquids. *Journal of Physical Chemistry B*, 110(34):16879–16886, 2006.

[36] James Bowers, Craig P Butts, Pamela J Martin, Marcos C Vergara-Gutierrez, and Richard K Heenan. Aggregation Behavior of Aqueous Solutions of Ionic Liquids. *Langmuir*, 20(6):2191–2198, mar 2004.

[37] James Bowers, Marcos C Vergara-Gutierrez, and John R P Webster. Surface Ordering of Amphiphilic Ionic Liquids. *Langmuir*, 20(2):309–312, jan 2004.

[38] A. E. Bradley, C. Hardacre, J. D. Holbrey, S. Johnston, S. E J McMath, and M. Nieuwenhuyzent. Small-angle x-ray scattering studies of liquid crystalline 1-alkyl-3-methylimidazolium salts. *Chemistry of Materials*, 14(2):629–635, 2002.

[39] Abigail F. Bratton, Sung Soo Kim, Christopher J. Ellison, and Kevin M. Miller. Thermomechanical and conductive properties of thiol-ene poly(ionic liquid) networks containing backbone and pendant imidazolium groups. *Industrial and Engineering Chemistry Research*, 57(48):16526–16536, 2018.

[40] P J Brown, A G Fox, E N Maslen, M A O Keefe, and B T M Willis. Internsity of diffracted intensities. In *International Tables for Crystallography*, volume C, chapter 6.1, pages 554–595. 2006.

[41] C Francisco Buitrago, Todd M Alam, Kathleen L Opper, Brian S Aitken, Kenneth B Wagener, and Karen I Winey. Morphological Trends in Precise Acid- and Ion-Containing Polyethylenes at Elevated Temperature. *Macromolecules*, 46(22):8995–9002, nov 2013.

[42] C. Francisco Buitrago, Dan S. Bolintineanu, Michelle E. Seitz, Kathleen L. Opper, Kenneth B. Wagener, Mark J. Stevens, Amalie L. Frischknecht, and Karen I. Winey. Direct comparisons of x-ray scattering and atomistic molecular dynamics simulations for precise acid copolymers and Ionomers. *Macromolecules*, 48(4):1210–1220, 2015.

[43] C Francisco Buitrago, Janelle E Jenkins, Kathleen L Opper, Brian S Aitken, Kenneth B Wagener, Todd M Alam, and Karen I Winey. Room Temperature Morphologies of Precise Acid- and Ion-Containing Polyethylenes. *Macromolecules*, 46(22):9003–9012, nov 2013.

[44] Giovanni Bussi, Davide Donadio, and Michele Parrinello. Canonical sampling through velocity rescaling. *Journal of Chemical Physics*, 126(1), 2007.

[45] N. Byrne, J. M. Pringle, C. Tiyapiboonchaiya, D. R. MacFarlane, and M. Forsyth. The additive effect of zwitterion and nano-particles on ion dissociation in polyelectrolytes. *Electrochimica Acta*, 50(13):2733–2738, 2005.

[46] Nolene Byrne, Patrick C. Howlett, Douglas R. MacFarlane, and Maria Forsyth. The zwitterion effect in ionic liquids: Towards practical rechargeable lithium-metal batteries. *Advanced Materials*, 17(20):2497–2501, 2005.

[47] José N. Canongia Lopes, Johnny Deschamps, and Agílio a. H. Pádua.

Modeling Ionic Liquids Using a Systematic All-Atom Force Field. *Journal of Physical Chemistry B*, 108(6):2038–2047, 2004.

[48] J Cardoso, R Manrique, M Albores Velasco, and A Huanosta. Properties of Three Different Methacrylate Polymers with Zwitterionic Pendant Groups. *Journal of Polymer Science: Part B: Polymer Physics*, 35:479–488, 1997.

[49] Judith Cardoso, Olivia Soria-Arteche, Gerardo Vázquez, Omar Solorza, and Ignacio González. Synthesis and Characterization of Zwitterionic Polymers with a Flexible Lateral Chain. *The Journal of Physical Chemistry C*, 114(33):14261–14268, aug 2010.

[50] ADRIAN J CARMICHAEL, CHRISTOPHER HARDACRE, JOHN D HOLBREY, MARK NIEUWENHUYZEN, and KENNETH R SEDDON. Molecular layering and local order in thin films of 1-alkyl-3-methylimidazolium ionic liquids using X-ray reflectivity. *Molecular Physics*, 99(10):795–800, may 2001.

[51] Jan Michael Y. Carrillo, Shiwang Cheng, Rajeev Kumar, Monojoy Goswami, Alexei P. Sokolov, and Bobby G. Sumpter. Untangling the Effects of Chain Rigidity on the Structure and Dynamics of Strongly Adsorbed Polymer Melts. *Macromolecules*, 48(12):4207–4219, 2015.

[52] Alberto Cavazzini, Luisa Pasti, Alessandro Massi, Nicola Marchetti, and Francesco Dondi. Recent applications in chiral high performance liquid

chromatography: A review. *Analytica Chimica Acta*, 706(2):205–222, 2011.

[53] V Chaban. Polarizability versus mobility: atomistic force field for ionic liquids. *Phys Chem Chem Phys*, 13(35):16055–16062, 2011.

[54] V V Chaban, I V Voroshylova, and O N Kalugin. A new force field model for the simulation of transport properties of imidazolium-based ionic liquids. *Phys Chem Chem Phys*, 13(17):7910–7920, 2011.

[55] Amalendu Chandra. Effects of ion atmosphere on hydrogen-bond dynamics in aqueous electrolyte solutions. *Physical Review Letters*, 85(4):768–771, 2000.

[56] Hong Chen, Jae-Hong Choi, David Salas-de la Cruz, Karen I. Winey, and Yossef A. Elabd. Polymerized Ionic Liquids: The Effect of Random Copolymer Composition on Ion Conduction. *Macromolecules*, 42(23):4809–4816, 2009.

[57] Shimou Chen, Suojiang Zhang, Xiaomin Liu, Jinquan Wang, Jianji Wang, Kun Dong, Jian Sun, and Baohua Xu. Ionic liquid clusters: structure, formation mechanism, and effect on the behavior of ionic liquids. *Physical Chemistry Chemical Physics*, 16(13):5893–5906, 2014.

[58] Yizi Cheng, Junhong Yang, Jui-Hsiang Hung, Tarak K Patra, and David S Simmons. Design Rules for Highly Conductive Polymeric Ionic Liquids

from Molecular Dynamics Simulations. *Macromolecules*, 51(17):6630–6644, 2018.

[59] U Hyeok Choi, Minjae Lee, Sharon Wang, Wenjuan Liu, Karen I Winey, Harry W Gibson, and Ralph H Colby. Ionic conduction and dielectric response of poly(imidazolium acrylate) ionomers. *Macromolecules*, 45(9):3974–3985, 2012.

[60] U Hyeok Choi, Anuj Mittal, Terry L Price, Minjae Lee, Harry W Gibson, James Runt, and Ralph H Colby. Molecular Volume Effects on the Dynamics of Polymerized Ionic Liquids and their Monomers. *Electrochimica Acta*, 175:55–61, 2015.

[61] U Hyeok Choi, Yuesheng Ye, David Salas De La Cruz, Wenjuan Liu, Karen I Winey, Yossef A Elabd, James Runt, and Ralph H Colby. Dielectric and viscoelastic responses of imidazolium-based ionomers with different counterions and side chain lengths. *Macromolecules*, 47(2):777–790, 2014.

[62] A. M. Christie, S. J. Lilley, E. Staunton, Y.G. Andreev, and P. G. Bruce. Increasing the conductivity of crystalline polymer electrolytes. *Nature*, 433(7021):50–53, 2005.

[63] Sandia Corporation. fix langevin command, 2019.

[64] Sandia Corporation. fix nve/limit command, 2019.

[65] Sandia Corporation. fix press/berendsen command, 2019.

[66] Daniel A. Crowl and Joseph F. Louvar. *Chemical Process Safety: Fundamentals with Applications*. Prentice Hall PTG, 3rd edition, 2011.

[67] Anthony J. D'Angelo and Matthew J. Panzer. Decoupling the Ionic Conductivity and Elastic Modulus of Gel Electrolytes: Fully Zwitterionic Copolymer Scaffolds in Lithium Salt/Ionic Liquid Solutions. *Advanced Energy Materials*, 8(26):1–13, 2018.

[68] Kostas Ch Daoulas and Marcus Müller. Single chain in mean field simulations: quasi-instantaneous field approximation and quantitative comparison with Monte Carlo simulations. *The Journal of chemical physics*, 125(18):184904, 2006.

[69] Kostas Ch Daoulas, Marcus Müller, Juan J de Pablo, Paul F Nealey, and Grant D Smith. Morphology of multi-component polymer systems: single chain in mean field simulation studies. *Soft Matter*, 2(7):573–583, 2006.

[70] Kostas Ch Daoulas, Victor Rühle, and Kurt Kremer. Simulations of nematic homopolymer melts using particle-based models with interactions expressed through collective variables. *Journal of physics. Condensed matter : an Institute of Physics journal*, 24(28):284121, 2012.

[71] Sudarshan Das, Sougata Santra, Pallab Mondal, Adinath Majee, and Alakananda Hajra. Zwitterionic Imidazolium Salt: Recent Advances in Organocatalysis. *Synthesis (Germany)*, 48(9):1269–1285, 2016.

[72] Jones De Andrade, Elvis S. Böes, and Hubert Stassen. Computational study of room temperature molten salts composed by 1-alkyl-3-methylimidazolium cations - Force-field proposal and validation. *Journal of Physical Chemistry B*, 106(51):13344–13351, 2002.

[73] Virginie Delhorbe, Dominic Bresser, Hakima Mendil-Jakani, Patrice Rannou, Laurent Bernard, Thibaut Gutel, Sandrine Lyonnard, and Lionel Picard. Unveiling the Ion Conduction Mechanism in Imidazolium-Based Poly(ionic liquids): A Comprehensive Investigation of the Structure-to-Transport Interplay. *Macromolecules*, 50(11):4309–4321, 2017.

[74] François A Detcheverry, Huiman Kang, Kostas Ch Daoulas, Marcus Müller, Paul F Nealey, and Juan J. De Pablo. Monte Carlo simulations of a coarse grain model for block copolymers and nanocomposites. *Macromolecules*, 41(13):4989–5001, 2008.

[75] Francois A. Detcheverry, Darin Q. Pike, Paul F. Nealey, Marcus M??ller, and Juan J. De Pablo. Monte Carlo simulation of coarse grain polymeric systems. *Physical Review Letters*, 102(19):2–5, 2009.

[76] Diddo Diddens, Andreas Heuer, and Oleg Borodin. Understanding the lithium transport within a rouse-based model for a PEO/LiTFSI polymer electrolyte. *Macromolecules*, 43(4):2028–2036, 2010.

[77] Changwoo Do, Peter Lunkenheimer, Diddo Diddens, Marion Gotz, Matthias Weib, Alois Loidl, Xiao Guang Sun, J??rgen Allgaier, and Michael Ohl.

Li+ transport in poly(ethylene oxide) based electrolytes: Neutron scattering, dielectric spectroscopy, and molecular dynamics simulations. *Physical Review Letters*, 111(1):1–5, 2013.

[78] Leela S Dodda, Israel Cabeza de Vaca, Julian Tirado-Rives, and William L Jorgensen. LigParGen web server: an automatic OPLS-AA parameter generator for organic ligands. *Nucleic Acids Research*, 45(W1):W331–W336, apr 2017.

[79] Florian Dommert, Katharina Wendler, Robert Berger, Luigi Delle Site, and Christian Holm. Force fields for studying the structure and dynamics of ionic liquids: A critical review of recent developments. *ChemPhysChem*, 13(7):1625–1637, 2012.

[80] Shichen Dou, Shihai Zhang, Robert J Klein, James Runt, Ralph H Colby, The Pennsyl, V State, V Uni, Uni V Park, and V Pennsyl. Synthesis and Characterization of Poly ( Ethylene Glycol ) -Based Single-Ion Conductors. *Chemistry of Materials*, 18(11):4288–4295, 2006.

[81] BURKHARD DÜNWEG and WOLFGANG PAUL. BROWNIAN DYNAMICS SIMULATIONS WITHOUT GAUSSIAN RANDOM NUMBERS. *International Journal of Modern Physics C*, 02(03):817–827, sep 1991.

[82] Ali Eftekhari and Tomonori Saito. Synthesis and properties of polymerized ionic liquids. *European Polymer Journal*, 90(March):245–272, 2017.

[83] Gebrekidan Gebresilassie Eshetu, David Mecerreyes, Maria Forsyth, Heng Zhang, and Michel Armand. Polymeric ionic liquids for lithium-based rechargeable batteries. *Molecular Systems Design & Engineering*, pages 294–309, 2019.

[84] P. Espa\˜nol and P. Warren. Statistical Mechanics of Dissipative Particle Dynamics. *EUROPHYSICS LETTERS Europhys. Lett*, 30:191, 1995.

[85] Christopher M. Evans, Colin R. Bridges, Gabriel E. Sanoja, Joshua Bartels, and Rachel A. Segalman. Role of Tethered Ion Placement on Polymerized Ionic Liquid Structure and Conductivity: Pendant versus Backbone Charge Placement. *ACS Macro Letters*, 5(8):925–930, 2016.

[86] Fei Fan, Weiyu Wang, Adam P Holt, Hongbo Feng, David Uhrig, Xinyi Lu, Tao Hong, Yangyang Wang, Nam Goo Kang, Jimmy Mays, and Alexei P Sokolov. Effect of molecular weight on the ion transport mechanism in polymerized ionic liquids. *Macromolecules*, 49(12):4557–4570, 2016.

[87] Fei Fan, Yangyang Wang, Tao Hong, Maximilian F Heres, Tomonori Saito, and Alexei P Sokolov. Ion Conduction in Polymerized Ionic Liquids with Different Pendant Groups. *Macromolecules*, 48(13):4461–4470, 2015.

[88] Maxim V Fedorov and Alexei A Kornyshev. Ionic Liquid Near a

Charged Wall: Structure and Capacitance of Electrical Double Layer. *The Journal of Physical Chemistry B*, 112(38):11868–11872, sep 2008.

[89] Maxim V Fedorov and Alexei A Kornyshev. Ionic Liquids at Electrified Interfaces. *Chemical Reviews*, 114(5):2978–3036, mar 2014.

[90] Maxim V Fedorov and R M Lynden-Bell. Probing the neutral graphene–ionic liquid interface: insights from molecular dynamics simulations. *Physical Chemistry Chemical Physics*, 14(8):2552–2556, 2012.

[91] Guang Feng and Peter T Cummings. Supercapacitor Capacitance Exhibits Oscillatory Behavior as a Function of Nanopore Size. *The Journal of Physical Chemistry Letters*, 2(22):2859–2864, nov 2011.

[92] Brian D Fitchett and John C Conboy. Structure of the Room-Temperature Ionic Liquid/SiO2 Interface Studied by Sum-Frequency Vibrational Spectroscopy. *The Journal of Physical Chemistry B*, 108(52):20255–20262, dec 2004.

[93] Raquel Fortunato, Carlos A.M. Afonso, Juana Benavente, E. Rodriguez-Castellón, and João G. Crespo. Stability of supported ionic liquid membranes as studied by X-ray photoelectron spectroscopy. *Journal of Membrane Science*, 256(1-2):216–223, 2005.

[94] Daniel Fragiadakis, Shichen Dou, Ralph H Colby, and James Runt. Molecular mobility, ion mobility and mobile ion concentration in polyethy-

lene oxide-based polyurethane ionomers. *Macromolecules*, 41(15):5723–5728, 2008.

[95] Daniel Fragiadakis, Shichen Dou, Ralph H. Colby, and James Runt. Molecular mobility and Li+ conduction in polyester copolymer ionomers based on poly(ethylene oxide). *Journal of Chemical Physics*, 130(6), 2009.

[96] Arthur France-Lanord and Jeffrey C. Grossman. Correlations from ion pairing and the nernst-einstein equation. *Phys. Rev. Lett.*, 122:136001, Apr 2019.

[97] Adilson Alves De Freitas, Karina Shimizu, Alexander M. Smith, Susan Perkin, and José Nuno Canongia Lopes. Structure and dynamics of mica-confined films of [C10C1Pyrr][NTf2] ionic liquid. *Journal of Chemical Physics*, 148(19), 2018.

[98] Falk Frenzel, Ryan Guterman, A. Markus Anton, Jiayin Yuan, and Friedrich Kremer. Molecular Dynamics and Charge Transport in Highly Conductive Polymeric Ionic Liquids. *Macromolecules*, 50(10):4022–4029, 2017.

[99] M. J. Frisch, G. W. Trucks, H. B. Schlegel, G. E. Scuseria, M. A. Robb, J. R. Cheeseman, G. Scalmani, V. Barone, G. A. Petersson, H. Nakatsuji, X. Li, M. Caricato, A. V. Marenich, J. Bloino, B. G. Janesko, R. Gomperts, B. Mennucci, H. P. Hratchian, J.V. Ortiz, A. F. Izmaylov,

J. L. Sonnenberg, D. Williams-Young, F. Ding, F. Lipparini, F. Egidi, J. Goings, B. Peng, A. Petrone, T. Henderson, D. Ranasinghe, V. G. Zakrzewski, J. Gao, N. Rega, G. Zheng, W. Liang, M. Hada, M. Ehara, K. Toyota, R. Fukuda, J. Hasegawa, M. Ishida, T. Nakajima, Y. Honda, O. Kitao, H. Nakai, T. Vreven, K. Throssell, J. A. Montgomery, Jr., J. E. Peralta, F. Ogliaro, M. J. Bearpark, J. J. Heyd, E. N. Brothers, K. N. Kudin, V. N. Staroverov, T. A. Keith, R. Kobayashi, J. Normand, and D. J. Fox. Gausian 16, 2016.

[100] Amalie L. Frischknecht and Karen I. Winey. The evolution of acidic and ionic aggregates in ionomers during microsecond simulations. *Journal of Chemical Physics*, 150(6), 2019.

[101] C. Gainaru, E. W. Stacy, V. Bocharova, M. Gobet, A. P. Holt, T. Saito, S. Greenbaum, and A. P. Sokolov. Mechanism of Conductivity Relaxation in Liquid and Polymeric Electrolytes: Direct Link between Conductivity and Diffusivity. *Journal of Physical Chemistry B*, 120(42):11074–11083, 2016.

[102] Monique Galin, Eve Marchal, André Mathis, and Jean Claude Galin. Poly(ammonioalkanesulfonate) blends with polar organic species and alkali metal salts: Structure, glass transition and ionic conductivity. *Polymers for Advanced Technologies*, 8(2):75–86, 1997.

[103] Venkat Ganesan. Ion transport in polymeric ionic liquids: recent developments and open questions. *Molecular Systems Design & Engineering*,

4(2):280–293, 2019.

[104] Thomas J Gannon, George Law, Philip R Watson, Adrian J Carmichael, and Kenneth R Seddon. First Observation of Molecular Composition and Orientation at the Surface of a Room-Temperature Ionic Liquid. *Langmuir*, 15(24):8429–8434, nov 1999.

[105] Xinpei Gao, Fei Lu, Bin Dong, Aoli Wu, Na Sun, and Liqiang Zheng. Anion exchange membranes with well-defined ion transporting nanochannels via self-assembly of polymerizable ionic liquids. *Journal of Materials Chemistry A*, 4(34):13316–13323, 2016.

[106] Gregorio García, Mert Atilhan, and Santiago Aparicio. Adsorption of choline benzoate ionic liquid on graphene, silicene, germanene and boron-nitride nanosheets: a DFT perspective. *Physical Chemistry Chemical Physics*, 17(25):16315–16326, 2015.

[107] Mohammad Hadi Ghatee and Fatemeh Moosavi. Physisorption of Hydrophobic and Hydrophilic 1-Alkyl-3-methylimidazolium Ionic Liquids on the Graphenes. *The Journal of Physical Chemistry C*, 115(13):5626–5636, apr 2011.

[108] Phwey S Gil, Sara J Jorgenson, Adriaan R Riet, and D J Lacks. Relationships between Molecular Structure, Interfacial Structure, and Dynamics of Ionic Liquids near Neutral and Charged Surfaces. *The Journal of Physical Chemistry C*, 122(48):27462–27468, dec 2018.

[109] G Gonnella, E Orlandini, and J M Yeomans. Spinodal Decomposition to a Lamellar Phase: Effects of Hydrodynamic Flow. *Phys. Rev. Lett.*, 78(9):1695–1698, mar 1997.

[110] Richard J Gowers, Max Linke, Jonathan Barnoud, Tyler J E Reddy, Manuel N Melo, Sean L Seyler, Jan Domański, David L Dotson, Sébastien Buchoux, Ian M Kenney, and Oliver Beckstein. {M}{D}{A}nalysis: {A} {P}ython {P}ackage for the {R}apid {A}nalysis of {M}olecular {D}ynamics {S}imulations. In Sebastian Benthall and Scott Rostrup, editors, *{P}roceedings of the 15th {P}ython in {S}cience {C}onference*, pages 98–105, 2016.

[111] Matthew D. Green, David Salas-De La Cruz, Yuesheng Ye, John M. Layman, Yossef A. Elabd, Karen I. Winey, and Timothy E. Long. Alkyl-substituted N-vinylimidazolium polymerized ionic liquids: Thermal properties and ionic conductivities. *Macromolecular Chemistry and Physics*, 212(23):2522–2528, 2011.

[112] Omar Green, Simonida Grubjesic, Sungwon Lee, and Millicent A Firestone. The Design of Polymeric Ionic Liquids for the Preparation of Functional Materials. *Journal of Macromolecular Science R , Part C: Polymer Reviews*, 49(March):339–360, 2009.

[113] Philip J. Griffin, Jessica L. Freyer, Nicholas Han, Noah Geller, Xiaodong Yin, Chirag D. Gheewala, Tristan H. Lambert, Luis M. Campos, and

Karen I. Winey. Ion Transport in Cyclopropenium-Based Polymerized Ionic Liquids. *Macromolecules*, page acs.macromol.7b02546, 2018.

[114] Philip J. Griffin, Jessica L. Freyer, Nicholas Han, Noah Geller, Xiaodong Yin, Chirag D. Gheewala, Tristan H. Lambert, Luis M. Campos, and Karen I. Winey. Ion transport in cyclopropenium-based polymerized ionic liquids. *Macromolecules*, 51(5):1681–1687, 2018.

[115] Philip J Griffin, Yangyang Wang, Adam P Holt, Alexei P Sokolov, Philip J Griffin, Yangyang Wang, Adam P Holt, and Alexei P Sokolov. Communication : Influence of nanophase segregation on ion transport in room temperature ionic liquids. *Journal of Chemical Physics*, 144:151104, 2016.

[116] Robert D. Groot and Patrick B. Warren. Dissipative particle dynamics: Bridging the gap between atomistic and mesoscopic simulation. *Journal of Chemical Physics*, 107(11):4423–4435, 1997.

[117] G. Guzmán, D. Nava, J. Vazquez-Arenas, J. Cardoso, and J. Alvarez-Ramirez. Polymer electrolytes through functionalization of poly (poly (ethylene glycol) methacrylate) with zwitterionic pendant groups: The role of ion clusters upon conductivity. *Solid State Ionics*, 320(December 2017):45–54, 2018.

[118] Gregorio Guzmán, Dora P Nava, Jorge Vazquez-Arenas, and Judith Cardoso. Design of a Zwitterion Polymer Electrolyte Based on Poly[poly

(ethylene glycol) methacrylate]: The Effect of Sulfobetaine Group on Thermal Properties and Ionic Conduction. *Macromolecular Symposia*, 374(1):1600136, aug 2017.

[119] Lisa M Hall, Michelle E Seitz, Karen I Winey, Kathleen L Opper, Kenneth B Wagener, Mark J Stevens, and Amalie L Frischknecht. Ionic Aggregate Structure in Ionomer Melts: Effect of Molecular Architecture on Aggregates and the Ionomer Peak. *Journal of the American Chemical Society*, 134(1):574–587, jan 2012.

[120] Lisa M Hall, Michelle E Seitz, Karen I Winey, Kathleen L Opper, Kenneth B Wagener, Mark J Stevens, and Amalie L Frischknecht. Ionic aggregate structure in ionomer melts: Effect of molecular architecture on aggregates and the ionomer peak. *Journal of the American Chemical Society*, 134(1):574–587, 2012.

[121] Lisa M Hall, Mark J Stevens, and Amalie L Frischknecht. Effect of polymer architecture and ionic aggregation on the scattering peak in model ionomers. *Physical Review Letters*, 106(12):127801, 2011.

[122] Lisa M Hall, Mark J Stevens, and Amalie L Frischknecht. Dynamics of Model Ionomer Melts of Various Architectures. *Macromolecules*, 45(19):8097–8108, oct 2012.

[123] Robert Hayes, Natalia Borisenko, Matthew K Tam, Patrick C Howlett, Frank Endres, and Rob Atkin. Double Layer Structure of Ionic Liquids

at the Au(111) Electrode Interface: An Atomic Force Microscopy Investigation. *The Journal of Physical Chemistry C*, 115(14):6855–6863, apr 2011.

[124] Hendrik Heinz, Tzu-Jen Lin, Ratan Kishore Mishra, and Fateme S Emami. Thermodynamically Consistent Force Fields for the Assembly of Inorganic, Organic, and Biological Nanostructures: The INTERFACE Force Field. *Langmuir*, 29(6):1754–1765, feb 2013.

[125] Maximilian Heres, Tyler Cosby, Emmanuel Urandu Mapesa, Hongjun Liu, Stefan Berdzinski, Veronika Strehmel, Mark Dadmun, Stephen J Paddison, and Joshua Sangoro. Ion Transport in Glassy Polymerized Ionic Liquids: Unraveling the Impact of the Molecular Structure. *Macromolecules*, 52(1):88–95, jan 2019.

[126] Maximilian Heres, Tyler Cosby, Emmanuel Urandu Mapesa, and Joshua Sangoro. Probing Nanoscale Ion Dynamics in Ultrathin Films of Polymerized Ionic Liquids by Broadband Dielectric Spectroscopy. *ACS Macro Letters*, 5(9):1065–1069, 2016.

[127] Maximilian Heres, Tyler Cosby, Emmanuel Urandu Mapesa, and Joshua Sangoro. Probing Nanoscale Ion Dynamics in Ultrathin Films of Polymerized Ionic Liquids by Broadband Dielectric Spectroscopy. *ACS Macro Letters*, 5(9):1065–1069, 2016.

[128] Steffen Hess, Margret Wohlfahrt-Mehrens, and Mario Wachtler. Flammability of Li-Ion Battery Electrolytes: Flash Point and Self-Extinguishing

Time Measurements. *Journal of The Electrochemical Society*, 162(2):A3084–A3097, 2015.

[129] Michiko Hirao, Kaori Ito, and Hiroyuki Ohno. Preparation and polymerization of new organic molten salts ; N -alkylimidazolium salt derivatives. 45:1291–1294, 2000.

[130] Michiko Hirao, Kaori Ito-akita, and Hiroyuki Ohno. Polymerization of Molten Salt Monomers having a Phenylimidazolium Group. 538(November 1999):534–538, 2000.

[131] R.W. Hockney and J.W. Eastwood. *Computer Simulation Using Particles*. CRC Press, 1988.

[132] P J Hoogerbrugge and J M V A Koelman. Simulating Microscopic Hydrodynamic Phenomena with Dissipative Particle Dynamics. *EUROPHYSICS LETTERS Europhys. Lett*, 19(3):155–160, 1992.

[133] C. Iacob, J. R. Sangoro, W. K. Kipnusu, R. Valiullin, J. Kärger, and F. Kremer. Enhanced charge transport in nano-confined ionic liquids. *Soft Matter*, 8(2):289–293, 2012.

[134] Ciprian Iacob, Atsushi Matsumoto, Marissa Brennan, Hongjun Liu, Stephen J. Paddison, Osamu Urakawa, Tadashi Inoue, Joshua Sangoro, and James Runt. Polymerized Ionic Liquids: Correlation of Ionic Conductivity with Nanoscale Morphology and Counterion Volume. *ACS Macro Letters*, 6:941–946, 2017.

[135] Takahiro Ichikawa. Zwitterions as building blocks for functional liquid crystals and block copolymers. *Polymer Journal*, 49(5):413–421, 2017.

[136] Toshifumi Iimori, Takashi Iwahashi, Hisao Ishii, Kazuhiko Seki, Yukio Ouchi, Ryosuke Ozawa, Hiro-o Hamaguchi, and Doseok Kim. Orientational ordering of alkyl chain at the air/liquid interface of ionic liquids studied by sum frequency vibrational spectroscopy. *Chemical Physics Letters*, 389(4):321–326, 2004.

[137] Toshifumi Iimori, Takashi Iwahashi, Kaname Kanai, Kazuhiko Seki, Jaeho Sung, Doseok Kim, Hiro-o Hamaguchi, and Yukio Ouchi. Local Structure at the Air/Liquid Interface of Room-Temperature Ionic Liquids Probed by Infrared-Visible Sum Frequency Generation Vibrational Spectroscopy: 1-Alkyl-3-methylimidazolium Tetrafluoroborates. *The Journal of Physical Chemistry B*, 111(18):4860–4866, may 2007.

[138] Vladislav Invnistsev and Maxim V. Fedorov. Insights from Molecular Simulations. *The Electrochemical Society Interface*, 23(1):65–69, 2014.

[139] Amjad Islam, Jianguo Li, Muhammad Pervaiz, Zheng Hong Lu, Mohini Sain, Lihui Chen, and Xinhua Ouyang. Zwitterions for Organic/Perovskite Solar Cells, Light-Emitting Devices, and Lithium Ion Batteries: Recent Progress and Perspectives. *Advanced Energy Materials*, 9(10):1–35, 2019.

[140] George Jaffe and John A. Rider. Polarization in Electrolytic Solutions.

Part I. Theory. *The Journal of Chemical Physics*, 20(7):1071–1077, 1952.

[141] H. Donald B. Jenkins, Helen K. Roobottom, Jack Passmore, and Leslie Glasser. Relationships among Ionic Lattice Energies, Molecular (Formula Unit) Volumes, and Thermochemical Radii. *Inorganic Chemistry*, 38(16):3609–3620, 1999.

[142] De-en Jiang, Zhehui Jin, and Jianzhong Wu. Oscillation of Capacitance inside Nanopores. *Nano Letters*, 11(12):5373–5377, dec 2011.

[143] Fangling Jiang, Cheng Li, Haiying Fu, Chenyang Wang, Xiaojing Guo, Zheng Jiang, Guozhong Wu, and Shimou Chen. Temperature-Induced Molecular Rearrangement of an Ionic Liquid Confined in Nanospaces: An in Situ X-ray Absorption Fine Structure Study. *Journal of Physical Chemistry C*, 119(39):22724–22731, 2015.

[144] William L Jorgensen, David S Maxwell, and Julian Tirado-Rives. Development and Testing of the OLPS All-Atom Force Field on Conformational Energetics and Properties of Organic Liquids. *J. Am. Chem. Soc.*, 118(15):11225–11236, 1996.

[145] William L Jorgensen, Julian Tirado-rives, and Force Fields. Potential energy functions for atomic-level simulations of water and organic and biomolecular systems. *PNAS*, 102(19):1–6, 2005.

[146] Ryan R. Julian and Martin F. Jarrold. Gas-phase zwitterions in the absence of a net charge. *Journal of Physical Chemistry A*, 108(49):10861–10864, 2004.

[147] Jordan Keith, Santosh Mogurampelly, Faisal Aldukhi, Bill Wheatle, and Venkat Ganesan. Influence of molecular weight on ion-transport properties of polymeric ionic liquids. *Phys Chem Chem Phys*, 19:29134, 2017.

[148] Jordan R. Keith, Santosh Mogurampelly, Bill K. Wheatle, and Venkat Ganesan. Influence of side chain linker length on ion-transport properties of polymeric ionic liquids. *Journal of Polymer Science Part B: Polymer Physics*, 55(23):1718–1723, 2017.

[149] Jordan R. Keith, Nathan J. Rebello, Benjamin J. Cowen, and Venkat Ganesan. Influence of Counterion Structure on Conductivity of Polymerized Ionic Liquids. *ACS Macro Letters*, 8:387–392, 2019.

[150] Ryunosuke Kikuchi. CO 2 Recovery and Reuse in the Energy Sector, Energy Resource Development and Others: Economic and Technical Evaluation of Large-Scale Co 2 Recycling . *Energy & Environment*, 14(4):383–395, 2003.

[151] Kento Kimura, Joh Motomatsu, and Yoichi Tominaga. Correlation between Solvation Structure and Ion-Conductive Behavior of Concentrated Poly(ethylene carbonate)-Based Electrolytes. *The Journal of Physical Chemistry C*, 120:12385–12391, 2016.

[152] Sergey A Kislenko, Igor S Samoylov, and Ravil H Amirov. Molecular dynamics simulation of the electrochemical interface between a graphite surface and the ionic liquid [BMIM][PF6]. *Physical Chemistry Chemical Physics*, 11(27):5584–5590, 2009.

[153] Robert J. Klein, Shihai Zhang, Shichen Dou, Brad H. Jones, Ralph H. Colby, and James Runt. Modeling electrode polarization in dielectric spectroscopy: Ion mobility and mobile ion concentration of single-ion polymer electrolytes. *Journal of Chemical Physics*, 124(14):144903, 2006.

[154] J M V A Koelman and P J Hoogerbrugge. Dynamic Simulations of Hard-Sphere Suspensions Under Steady Shear. *Europhysics Letters (EPL)*, 21(3):363–368, 1993.

[155] Lingxi Kong, Chuan Li, Jiuchun Jiang, and Michael G. Pecht. Li-ion battery fire hazards and safety strategies. *Energies*, 11(9):1–11, 2018.

[156] Alexei A Kornyshev. Double-Layer in Ionic Liquids: Paradigm Change? *The Journal of Physical Chemistry B*, 111(20):5545–5557, may 2007.

[157] M. H. Kowsari, Saman Alavi, Mahmud Ashrafizaadeh, and Bijan Najafi. Molecular dynamics simulation of imidazolium-based ionic liquids. II. Transport coefficients. *Journal of Chemical Physics*, 130(1):014703, 2009.

[158] Friedrich Kremer and Andreas Schonhals, editors. *Broadband Dielectric Spectroscopy*. Springer-Verlag Berlin Heidelberg, New York, NY, 1 edition, 2003.

[159] Sarkyt Kudaibergenov, Werner Jaeger, and Andre Laschewsky. Polymeric Betaines: Synthesis, Characterization, and Application. In *Supramolecular Polymers Polymeric Betains Oligomers*, pages 157–224. Springer-Verlag Berlin Heidelberg, Berlin, Heidelberg, 2006.

[160] Nikki H. Lafemina, Quan Chen, Ralph H. Colby, and Karl T. Mueller. The diffusion and conduction of lithium in poly(ethylene oxide)-based sulfonate ionomers. *Journal of Chemical Physics*, 145(11):114903, 2016.

[161] Oliver J Lanning and Paul A Madden. Screening at a Charged Surface by a Molten Salt. *The Journal of Physical Chemistry B*, 108(30):11069–11072, jul 2004.

[162] Uwe Lappan and Ulrich Scheler. Influence of the Nature of the Ion Pairs on the Segmental Dynamics in Polyelectrolyte Complex Coacervate Phases. *Macromolecules*, page acs.macromol.7b01858, 2017.

[163] André Laschewsky. Structures and synthesis of zwitterionic polymers. *Polymers*, 6(5):1544–1601, 2014.

[164] George Law and Philip R Watson. Surface orientation in ionic liquids. *Chemical Physics Letters*, 345(1):1–4, 2001.

[165] George Law and Philip R Watson. Surface Tension Measurements of N-Alkylimidazolium Ionic Liquids. *Langmuir*, 17(20):6138–6141, oct 2001.

[166] George Law, Philip R Watson, Adrian J Carmichael, and Kenneth R Seddon. Molecular composition and orientation at the surface of room-temperature ionic liquids: Effect of molecular structure. *Physical Chemistry Chemical Physics*, 3(14):2879–2885, 2001.

[167] J. Le Bideau, P. Gaveau, S. Bellayer, M. A. Néouze, and A. Vioux. Effect of confinement on ionic liquids dynamics in monolithic silica ionogels: 1H NMR study. *Physical Chemistry Chemical Physics*, 9(40):5419–5422, 2007.

[168] Minjae Lee, U. Hyeok Choi, Ralph H. Colby, and Harry W. Gibson. Ion conduction in imidazolium acrylate ionic liquids and their polymers. *Chemistry of Materials*, 22(21):5814–5822, 2010.

[169] Minjae Lee, U. Hyeok Choi, David Salas-De La Cruz, Anuj Mittal, Karen I. Winey, Ralph H. Colby, and Harry W. Gibson. Imidazolium polyesters: Structure-property relationships in thermal behavior, ionic conductivity, and morphology. *Advanced Functional Materials*, 21(4):708–717, 2011.

[170] Qi Lei, Chen Zheng, Fang He, Jia Zhao, Yang Liu, Xiaopeng Zhao, and Jianbo Yin. Enhancing Electroresponsive Electrorheological Effect and

Temperature Dependence of Poly(ionic liquid) Particles by Hard Core Confinement. *Langmuir*, 34(51):15827–15838, dec 2018.

[171] Dennis Y.C. Leung, Giorgio Caramanna, and M. Mercedes Maroto-Valer. An overview of current status of carbon dioxide capture and storage technologies. *Renewable and Sustainable Energy Reviews*, 39:426–443, 2014.

[172] Thomas Lewis and Venkat Ganesan. Mean-field modeling of the encapsulation of weakly acidic molecules in polyelectrolyte dendrimers. *Journal of Physical Chemistry B*, 116(28):8269–8281, 2012.

[173] Linlin Li, Siyuan Li, and Yingying Lu. Suppression of dendritic lithium growth in lithium metal-based batteries. *Chemical Communications*, 54(50):6648–6661, 2018.

[174] Mian-Gang Li, Li Chen, Yun-Xin Zhong, Zhao-Bin Chen, Jia-Wei Yan, and Bing-Wei Mao. The electrochemical interface of Ag(111) in 1-ethyl-3-methylimidazolium bis(trifluoromethylsulfonyl)imide ionic liquid—A combined in-situ scanning probe microscopy and impedance study. *Electrochimica Acta*, 197:282–289, 2016.

[175] Qi Li, Juner Chen, Lei Fan, Xueqian Kong, and Yingying Lu. Progress in electrolytes for rechargeable Li-based batteries and beyond. *Green Energy & Environment*, 1(1):18–42, 2016.

[176] Siwei Liang, U Hyeok Choi, Wenjuan Liu, James Runt, and Ralph H Colby. Synthesis and Lithium Ion Conduction of Polysiloxane Single-Ion Conductors Containing Novel Weak-Binding Borates. *Chemistry of Materials*, 24(12):2316–2323, jun 2012.

[177] Kan-Ju Lin, Katherine Li, and Janna K. Maranas. Differences between polymer/salt and single ion conductor solid polymer electrolytes. *RSC Advances*, 3:1564–1571, 2013.

[178] Kan Ju Lin and Janna K. Maranas. Cation coordination and motion in a poly(ethylene oxide)-based single ion conductor. *Macromolecules*, 45(15):6230–6240, 2012.

[179] Kan-Ju Lin and Janna K Maranas. Does decreasing ion-ion association improve cation mobility in single ion conductors? *Physical chemistry chemical physics : PCCP*, 15:16143–51, 2013.

[180] Yue Lin, Jie Li, Yanqing Lai, Changfu Yuan, Yun Cheng, and Jin Liu. A wider temperature range polymer electrolyte for all-solid-state lithium ion batteries. *RSC Advances*, 3(27):10722, 2013.

[181] Fatin Lind, Luis Rebollar, Prity Bengani-Lutz, Ayse Asatekin, and Matthew J. Panzer. Zwitterion-Containing Ionogel Electrolytes. *Chemistry of Materials*, 28(23):8480–8483, 2016.

[182] Martin Lísal, John K. Brennan, and Josep Bonet Avalos. Dissipative particle dynamics at isothermal, isobaric, isoenergetic, and isoenthalpic

conditions using Shardlow-like splitting algorithms. *Journal of Chemical Physics*, 135(20), 2011.

[183] Hongjun Liu and Edward Maginn. A molecular dynamics investigation of the structural and dynamic properties of the ionic liquid 1-n-butyl-3-methylimidazolium bis ( trifluoromethanesulfonyl ) imide A molecular dynamics investigation of the structural and dynamic properties of the ionic l. *J. Chem. Phys*, 135:124507, 2011.

[184] Hongjun Liu and Stephen J. Paddison. Direct Comparison of Atomistic Molecular Dynamics Simulations and X-ray Scattering of Polymerized Ionic Liquids. *ACS Macro Letters*, 5(4):537–543, 2016.

[185] Mingzhu Liu, Biyu Jin, Qinghua Zhang, Xiaoli Zhan, and Fengqiu Chen. High-performance solid polymer electrolytes for lithium ion batteries based on sulfobetaine zwitterion and poly (ethylene oxide) modified polysiloxane. *Journal of Alloys and Compounds*, 742:619–628, 2018.

[186] Yao Liu, Volodimyr V. Duzhko, Zachariah A. Page, Todd Emrick, and Thomas P. Russell. Conjugated Polymer Zwitterions: Efficient Interlayer Materials in Organic Electronics. *Accounts of Chemical Research*, 49(11):2478–2488, 2016.

[187] Yaodong Liu, Yi Zhang, Guozhong Wu, and Jun Hu. Coexistence of Liquid and Solid Phases of Bmim-PF6 Ionic Liquid on Mica Surfaces at Room Temperature. *Journal of the American Chemical Society*, 128(23):7456–7457, jun 2006.

[188] José N.Canongia Lopes and Agílio A.H. Pádua. Molecular force field for ionic liquids composed of triflate or bistriflylimide anions. *Journal of Physical Chemistry B*, 108(43):16893–16898, 2004.

[189] M. S. Loth, Brian Skinner, and B. I. Shklovskii. Anomalously large capacitance of an ionic liquid described by the restricted primitive model. *Physical Review E - Statistical, Nonlinear, and Soft Matter Physics*, 82(5):1–7, 2010.

[190] Andrew B Lowe and Charles L McCormick. Synthesis and Solution Properties of Zwitterionic Polymers. *Chemical Reviews*, 102(11):4177–4190, nov 2002.

[191] Fei Lu, Xinpei Gao, Aoli Wu, Na Sun, Lijuan Shi, and Liqiang Zheng. Lithium-Containing Zwitterionic Poly(Ionic Liquid)s as Polymer Electrolytes for Lithium-Ion Batteries. *Journal of Physical Chemistry C*, 121(33):17756–17763, 2017.

[192] Keran Lu, Janna K. Maranas, and Scott T. Milner. Ion-mediated charge transport in ionomeric electrolytes. *Soft Matter*, 12(17):3943–3954, 2016.

[193] Keran Lu, Joseph F. Rudzinski, William G. Noid, Scott T. Milner, and Janna K. Maranas. Scaling behavior and local structure of ion aggregates in single-ion conductors. *Soft Matter*, 10:978–989, 2014.

[194] R M Lynden-Bell, J Kohanoff, and M G Del Popolo. Simulation of interfaces between room temperature ionic liquids and other liquids. *Faraday Discussions*, 129(0):57–67, 2005.

[195] R.M. Lynden-Bell. Gas-liquid interfaces of room temperature ionic liquids. *Molecular Physics*, 101(16):2625–2633, aug 2003.

[196] Qiang Ma, Heng Zhang, Chongwang Zhou, Liping Zheng, Pengfei Cheng, Jin Nie, Wenfang Feng, Yong-Sheng Hu, Hong Li, Xuejie Huang, Liquan Chen, Michel Armand, and Zhibin Zhou. Single Lithium-Ion Conducting Polymer Electrolytes Based on a Super-Delocalized Polyanion. *Angewandte Chemie International Edition*, 55(7):2521–2525, feb 2016.

[197] J Ross Macdonald. Theory of ac space-charge polarization effects in photoconductors, semiconductors, and electrolytes. *Physical Review*, 92(1):4–17, 1953.

[198] J. Ross Macdonald. Simplified impedance/frequency-response results for intrinsically conducting solids and liquids. *The Journal of Chemical Physics*, 61(10):3977–3996, 1974.

[199] Guomin Mao, Ricardo Fernandez Perea, W. Spencer Howells, David L. Price, and Marie-Louise Saboungi. Relaxation in polymer electrolytes on the nanosecond timescale. *Nature*, 405(6783):163–165, 2000.

[200] Guomin Mao, Marie-louise Saboungi, and David L Price. alpha-Relaxation in PEO - LiTFSI Polymer Electrolytes. *Macromolecules*, 35:415–419,

2002.

[201] Sha Maolin, Zhang Fuchun, Wu Guozhong, Fang Haiping, Wang Chunlei, Chen Shimou, Zhang Yi, and Hu Jun. Ordering layers of [bmim][PF6] ionic liquid on graphite surfaces: Molecular dynamics simulation. *The Journal of Chemical Physics*, 128(13):134504, apr 2008.

[202] M. Marcinek, J. Syzdek, M. Marczewski, M. Piszcz, L. Niedzicki, M. Kalita, A. Plewa-Marczewska, A. Bitner, P. Wieczorek, T. Trzeciak, M. Kasprzyk, P. Lezak, Z. Zukowska, A. Zalewska, and W. Wieczorek. Electrolytes for Li-ion transport - Review. *Solid State Ionics*, 276:107–126, 2015.

[203] Yizhak Marcus. Ionic and molar volumes of room temperature ionic liquids. *Journal of Molecular Liquids*, 209:289–293, 2015.

[204] Henrik Markusson, Hiroyuki Tokuda, Masayoshi Watanabe, Patrik Johansson, and Per Jacobsson. IR spectroscopy and quantum mechanical calculations of lithium ion transport conditions in a single ion conducting polymer electrolyte. *Polymer*, 45(26):9057–9065, 2004.

[205] Imee Su Martinez and Steven Baldelli. On the Arrangement of Ions in Imidazolium-Based Room Temperature Ionic Liquids at the Gas-Liquid Interface, Using Sum Frequency Generation, Surface Potential, and Surface Tension Measurements. *The Journal of Physical Chemistry C*, 114(26):11564–11575, jul 2010.

[206] L. Martinez, R. Andrade, E.G. Birgin, and J.M. Martinez. Packmol: A Package for Building Initial Configurations forMolecular Dynamics Simulations. *Journal of computational chemistry*, 30(13):2157–2164, 2009.

[207] Glenn J. Martyna, Douglas J. Tobias, and Michael L. Klein. Constant pressure molecular dynamics algorithms. *The Journal of Chemical Physics*, 101(September):4177–4189, 1994.

[208] Jesse G McDaniel, Eunsong Choi, Chang-Yun Son, J R Schmidt, and Arun Yethiraj. Conformational and Dynamic Properties of Poly(ethylene oxide) in an Ionic Liquid: Development and Implementation of a First-Principles Force Field. *Journal of Physical Chemistry B*, 120(1):231–243, 2016.

[209] David Mecerreyes. Polymeric ionic liquids: Broadening the properties and applications of polyelectrolytes. *Progress in Polymer Science (Oxford)*, 36(12):1629–1648, 2011.

[210] Kelly M Meek and Yossef A Elabd. Polymerized ionic liquid block copolymers for electrochemical energy. *J. Mater. Chem. A*, 3:24187–24194, 2015.

[211] Kelly M Meek, Sharon Sharick, Yuesheng Ye, Karen I Winey, and Yossef A Elabd. Bromide and Hydroxide Conductivity-Morphology Relationships in Polymerized Ionic Liquid Block Copolymers. *Macromolecules*, 48(14):4850–4862, 2015.

[212] Naveen Michaud-Agrawal, Elizabeth J Denning, Thomas B Woolf, and Oliver Beckstein. MDAnalysis: A toolkit for the analysis of molecular dynamics simulations. *Journal of Computational Chemistry*, 32(10):2319–2327, jul 2011.

[213] Santosh Mogurampelly, Oleg Borodin, and Venkat Ganesan. Computer Simulations of Ion Transport in Polymer Electrolyte Membranes. *Annual Review of Chemical and Biomolecular Engineering*, 7(1):349–371, 2016.

[214] Santosh Mogurampelly and Venkat Ganesan. Effect of nanoparticles on ion transport in polymer electrolytes. *Macromolecules*, 48(8):2773–2786, 2015.

[215] Santosh Mogurampelly and Venkat Ganesan. Ion Transport in Polymerized Ionic Liquid–Ionic Liquid Blends. *Macromolecules*, 51:acs.macromol.8b01460, 2018.

[216] Santosh Mogurampelly, Jordan Keith, and Venkat Ganesan. Structural Relaxations of Ion Association Facilitate Ion Transport in Polymerized Ionic Liquids. *Journal of the American Chemical Society*, 139(28):9511–9514, 2017.

[217] Santosh Mogurampelly, Jordan R. Keith, and Venkat Ganesan. Mechanisms Underlying Ion Transport in Polymerized Ionic Liquids. *Journal of the American Chemical Society*, 139(28):9511–9514, 2017.

[218] Anirban Mondal and Sundaram Balasubramanian. Quantitative Prediction of Physical Properties of Imidazolium Based Room Temperature Ionic Liquids through Determination of Condensed Phase Site Charges: A Refined Force Field. *Journal of Physical Chemistry B*, 118:3409–3422, 2014.

[219] Jagannath Mondal, Eunsong Choi, and Arun Yethiraj. Atomistic Simulations of Poly ( ethylene oxide ) in Water and an Ionic Liquid at Room Temperature. *Macromolecules*, 47:438–446, 2013.

[220] Katrina Irene S Mongcopa, Madhusudan Tyagi, Jonathan P Mailoa, Georgy Samsonidze, Boris Kozinsky, Scott A Mullin, Daniel A Gribble, Hiroshi Watanabe, and Nitash P Balsara. Relationship between Segmental Dynamics Measured by Quasi-Elastic Neutron Scattering and Conductivity in Polymer Electrolytes. *ACS Macro Letters*, 7(4):504–508, apr 2018.

[221] Charles Monroe and John Newman. The Impact of Elastic Deformation on Deposition Kinetics at Lithium/Polymer Interfaces. *Journal of The Electrochemical Society*, 152(2):A396, 2005.

[222] Timothy I Morrow and Edward J Maginn. Molecular Dynamics Study of the Ionic Liquid 1- n -Butyl-3-methylimidazolium Hexafluorophosphate. *The Journal of Physical Chemistry B*, 106(49):12807–12813, 2002.

[223] Marcus Müller and Juan J. de Pablo. Computational Approaches for

the Dynamics of Structure Formation in Self-Assembling Polymeric Materials. *Annual Review of Materials Research*, 43(1):1–34, 2013.

[224] Kenji Nakamura, Koji Fukao, and Tadashi Inoue. Dielectric relaxation and viscoelastic behavior of polymerized ionic liquids with various counteranions. *Macromolecules*, 45(9):3850–3858, 2012.

[225] Kenji Nakamura, Tatsuya Saiwaki, and Koji Fukao. Dielectric relaxation behavior of polymerized ionic liquid. *Macromolecules*, 43(14):6092–6098, 2010.

[226] Kenji Nakamura, Tatsuya Saiwaki, Koji Fukao, and Tadashi Inoue. Viscoelastic Behavior of the Polymerized Ionic Liquid Poly(1-ethyl-3-vinylimidazolium bis(trifluoromethanesulfonylimide)). *Macromolecules*, 44(19):7719–7726, 2011.

[227] Sylvie Neyertz and David Brown. Local structure and mobility of ions in polymer electrolytes: A molecular dynamics simulation study of the amorphous PEO <sub> x </sub> NaI system. *The Journal of Chemical Physics*, 104(10):3797–3809, 1996.

[228] P. Nikunen, M. Karttunen, and I. Vattulainen. How would you integrate the equations of motion in dissipative particle dynamics simulations? *Computer Physics Communications*, 153(3):407–423, 2003.

[229] Naomi Nishimura and Hiroyuki Ohno. 15th anniversary of polymerised ionic liquids. *Polymer (United Kingdom)*, 55(16):3289–3297, aug 2014.

[230] Hiroyuki Ohno. Ohno - molten salt type polymer electrolytes. *Electrochimica Acta*, 46:1407–1411, 2001.

[231] Hiroyuki Ohno. Functional design of ionic liquids. *Bulletin of the Chemical Society of Japan*, 79(11):1665–1680, 2006.

[232] Hiroyuki Ohno and Kaori Ito. Room-Temperature Molten Salt Polymers as a Matrix for Fast Ion Conduction. *Chemistry Letters*, 27:751–752, 1998.

[233] Hiroyuki Ohno, Masahiro Yoshizawa-Fujita, and Yuki Kohno. Design and properties of functional zwitterions derived from ionic liquids. *Physical Chemistry Chemical Physics*, 20(16):10978–10991, 2018.

[234] Michael V. O'Reilly, Hanqing Masser, Daniel R. King, Paul C. Painter, Ralph H. Colby, Karen I. Winey, and James Runt. Ionic aggregate dissolution and conduction in a plasticized single-ion polymer conductor. *Polymer (United Kingdom)*, 59:133–143, 2015.

[235] I Pagonabarraga, M H J Hagen, and D Frenkel. Self-consistent dissipative particle dynamics algorithm. *Europhys. Lett.*, 42(4):377–382, may 1998.

[236] Tamás Pajkossy, Claus Müller, and Timo Jacob. The metal–ionic liquid interface as characterized by impedance spectroscopy and in situ scanning tunneling microscopy. *Physical Chemistry Chemical Physics*, 20(33):21241–21250, 2018.

[237] Moon Jeong Park. Confinement-entitled morphology and ion transport in ion-containing polymers. *Molecular Systems Design & Engineering*, 4(2):239, 2019.

[238] M. Parrinello and A. Rahman. Polymorphic transitions in single crystals: A new molecular dynamics method. *Journal of Applied Physics*, 52(12):7182–7190, 1981.

[239] Danielle M Pesko, Michael A Webb, Yukyung Jung, Qi Zheng, Thomas F Miller, Geoffrey W Coates, and Nitash P Balsara. Universal Relationship between Conductivity and Solvation-Site Connectivity in Ether-Based Polymer Electrolytes. *Macromolecules*, 49(14):5244–5255, jul 2016.

[240] C Peter and K Kremer. Multiscale simulation of soft matter systems. *Faraday Discussions*, 144:9, 2010.

[241] Carlos Pinilla, M. G. Del Pópolo, Jorge Kohanoff, and R. M. Lynden-Bell. Polarization relaxation in an ionic liquid confined between electrified walls. *Journal of Physical Chemistry B*, 111(18):4877–4884, 2007.

[242] Carlos Pinilla, Mario G Del Pópolo, Ruth M Lynden-Bell, and Jorge Kohanoff. Structure and Dynamics of a Confined Ionic Liquid. Topics of Relevance to Dye-Sensitized Solar Cells. *The Journal of Physical Chemistry B*, 109(38):17922–17927, sep 2005.

[243] Steve Plimpton. Fast Parallel Algorithms for Short-Range Molecular Dynamics. *Journal of Computational Physics*, 117(1):1–19, 1995.

[244] Steve Plimpton, Roy Pollock, and Mark J. Stevens. Particle Mesh Ewald and rRESPA for Parallel Molecular Dynamics Simulations. In *Proceedings of the Eighth Siam Conference on Parallel Processing for Scientific Computing*, pages 1–13, 1997.

[245] Luca Porcarelli, Petr S Vlasov, Denis O Ponkratov, Elena I Lozinskaya, Dmitrii Y Antonov, Jijeesh R Nair, Claudio Gerbaldi, David Mecerreyes, and Alexander S Shaplov. Design of ionic liquid like monomers towards easy-accessible single-ion conducting polymer electrolytes. *European Polymer Journal*, 107:218–228, 2018.

[246] Victor Pryamitsyn and Venkat Ganesan. Interplay between depletion and electrostatic interactions in polyelectrolyte-nanoparticle systems. *Macromolecules*, 47(17):6095–6112, 2014.

[247] Wenjing Qian, John Texter, and Feng Yan. Frontiers in poly(ionic liquid)s: Syntheses and applications. *Chemical Society Reviews*, 46(4):1124–1159, 2017.

[248] Nav Nidhi Rajput, Joshua Monk, and Francisco R. Hung. Structure and dynamics of an ionic liquid confined inside a charged slit graphitic nanopore. *Journal of Physical Chemistry C*, 116(27):14504–14513, 2012.

[249] D.R. Reidmiller, C.W. Avery, D.R. Easterling, K.E. Kunkel, K.L.M. Lewis, T.K. Maycock, and B.C. Stewart. Impacts, Risks, and Adaptation in the United States: Fourth National Climate Assessment, Volume II. 2018.

[250] Julie B Rollins, Brian D Fitchett, and John C Conboy. Structure and Orientation of the Imidazolium Cation at the Room-Temperature Ionic Liquid/SiO2 Interface Measured by Sum-Frequency Vibrational Spectroscopy. *The Journal of Physical Chemistry B*, 111(18):4990–4999, may 2007.

[251] Casey Romero and Steven Baldelli. Sum Frequency Generation Study of the Room-Temperature Ionic Liquids/Quartz Interface. *The Journal of Physical Chemistry B*, 110(12):6213–6223, mar 2006.

[252] Casey Romero, H Justin Moore, T Randall Lee, and Steven Baldelli. Orientation of 1-Butyl-3-methylimidazolium Based Ionic Liquids at a Hydrophobic Quartz Interface Using Sum Frequency Generation Spectroscopy. *The Journal of Physical Chemistry C*, 111(1):240–247, jan 2007.

[253] David Salas-de-la Cruz, Matthew D. Green, Yuesheng Ye, Yossef A. Elabd, Timothy E. Long, and Karen I. Winey. Correlating backbone-to-backbone distance to ionic conductivity in amorphous polymerized ionic liquids. *Journal of Polymer Science Part B: Polymer Physics*, 50(5):338–346, mar 2012.

[254] Somisetti V Sambasivarao and Orlando Acevedo. Development of OPLS-AA force field parameters for 68 unique ionic liquids. *Journal of Chemical Theory and Computation*, 5(4):1038–1050, 2009.

[255] J. Sangoro, C. Iacob, A. Serghei, S. Naumov, P. Galvosas, J. Kärger, C. Wespe, F. Bordusa, A. Stoppa, J. Hunger, R. Buchner, and F. Kremer. Electrical conductivity and translational diffusion in the 1-butyl-3-methylimidazolium tetrafluoroborate ionic liquid. *Journal of Chemical Physics*, 128(21):214509, 2008.

[256] J R Sangoro, C Iacob, A L Agapov, Y Wang, S Berdzinski, H Rexhausen, V Strehmel, C Friedrich, A P Sokolov, and F Kremer. Decoupling of ionic conductivity from structural dynamics in polymerized ionic liquids. *Soft Matter*, 10:3536–3540, 2014.

[257] J R Sangoro, C Iacob, A Serghei, C Friedrich, and F Kremer. Universal scaling of charge transport in glass-forming ionic liquids. *Physical chemistry chemical physics : PCCP*, 11(6):913–916, 2009.

[258] Gabriel E. Sanoja, Bhooshan C. Popere, Bryan S. Beckingham, Christopher M. Evans, Nathaniel A. Lynd, and Rachel A. Segalman. Structure-Conductivity Relationships of Block Copolymer Membranes Based on Hydrated Protic Polymerized Ionic Liquids: Effect of Domain Spacing. *Macromolecules*, 49(6):2216–2223, 2016.

[259] Gabriel E. Sanoja, Nicole S. Schauser, Joshua M. Bartels, Christopher M. Evans, Matthew E. Helgeson, Ram Seshadri, and Rachel A. Segalman.

Ion Transport in Dynamic Polymer Networks Based on Metal-Ligand Coordination: Effect of Cross-Linker Concentration. *Macromolecules*, 51(5):2017–2026, 2018.

[260] Cherry S Santos and Steven Baldelli. Surface Orientation of 1-Methyl-, 1-Ethyl-, and 1-Butyl-3-methylimidazolium Methyl Sulfate as Probed by Sum-Frequency Generation Vibrational Spectroscopy. *The Journal of Physical Chemistry B*, 111(18):4715–4723, may 2007.

[261] T. Schneider and E. Stoll. Molecular-dynamics study of a three-dimensional one-component model for distortive phase transitions. *Physical Review B*, 17(3):1302–1322, 1978.

[262] Christian Schröder and Othmar Steinhauser. On the dielectric conductivity of molecular ionic liquids. *Journal of Chemical Physics*, 131(11):114504, 2009.

[263] S. S. Sekhon, Boor Singh Lalia, Jin Soo Park, Chang Soo Kim, and K. Yamada. Physicochemical properties of proton conducting membranes based on ionic liquid impregnated polymer for fuel cells. *Journal of Materials Chemistry*, 16(23):2256–2265, 2006.

[264] Luis A Selis and Jorge M. Seminario. Dendrite formation in silicon anodes of lithium-ion batteries. *RSC Advances*, 8(10):5255–5267, 2018.

[265] Debabrata Seth, Anjan Chakraborty, Palash Setua, and Nilmoni Sarkar. Dynamics of Solvent and Rotational Relaxation of Coumarin-153 in

Room-Temperature Ionic Liquid 1-Butyl-3-methyl Imidazolium Tetrafluoroborate Confined in Poly(oxyethylene glycol) Ethers Containing Micelles. *The Journal of Physical Chemistry B*, 111(18):4781–4787, may 2007.

[266] Vaidyanathan Sethuraman, Santosh Mogurampelly, and Venkat Ganesan. Ion transport mechanisms in lamellar phases of salt-doped PS–PEO block copolymer electrolytes. *Soft Matter*, 13(42):7793–7803, 2017.

[267] Vaidyanathan Sethuraman, Santosh Mogurampelly, and Venkat Ganesan. Multiscale Simulations of Lamellar PS-PEO Block Copolymers Doped with LiPF6 Ions. *Macromolecules*, 50(11):4542–4554, 2017.

[268] Maolin Sha, Guozhong Wu, Haiping Fang, Guanglai Zhu, and Yusheng Liu. Liquid-to-Solid Phase Transition of a 1,3-Dimethylimidazolium Chloride Ionic Liquid Monolayer Confined between Graphite Walls. *The Journal of Physical Chemistry C*, 112(47):18584–18587, nov 2008.

[269] Maolin Sha, Guozhong Wu, Yusheng Liu, Zhongfeng Tang, and Haiping Fang. Drastic Phase Transition in Ionic Liquid [Dmim][Cl] Confined Between Graphite Walls: New Phase Formation. *The Journal of Physical Chemistry C*, 113(11):4618–4622, mar 2009.

[270] Nima Shahkaramipour, Thien N. Tran, Sankara Ramanan, and Haiqing Lin. Membranes with surface-enhanced antifouling properties for water purification. *Membranes*, 7(1):1–19, 2017.

[271] Qing Shao, Yi He, and Shaoyi Jiang. Molecular Dynamics Simulation Study of Ion Interactions with Zwitterions. *The Journal of Physical Chemistry B*, 115(25):8358–8363, jun 2011.

[272] Qing Shao and Shaoyi Jiang. Effect of Carbon Spacer Length on Zwitterionic Carboxybetaines. *The Journal of Physical Chemistry B*, 117(5):1357–1366, feb 2013.

[273] Qing Shao and Shaoyi Jiang. Influence of Charged Groups on the Properties of Zwitterionic Moieties: A Molecular Simulation Study. *The Journal of Physical Chemistry B*, 118(27):7630–7637, jul 2014.

[274] Qing Shao and Shaoyi Jiang. Molecular understanding and design of zwitterionic materials. *Advanced Materials*, 27(1):15–26, 2015.

[275] Qing Shao, Luo Mi, Xia Han, Tao Bai, Sijun Liu, Yuting Li, and Shaoyi Jiang. Differences in Cationic and Anionic Charge Densities Dictate Zwitterionic Associations and Stimuli Responses. *The Journal of Physical Chemistry B*, 118(24):6956–6962, jun 2014.

[276] Alexander S. Shaplov, Rebeca Marcilla, and David Mecerreyes. Recent Advances in Innovative Polymer Electrolytes based on Poly(ionic liquid)s. *Electrochimica Acta*, 175:18–34, 2015.

[277] Tony Shardlow. Splitting for dissipative particle dynamics. *SIAM J. Sci. Comput.*, 24(4):1267–1282, 2003.

[278] Chengtian Shen, Qiujie Zhao, and Christopher M. Evans. Ion specific, odd–even glass transition temperatures and conductivities in precise network polymerized ionic liquids. *Molecular Systems Design & Engineering*, 2019.

[279] Wataru Shinoda, Motoyuki Shiga, and Masuhiro Mikami. Rapid estimation of elastic constants by molecular dynamics simulation under constant stress. *Physical Review B - Condensed Matter and Materials Physics*, 69(13):134103, 2004.

[280] Meenakshi Singh and Nazia Tarannum. Polyzwitterions. In Anilkumar Parambath, editor, *Engineering of Biomaterials for Drug Delivery Systems*, chapter 4, pages 69–101. Woodhead Publishing, 2018.

[281] Mohit Singh, Omolola Odusanya, Gregg M. Wilmes, Hany B. Eitouni, Enrique D. Gomez, Amish J. Patel, Vincent L. Chen, Moon Jeong Park, Panagiota Fragouli, Hermis Iatrou, Nikos Hadjichristidis, David Cookson, and Nitash P. Balsara. Effect of Molecular Weight on the Mechanical and Electrical Properties of Block Copolymer Electrolytes. *Macromolecules*, 40(13):4578–4585, jun 2007.

[282] Ramesh Singh, Joshua Monk, and Francisco R. Hung. A computational study of the behavior of the ionic liquid [BMIM+][PF6-] confined inside multiwalled carbon nanotubes. *Journal of Physical Chemistry C*, 114(36):15478–15485, 2010.

[283] U. C. Singh and P. A. Kollman. An approach to computing electrostatic charges for molecules. *J. Comput. Chem.*, 5:129–145, 1984.

[284] Kokonad Sinha and Janna Maranas. Does Ion Aggregation Impact Polymer Dynamics and Conductivity in PEO-Based Single Ion Conductors? *Macromolecules*, 47(8):2718–2726, apr 2014.

[285] Kokonad Sinha and Janna K Maranas. Segmental Dynamics and Ion Association in PEO-Based Single Ion Conductors. *Macromolecules*, 44(13):5381–5391, jul 2011.

[286] John M. Slattery, Corinne Daguenet, Paul J. Dyson, Thomas J.S. Schubert, and Ingo Krossing. How to predict the physical properties of ionic liquids: A volume-based approach. *Angewandte Chemie - International Edition*, 46(28):5384–5388, 2007.

[287] Eli Sloutskin, Benjamin M Ocko, Lilach Tamam, Ivan Kuzmenko, Thomas Gog, and Moshe Deutsch. Surface Layering in Ionic Liquids: An X-ray Reflectivity Study. *Journal of the American Chemical Society*, 127(21):7796–7804, jun 2005.

[288] Chang Yun Son, Jesse G. McDaniel, J. R. Schmidt, Qiang Cui, and Arun Yethiraj. First-Principles United Atom Force Field for the Ionic Liquid BMIM+BF4-: An Alternative to Charge Scaling. *Journal of Physical Chemistry B*, 120(14):3560–3568, 2016.

[289] J.Y. Song, Y.Y. Wang, and C.C. Wan. Review of gel-type polymer electrolytes for lithium-ion batteries. *Journal of Power Sources*, 77(2):183–197, 1999.

[290] E. Spohr. Effect of electrostatic boundary conditions and system size on the interfacial properties of water and aqueous solutions. *Journal of Chemical Physics*, 107(16):6342–6348, 1997.

[291] H. V. Spohr and G. N. Patey. Structural and dynamical properties of ionic liquids: The influence of ion size disparity. *Journal of Chemical Physics*, 129(6):064517, 2008.

[292] H. V. Spohr and G. N. Patey. Structural and dynamical properties of ionic liquids: The influence of charge location. *Journal of Chemical Physics*, 130(10):104506, 2009.

[293] Heidrun V. Spohr and G. N. Patey. Structural and dynamical properties of ionic liquids: Competing influences of molecular properties. *Journal of Chemical Physics*, 132(15):154504, 2010.

[294] K. G. Sprenger, Vance W. Jaeger, and Jim Pfaendtner. The general AMBER force field (GAFF) can accurately predict thermodynamic and transport properties of many ionic liquids. *Journal of Physical Chemistry B*, 119(18):5882–5895, 2015.

[295] Mitsutake Suematsu, Masahiro Yoshizawa-Fujita, Haijin Zhu, Maria Forsyth, Yuko Takeoka, and Masahiro Rikukawa. Effect of zwitterions on elec-

trochemical properties of oligoether-based electrolytes. *Electrochimica Acta*, 175:209–213, 2015.

[296] H. Sun. COMPASS: An ab Initio Force-Field Optimized for Condensed-Phase ApplicationsOverview with Details on Alkane and Benzene Compounds. *The Journal of Physical Chemistry B*, 102(38):7338–7364, 1998.

[297] J. Sun, D. R. MacFarlane, N. Byrne, and M. Forsyth. Zwitterion effect in polyelectrolyte gels based on lithium methacrylate-N,N-dimethyl acrylamide copolymer. *Electrochimica Acta*, 51(19):4033–4038, 2006.

[298] Jiazeng Sun, Churat Tiyapiboonchaiya, Patrick C. Howlett, Douglas R. MacFarlane, Nolene Byrne, Jennifer M. Pringle, and Maria Forsyth. The zwitterion effect in high-conductivity polyelectrolyte materials. *Nature Materials*, 3(1):29–32, 2004.

[299] Na Sun, Xinpei Gao, Aoli Wu, Fei Lu, and Liqiang Zheng. Mechanically strong ionogels formed by immobilizing ionic liquid in polyzwitterion networks. *Journal of Molecular Liquids*, 248:759–766, 2017.

[300] Xiao Guang Sun, Craig L Reeder, and John B Kerr. Synthesis and characterization of network type single ion conductors. *Macromolecules*, 37(6):2219–2227, 2004.

[301] Anurag Prakash Sunda, Anirban Mondal, and Sundaram Balasubramanian. Atomistic simulations of ammonium-based protic ionic liquids:

steric effects on structure, low frequency vibrational modes and electrical conductivity. *Phys. Chem. Chem. Phys*, 17:4625–4633, 2015.

[302] Masahiro Tamada, Saori Ueda, Takahiro Hayashi, and Hiroyuki Ohno. Thermally Stable Polymer Gel Electrolytes Composed of Branched Polyimide and Ionic Liquid/Zwitterion Mixture Prepared by In Situ Polycondensation. *Chemistry Letters*, 37(1):86–87, 2007.

[303] J Tarascon. Issues and challenges facing rechargeable lithium batteries. *Nature*, 414(November):359–367, 2001.

[304] Magdalena Tarnacka, Anna Chrobok, Karolina Matuszek, Sylwia Golba, Paulina Maksym, Kamil Kaminski, and Marian Paluch. Polymerization of Monomeric Ionic Liquid Confined within Uniaxial Alumina Pores as a New Way of Obtaining Materials with Enhanced Conductivity. *ACS Applied Materials and Interfaces*, 8(43):29779–29790, 2016.

[305] Morgan E. Taylor and Matthew J. Panzer. Fully-Zwitterionic Polymer-Supported Ionogel Electrolytes Featuring a Hydrophobic Ionic Liquid. *Journal of Physical Chemistry B*, 122(35):8469–8476, 2018.

[306] Sami Tazi, Mathieu Salanne, Christian Simon, Pierre Turq, Michael Pounds, and Paul A. Madden. Potential-induced ordering transition of the adsorbed layer at the ionic liquid/electrified metal interface. *Journal of Physical Chemistry B*, 114(25):8453–8459, 2010.

[307] Christina L Ting, Karen E Sorensen-Unruh, Mark J Stevens, and Amalie L Frischknecht. Nonequilibrium simulations of model ionomers in an oscillating electric field. *The Journal of Chemical Physics*, 145(4):44902, jul 2016.

[308] Christina L Ting, Mark J Stevens, and Amalie L Frischknecht. Structure and Dynamics of Coarse-Grained Ionomer Melts in an External Electric Field. *Macromolecules*, 48(3):809–818, feb 2015.

[309] Abdulnour Y. Toukmaji and John A. Board. Ewald summation techniques in perspective: a survey. *Computer Physics Communications*, 95(2-3):73–92, 2003.

[310] Edward B. Trigg and Karen I. Winey. Nanoscale layers in polymers to promote ion transport. *Molecular Systems Design & Engineering*, 4(2):252–262, 2019.

[311] Alessandro Triolo, Olga Russina, Hans-Jurgen Bleif, and Emanuela Di Cola. Nanoscale Segregation in Room Temperature Ionic Liquids†. *Journal of Physical Chemistry B*, 111(18):4641–4644, 2007.

[312] Seiji Tsuzuki, Hajime Matsumoto, Wataru Shinoda, and Masuhiro Mikami. Effects of conformational flexibility of alkyl chains of cations on diffusion of ions in ionic liquids. *Physical Chemistry Chemical Physics*, 13(13):5987–5993, 2011.

[313] Seiji Tsuzuki, Wataru Shinoda, Hiroaki Saito, Masuhiro Mikami, Hiroyuki Tokuda, and Masayoshi Watanabe. Molecular dynamics simulations of ionic liquids: Cation and anion dependence of self-diffusion coefficients of ions. *Journal of Physical Chemistry B*, 113(31):10641–10649, 2009.

[314] Mark E Tuckerman, José Alejandre, Roberto López-Rendón, Andrea L Jochim, and Glenn J Martyna. A Liouville-operator derived measure-preserving integrator for molecular dynamics simulations in the isothermal–isobaric ensemble. *Journal of Physics A: Mathematical and General*, 39(19):5629–5651, 2006.

[315] Gregory J Tudryn, Michael V. O'Reilly, Shichen Dou, Daniel R King, Karen I Winey, James Runt, and Ralph H Colby. Molecular mobility and cation conduction in polyether-ester-sulfonate copolymer ionomers. *Macromolecules*, 45(9):3962–3973, 2012.

[316] Kurt Ueberreiter and Gerhard Kanig. Self-plasticization of polymers. *Journal of Colloid Science*, 7(6):569–583, 1952.

[317] Sérgio M. Urahata and Mauro C C Ribeiro. Single particle dynamics in ionic liquids of 1-alkyl-3-methylimidazolium cations. *Journal of Chemical Physics*, 122(2):1–10, 2005.

[318] I. Vattulainen, M. Karttunen, G. Besold, and J. M. Polson. Integration schemes for dissipative particle dynamics simulations: From softly in-

teracting systems towards hybrid models. *Journal of Chemical Physics*, 116(10):3967–3979, 2002.

[319] J M Wang, R M Wolf, J W Caldwell, P A Kollman, and D A Case. Development and testing of a general amber force field. *J. Comput. Chem.*, 25(9):1157–1174, 2004.

[320] Junmei Wang, Wei Wang, Peter A Kollman, and David A Case. Automatic atom type and bond type perception in molecular mechanical calculations. *Journal of Molecular Graphics and Modelling*, 25(2):247–260, 2006.

[321] Qiang Wang, Takashi Taniguchi, and Glenn H Fredrickson. Self-consistent field theory of polyelectrolyte systems. *Journal of Physical Chemistry B*, 108(21):6733–6744, 2004.

[322] Shih-Wa Wang, Wenjuan Liu, and Ralph H. Colby. Counterion Dynamics in Polyurethane-Carboxylate Ionomers with Ionic Liquid Counterions. *Chemistry of Materials*, 23(7):1862–1873, 2011.

[323] Yangyang Wang, Alexander L. Agapov, Fei Fan, Kunlun Hong, Xiang Yu, Jimmy Mays, and Alexei P. Sokolov. Decoupling of ionic transport from segmental relaxation in polymer electrolytes. *Physical Review Letters*, 108(8):1–5, 2012.

[324] Yangyang Wang and Alexei P. Sokolov. Design of superionic polymer electrolytes. *Current Opinion in Chemical Engineering*, 7:113–119,

2015.

[325] Yong Lei Wang and Aatto Laaksonen. Interfacial structure and orientation of confined ionic liquids on charged quartz surfaces. *Physical Chemistry Chemical Physics*, 16(42):23329–23339, 2014.

[326] Masayoshi Watanabe, Yusuke Suzuki, and Astushi Nishimoto. Single ion conduction in polyether electrolytes alloyed with lithium salt of a perfluorinated polyimide. *Electrochimica Acta*, 45(8):1187–1192, 2000.

[327] S Watanabe, M Nakano, K Miyake, R Tsuboi, and S Sasaki. Effect of Molecular Orientation Angle of Imidazolium Ring on Frictional Properties of Imidazolium-Based Ionic Liquid. *Langmuir*, 30(27):8078–8084, jul 2014.

[328] Michael A Webb, Yukyung Jung, Danielle M Pesko, Brett M Savoie, Umi Yamamoto, Geoffrey W Coates, Nitash P Balsara, Zhen-Gang Wang, and Thomas F Miller. Systematic Computational and Experimental Investigation of Lithium-Ion Transport Mechanisms in Polyester-Based Polymer Electrolytes. *ACS Central Science*, 1(4):198–205, jul 2015.

[329] Alexander Weyman, Markus Bier, Christian Holm, and Jens Smiatek. Microphase separation and the formation of ion conductivity channels in poly(ionic liquid)s: A coarse-grained molecular dynamics study. *Journal of Chemical Physics*, 148(19), 2018.

[330] Bill K. Wheatle, Jordan R. Keith, Santosh Mogurampelly, Nathaniel A. Lynd, and Venkat Ganesan. Influence of Dielectric Constant on Ionic Transport in Polyether-Based Electrolytes. *ACS Macro Letters*, 6(12):1362–1367, 2017.

[331] Bill K Wheatle, Nathaniel A Lynd, and Venkat Ganesan. Effect of Polymer Polarity on Ion Transport: A Competition between Ion Aggregation and Polymer Segmental Dynamics. *ACS Macro Letters*, 7(10):1149–1154, oct 2018.

[332] F. Wohde, R. Bhandary, J. M. Moldrickx, J. Sundermeyer, M. Schönhoff, and B. Roling. Li+ ion transport in ionic liquid-based electrolytes and the influence of sulfonate-based zwitterion additives. *Solid State Ionics*, 284:37–44, 2016.

[333] Z Wojnarowska, J Knapik, M Díaz, A. Ortiz, I Ortiz, and M Paluch. Conductivity Mechanism in Polymerized Imidazolium-Based Protic Ionic Liquid [HSO 3 –BVIm][OTf]: Dielectric Relaxation Studies. *Macromolecules*, 47(12):4056–4065, 2014.

[334] Chun Y. Wong, Hani Al-Salami, and Crispin R. Dass. Potential of insulin nanoparticle formulations for oral delivery and diabetes treatment. *Journal of Controlled Release*, 264(August):247–275, 2017.

[335] Peng Wu, Jingsong Huang, Vincent Meunier, Bobby G Sumpter, and Rui Qiao. Complex Capacitance Scaling in Ionic Liquids-Filled Nanopores. *ACS Nano*, 5(11):9044–9051, nov 2011.

[336] D.J. Wuebbles, D.W. Fahey, K.A. Hibbard, D.J. Dokken, B.C. Stewart, and T.K. Maycock. Climate Science Special Report: Fourth National Climate Assessment, Volume I. Technical report, U.S. Grobal Climate Research Program, Washington DC, USA, 2017.

[337] Siyun Xu, Sirui Xing, Shin-Shem Pei, and Steven Baldelli. Sum Frequency Generation Spectroscopy Study of an Ionic Liquid at a Graphene-BaF2 (111) Interface. *The Journal of Physical Chemistry B*, 118(19):5203–5210, may 2014.

[338] Siyun Xu, Sirui Xing, Shin Shem Pei, Vladislav Ivaništšev, Ruth Lynden-Bell, and Steven Baldelli. Molecular Response of 1-Butyl-3-Methylimidazolium Dicyanamide Ionic Liquid at the Graphene Electrode Interface Investigated by Sum Frequency Generation Spectroscopy and Molecular Dynamics Simulations. *Journal of Physical Chemistry C*, 119(46):26009–26019, 2015.

[339] Seitaro Yamaguchi, Masahiro Yoshizawa-Fujita, Haijin Zhu, Maria Forsyth, Yuko Takeoka, and Masahiro Rikukawa. Improvement of charge/discharge properties of oligoether electrolytes by zwitterions with an attached cyano group for use in lithium-ion secondary batteries. *Electrochimica Acta*, 186:471–477, 2015.

[340] Yuesheng Ye, Jae Hong Choi, Karen I. Winey, and Yossef A. Elabd. Polymerized ionic liquid block and random copolymers: Effect of weak

microphase separation on ion transport. *Macromolecules*, 45(17):7027–7035, 2012.

[341] Yuesheng Ye and Yossef A. Elabd. Anion exchanged polymerized ionic liquids: High free volume single ion conductors. *Polymer*, 52(5):1309–1317, 2011.

[342] Yuesheng Ye, Sharon Sharick, Eric M. Davis, Karen I. Winey, and Yossef A. Elabd. High hydroxide conductivity in polymerized ionic liquid block copolymers. *ACS Macro Letters*, 2(7):575–580, 2013.

[343] In-Chul Yeh and Max L Berkowitz. Ewald summation for systems with slab geometry. *The Journal of Chemical Physics*, 111(7):3155–3162, aug 1999.

[344] Tristan G A Youngs and Christopher Hardacre. Application of static charge transfer within an ionic-liquid force field and its effect on structure and dynamics. *ChemPhysChem*, 9(11):1548–1558, 2008.

[345] Yang Yu, Fei Lu, Na Sun, Aoli Wu, Wei Pan, and Liqiang Zheng. Single lithium-ion polymer electrolytes based on poly(ionic liquid)s for lithium-ion batteries. *Soft Matter*, 14(30):6313–6319, 2018.

[346] Zhou Yu, Chao Fang, Jingsong Huang, Bobby G. Sumpter, and Rui Qiao. Molecular Structure and Dynamics of Interfacial Polymerized Ionic Liquids. *Journal of Physical Chemistry C*, 122(39):22494–22503, 2018.

[347] Jiayin Yuan and Markus Antonietti. Poly(ionic liquid)s: Polymers expanding classical property profiles. *Polymer*, 52(7):1469–1482, 2011.

[348] Jiayin Yuan, David Mecerreyes, and Markus Antonietti. Poly(ionic liquid)s: An update. *Progress in Polymer Science*, 38(7):1009–1036, 2013.

[349] Heng Zhang, Wenfang Feng, Zhibin Zhou, and Jin Nie. Composite electrolytes of lithium salt / polymeric ionic liquid with bis ( fl uorosulfonyl ) imide. *Solid State Ionics*, 256:61–67, 2014.

[350] Heng Zhang, Chunmei Li, Michal Piszcz, Estibaliz Coya, Teofilo Rojo, Lide M. Rodriguez-Martinez, Michel Armand, and Zhibin Zhou. Single lithium-ion conducting solid polymer electrolytes: Advances and perspectives. *Chemical Society Reviews*, 46(3):797–815, 2017.

[351] Yong Zhang and Edward J. Maginn. A simple AIMD approach to derive atomic charges for condensed phase simulation of ionic liquids. *Journal of Physical Chemistry B*, 116(33):10036–10048, 2012.

[352] Yong Zhang and Edward J Maginn. Direct Correlation between Ionic Liquid Transport Properties and Ion Pair Lifetimes: A Molecular Dynamics Study. *The Journal of Physical Chemistry Letters*, 705(3):700–705, 2015.

[353] Yong Zhang, Lianjie Xue, Fardin Khabaz, Rose Doerfler, Edward L. Quitevis, Rajesh Khare, and Edward J. Maginn. Molecular Topology

and Local Dynamics Govern the Viscosity of Imidazolium-Based Ionic Liquids. *Journal of Physical Chemistry B*, 119(47):14934–14944, 2015.

[354] Wei Zhao, Frederic Leroy, Berit Heggen, Stefan Zahn, Barbara Kirchner, Sundaram Balasubramanian, and Florian M??ller-Plathe. Are there stable ion-pairs in room-temperature ionic liquids? Molecular dynamics simulations of 1-n-butyl-3-methylimidazolium hexafluorophosphate. *Journal of the American Chemical Society*, 131(43):15825–15833, 2009.

[355] Liuchun Zheng, Harihara S. Sundaram, Zhiyong Wei, Chuncheng Li, and Zhefan Yuan. Applications of zwitterionic polymers. *Reactive and Functional Polymers*, 118(June):51–61, 2017.

[356] Yun-Xin Zhong, Jia-Wei Yan, Mian-Gang Li, Xiao Zhang, Ding-Wen He, and Bing-Wei Mao. Resolving Fine Structures of the Electric Double Layer of Electrochemical Interfaces in Ionic Liquids with an AFM Tip Modification Strategy. *Journal of the American Chemical Society*, 136(42):14682–14685, oct 2014.

[357] Ming Zhou, Sisi Li, Ze Zhang, Chengwen Wang, Gang Luo, and Jinzhou Zhao. Progress in the Synthesis of Zwitterionic Gemini Surfactants. *Journal of Surfactants and Detergents*, 20(6):1243–1254, 2017.

# Vita

Jordan Reynolds Keith is a graduate of R.J. Reynolds High School in Winston-Salem, NC, USA and North Carolina State University in Raleigh, NC, USA, where he earned a Bachelor of Science in Chemical Engineering. He was an accomplished student, earning a 4.0 GPA and volunteering for the student chapter of the American Institute for Chemical Engineers (AIChE), ultimately serving as President for the chapter in 2011-2012. Jordan received the NC State Merit Recognition Scholarship, the Francis P. O'Dell Outstanding Engineer Scholarship, the AIChE Donald F. and Mildred Topp Othmer National Scholarship Award, and the NC State Chemical and Biomolecular Engineering Departmental Award for Leadership. After three years at Eastman Chemical Company in Kingsport, TN, USA, where he worked as a process design engineer, Jordan was inspired to return to graduate school. He began in 2015 at the University of Texas at Austin with the Bruce B. Jackson Endowed Graduate Fellowship in Engineering.

Permanent address: jrkws1@aol.com

This dissertation was typeset with LaTeX[†] by the author.

[†]LaTeX is a document preparation system developed by Leslie Lamport as a special version of Donald Knuth's TeX Program.